AD_____

Award Number: DAMD17-00-1-0249

TITLE: FCCC Institutional Breast Cancer Training Program (FCCC-IBCTP)

PRINCIPAL INVESTIGATOR: Jose Russo, M.D.

CONTRACTING ORGANIZATION: Fox Chase Cancer Center
Philadelphia, Pennsylvania 19111

REPORT DATE: July 2004

TYPE OF REPORT: Annual Summary

PREPARED FOR: U.S. Army Medical Research and Materiel Command
Fort Detrick, Maryland 21702-5012

DISTRIBUTION STATEMENT: Approved for Public Release;
Distribution Unlimited

REPORT DOCUMENTATION PAGE

Form Approved
OMB No. 074-0188

1. AGENCY USE ONLY (Leave blank)	2. REPORT DATE	3. REPORT TYPE AND DATES COVERED
	July 2004	Annual Summary (1 Jul 2003 – 30 Jun 2004)

4. TITLE AND SUBTITLE
FCCC Institutional Breast Cancer Training Program (FCCC-IBCTP)

5. FUNDING NUMBERS
DAMD17-00-1-0249

6. AUTHOR(S)
Jose Russo, M.D.

7. PERFORMING ORGANIZATION NAME(S) AND ADDRESS(ES)
Fox Chase Cancer Center
Philadelphia, Pennsylvania 19111

E-Mail: Jose.russo@fccc.edu

8. PERFORMING ORGANIZATION REPORT NUMBER

9. SPONSORING / MONITORING AGENCY NAME(S) AND ADDRESS(ES)
U.S. Army Medical Research and Materiel Command
Fort Detrick, Maryland 21702-5012

10. SPONSORING / MONITORING AGENCY REPORT NUMBER

11. SUPPLEMENTARY NOTES
Original contains color plates: All DTIC reproductions will be in black and white.

12a. DISTRIBUTION / AVAILABILITY STATEMENT
Approved for Public Release; Distribution Unlimited

12b. DISTRIBUTION CODE

13. ABSTRACT (Maximum 200 Words)

The Institutional Breast Cancer Training Program offers to the postdoctoral trainees practical experience in the fields of cellular and molecular biology, drug resistance and targeted immunotherapy, genetic epidemiology and control, psychosocial and behavioral medicine, as well as breast cancer prevention, diagnosis, and treatment. During the fourth year of the grant awarded we have been implementing the training phase of the program by monitoring each of the individual projects. The trainees have been attending at least one general lecture a week from those offered by the Fox Chase Cancer Center and a special seminar targeted to the formation of the trainees addressing critical subjects in breast cancer. We have established a half-day seminar twice a year in which the trainees present their work. In this last year of the program that ends in June 30 of 2004 we have requested and additional six months extension for allowing the completion of the program of those trainees that started in January 1, 2003. During this period the main emphasis has been and will be the data collection, analysis and preparation of abstracts and manuscripts.

14. SUBJECT TERMS
Genomic instability, Proline 47 polymorphism, p53, Appl Gene, mammary gland

15. NUMBER OF PAGES
138

16. PRICE CODE

17. SECURITY CLASSIFICATION OF REPORT	18. SECURITY CLASSIFICATION OF THIS PAGE	19. SECURITY CLASSIFICATION OF ABSTRACT	20. LIMITATION OF ABSTRACT
Unclassified	Unclassified	Unclassified	Unlimited

Table of Contents

A-INTRODUCTION

The focus of the FCCC Institutional Breast Cancer Training Program (IBCTP) is to integrate the unique talents and interests of the Center's basic scientists, clinical investigators and behavioral scientists to create a comprehensive effort to approach the problems of breast cancer. The rich scientific and intellectual environment of FCCC is nurtured by a cohesive interdisciplinary program that is based on expertise in areas of high relevance to breast cancer. The Institutional Breast Cancer Training Program offers to the postdoctoral trainees practical experience in the fields of cellular and molecular biology, drug resistance and targeted immunotherapy, genetic epidemiology and control, psychosocial and behavioral medicine, as well as breast cancer prevention, diagnosis, and treatment.

B-BODY

B-i. Organization of the FCCC-Institutional Breast Cancer Training Program. Following our statement of work we have accomplished the following tasks:

Tasks4-7. During the fourth year of the grant awarded we have been implementing the training phase of the program by monitoring each of the individual projects. The trainees have been attending at least one general lecture a week from those offered by the Fox Chase Cancer Center and a special seminar targeted to the formation of the trainees addressing critical subjects in breast cancer. We have established a half-day seminar twice a year in which the trainees present their work in front of the Faculty and the Advisory Panel.

Task 8. In this last year of the program that ends in June 30 of 2004 (for Dr. S. Fernandez), we have requested and additional six months extension for allowing the completion of the program of those trainees (Drs E. Pugacheva, X. Li and H. You) that started in January 1, 2003. During this period the main emphasis has been and will be the data collection, analysis and preparation of abstracts and manuscripts. This will be an indicator of the success of our training program.

B-ii- . Predisposition to genomic instability in breast cancer: analysis of molecular mechanisms.

Trainee: Elena Pugacheva, PhD
Mentor: Erica Golemis, Ph.D.
Period reported: August 1, 2003 – to June 30, 2004

Introduction:

The goal of this research is to better understand intrinsic genetic factors leading to genome instability, with the intent of improving diagnosis and treatment for breast cancer. Based on our extensive preliminary data, which define HEF1 and p130Cas as novel factors controlling centrosome dynamics and spindle formation, we are exploring HEF1 and p130Cas status as contributing factors to acquisition of a malignant phenotype and drug resistance in breast cancer.

Background.

The **HEF1** scaffolding protein has a well-defined role in mediating integrin-dependent attachment signaling at focal adhesions. We had previously shown that HEF1 relocalizes to the spindle asters at mitosis, but the significance of this migration was unclear. We here report that HEF1 status controls mitotic spindle formation through action at centrosomes in the G2 phase of cell cycle. We have demonstrated that increased levels of HEF1 cause the development of supernumerary centrosomes, and a multipolar spindle. Conversely, depletion of HEF1, or over expression of a dominant-negative HEF1 derivative, results in premature centrosome splitting and frequent appearance of monoastral spindles. Association of endogenous HEF1 with the centrosome peaks in late G2 phase of cell cycle, and is followed by HEF1 movement from the centrosome to the spindle. We show that HEF1 controls recruitment of activated Aurora A kinase to the centrosome, in an interaction involving association with the AurA activation partner Ajuba. In summary, these results provide a novel mechanism for the coordination of cell attachment status with cell division which malfunctions in tumor cells.

Aims of our study are: **1**- To delineate HEF1 sequence motifs responsible for delivery of the protein to the centrosome and to the mitotic spindle. **2**- Identify the proteins interacting with HEF1 during onset of mitosis and modulating HEF1 localization. **3**-To investigate how phosphorylation of HEF1 affects the localization of the HEF1 protein to the mitotic apparatus. **4**-To clarify the relation between HEF1 and the closely related p130Cas protein in the regulation of centrosome dynamics in tumor and normal breast epithelial cells.

Results

i. Localization of HEF1 to the centrosome.

We are exploring the function of HEF1 in mitosis. We believe phosphorylation of HEF1 is an important controlling mechanism governing HEF1 mitotic localization and interaction with target proteins. We have identified potential phosphorylation sites on HEF1 for cdc2/cyclin B and GSK3-beta, kinases that play pivotal roles in mitotic progression. We are currently investigating the significance of interactions of HEF1 with these kinases for the observed phenotypes induced by HEF1 on the spindle and centrosomes.

Using HEF1-specific antibodies in high resolution confocal and immunofluorescence analysis, we have now determined that a population of endogenous HEF1 associates with the centrosome. Using a set of deletion mutants of the HEF1 protein (Fig.1a.) we have delineated the exact region responsible for the delivery of HEF1 to the centrosome (compare clone p55 and p55+). This 31 aa fragment of HEF1 consists of 18 Ser/Thr residues which are highly phosphorylated during mitosis. Four potential consensus phosphorylation sites for the GSK3-beta kinase were identified in this region by the

NetPhos 2.0 program (Fig.1b). In immunofluorescence assays, we showed that the mutations in the crucial serine residues (S371, S386, S391) in three out of four identified consensuses completely prevent (abolished) delivery of HEF1 to the centrosome, but do not interfere with localization of HEF1 to the focal adhesion (Fig1.c).

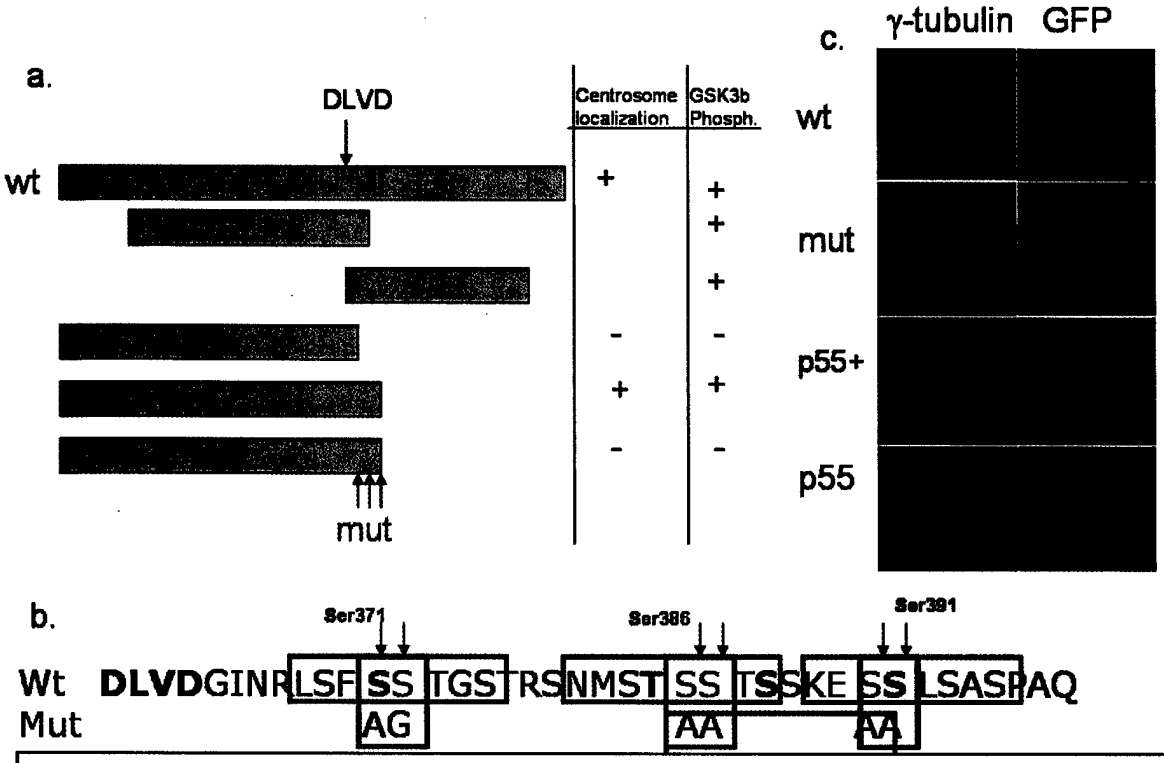

Figure 1. *Localization of HEF1 to the centrosome.* **a.** Schematic representation of HEF1 mutants used for the experiments. **b.** Sequence of the (+) motif in the p55+ part of HEF1 containing the 31 amino acid localization motif. Mutated serines are marked by red arrows. GSK3-beta consensus sites marked with blue boxes. c.Immunofluorescence of cells transfected with GFP-tagged HEF1 variants (Green), co-stained with γ-tubulin (Red).

HEF1 fragments containing or lacking this motif were used in *in vitro* kinase assays, indicating that this motif is important for phosphorylation by GSK3-beta (Fig2.b). It is possible, that GSK3b dependent phosphorylation of HEF1 accrue at the beginning of mitosis, since we have shown in vivo analysis that two well characterized inhibitors of GSK3-beta kinase (LiCl or thiadiazolidinone (Calbiochem)), caused reduction of endogenous HEF1 levels in cells. (Fig2.a).

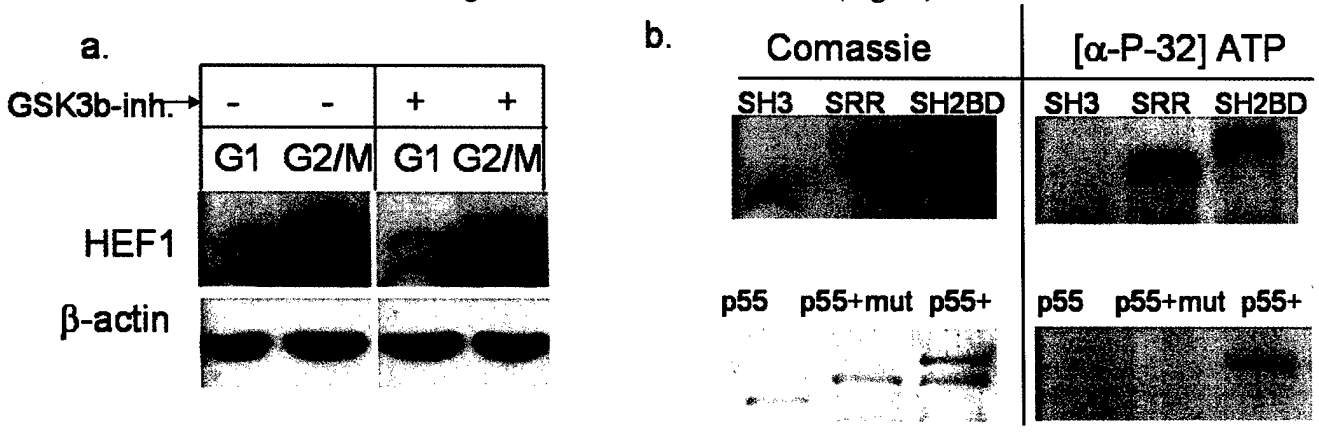

Figure 2. *HEF1is a potential GSK3b phosphorylation target.* **a.** Western analysis of MCF-7 cells treated (+) or untreated (-) with specific GSK3b inhibitor (Calbiochem). Thymidine and nocodazole treated cells were used for analysis of G1 and G2/M population of cells. β-actin was shown as a loading control. **b.** *In vitro* kinase assay with GSK3-beta kinase, using the HEF1 variants presented in Fig1a. Coomassie staining indicates equal loading of proteins in the assay.

ii. HEF1is involved in and required for the centrosomal accumulation of phosphorylated AuroraA kinase

As we have previously reported, manipulation of the levels of HEF1 or p130Cas leads to profound changes in centrosome integrity and dynamics. Over-expression of HEF1, or stabilization of endogenous HEF1 at mitosis with targeted peptides, in each case result in centrosome amplification, with cells containing in excess of 4 centrosomes. In contrast, depletion of HEF1 resulted in a separate centrosome defect: the premature splitting of the centrosomes in >70% of the cell population (manuscript in preparation). Intriguingly, the two phenotypes associated with over-expressed HEF1 are very similar to those reported for Aurora A kinase in breast carcinoma (1, 2). Initial activation of cyclin B1 at mitosis has been proposed to depend on an initial recruitment of activated AurA kinase to the centrosome in late G2, following AurA interaction with the LIM domain protein Ajuba (3). We investigated the interactions of HEF1, Aurora A and Ajuba.

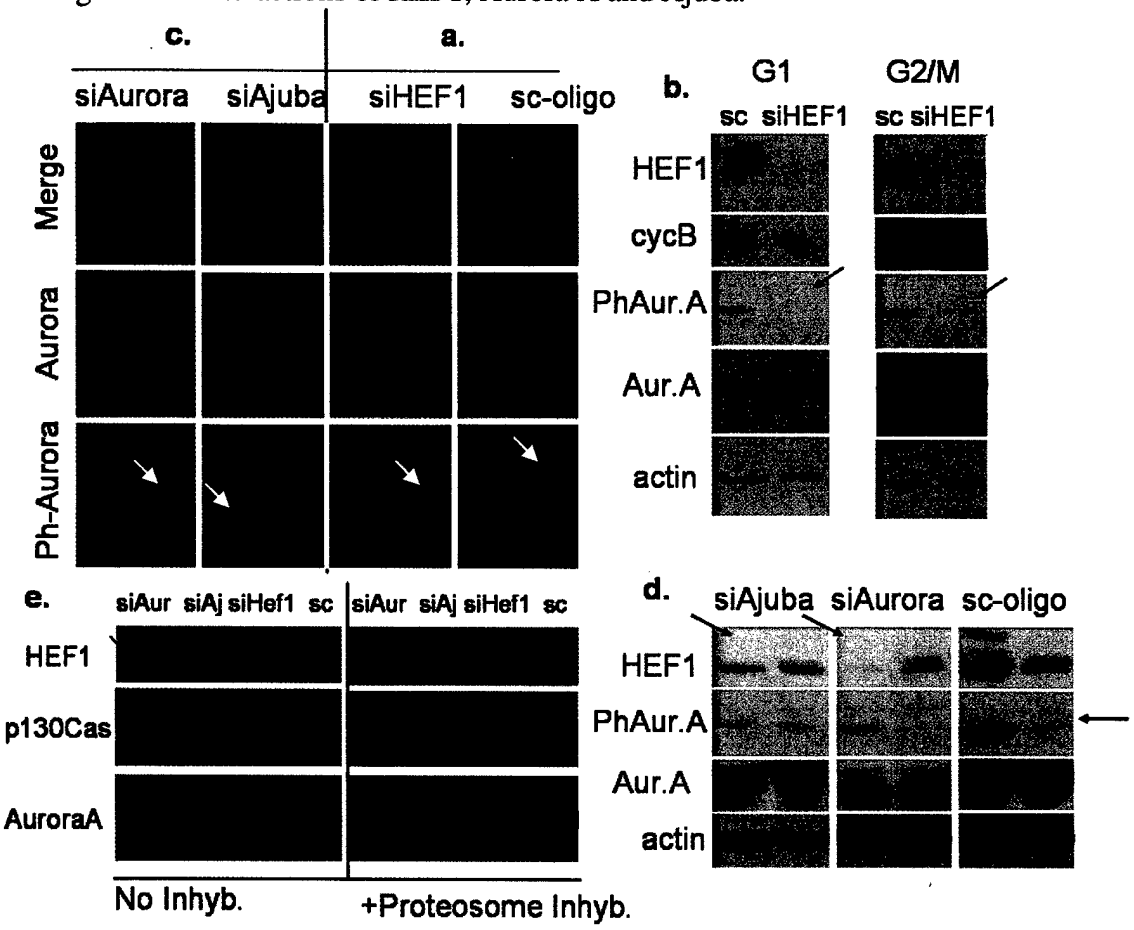

Figure 3.. *HEF1 is required for the centrosomal accumulation of phosphorylated AuroraA kinase* **a.** and **c.** Immunofluorescence of cells transfected with small interfering RNA against HEF1 (siHEF1) or scrambled control oligo (a, c), or siRNA to Aurora or Ajuba (c). **b.** Western analysis of the siHEF1 treated cells with the antibody against phosphorylated active Aurora, Aurora (total), cyclin B to confirm the cell cycle stage, HEF1, or an actin loading control. **d.** Western analysis of the siAurora or siAjuba treated cells with the antibody HEF1, Phospho-Aurora, Aurora total and actin as loading control. **e.** Western blot analysis of the sc-oligo, siHEF1, siAurora or siAjuba treated cells in the presence (+) or absence (-) of lactacystin (Sigma), using antibody against Aurora (total), p130Cas and HEF1.

For all experiments we used cells synchronized at different stages of cell cycle, to discriminate mitosis-specific activities of HEF1. To synchronize cells at G1 we applied a 2mM thymidine solution to MCF-7 cells for 18 hours and confirmed the accumulation of cells in the G1 phase by FACS analysis (data not shown). Nocodazole treatment was used to synchronize cells at G2/M boundary. Through immunofluorescence and Western blot analysis of synchronized breast carcinoma cell lines (MCF-7 and others), we have found that HEF1 depletion causes a dramatic decrease in the amount of phosphorylated Aurora A protein at the onset of mitosis (Fig3a.,b). Reciprocally, depletion of Aurora A or its partner Ajuba, reduces the total amount of HEF1 protein and eliminates its localization at the centrosome (Fig 3c, d). This reduction of HEF1 level by Aurora A depletion could be blocked by incubating cells with the 26S proteosome inhibitor lactacystin (4) (Fig.3e), suggesting that this reduction in protein level was due to increased sensitivity of HEF to degradation because of destruction of a protective complex involving between Ajuba, Aurora and HEF1.

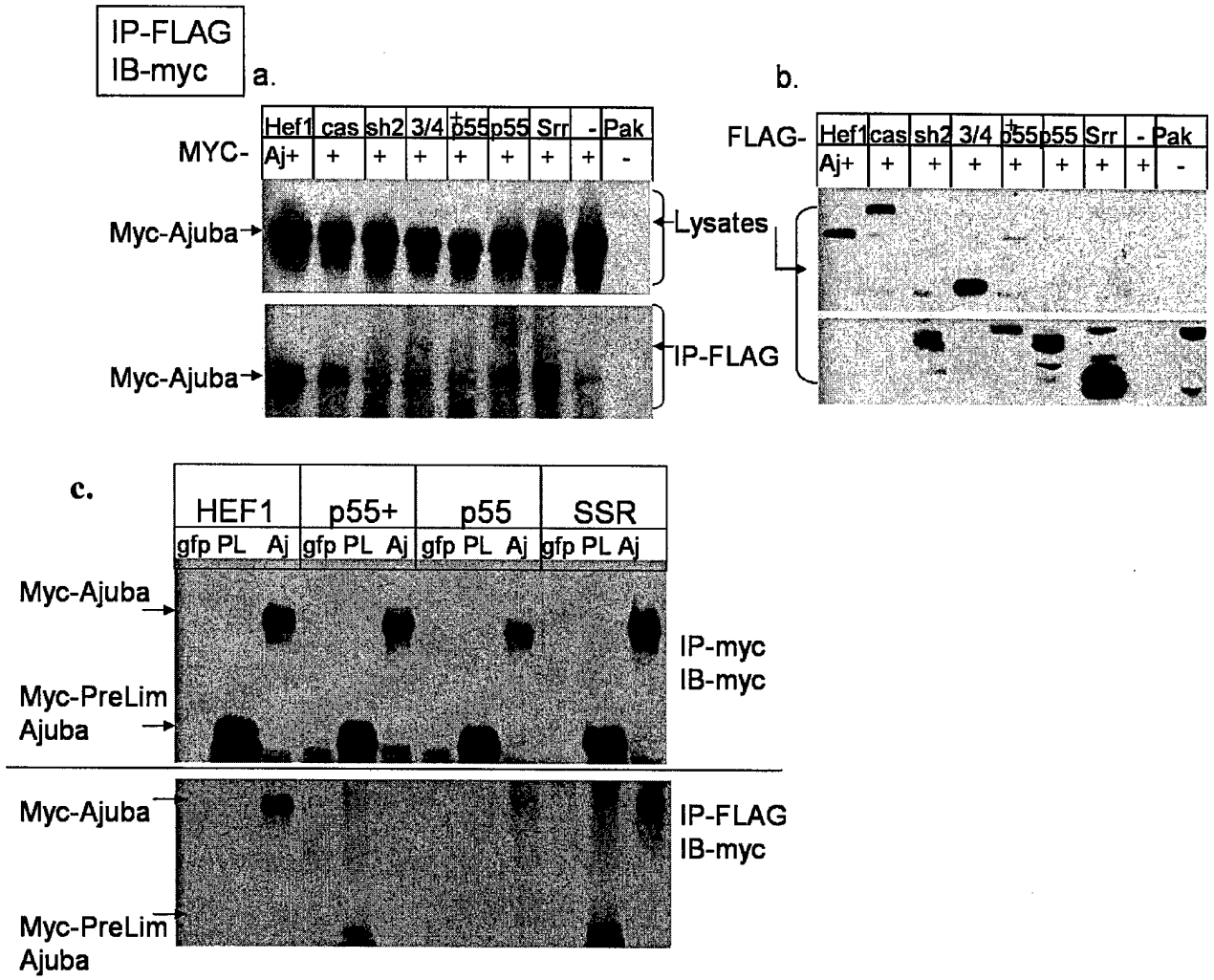

Figure 4.. *HEF1 directly interacts with Ajuba.* **a, b, c.** MCF-7 cells were co-transfected with the FLAG-HEF1 constructs and myc-tagged-Ajuba, lysed 24 hours post transfection and antibodies to FLAG-or Myc- used for immuno-precipitation (IP)from lysate, followed by Western blot (IB). **b.** Western analysis of the expression level of myc-Ajuba (a) or FLAG-HEF1 (b). **c.** MCF-7 cells were co-transfected by myc-tagged Pre-LIM domain of Ajuba, full length Ajuba or GFP (as non-specific control) with combination of FLAG-tagged full length HEF1 or deletion variants.

iii. HEF1 directly interacts with Ajuba

Using co-immuno-precipitation as a method for protein-protein interaction analysis, we have found that both Aurora A and Ajuba directly interact with HEF1.Using a panel of FLAG epitope-tagged deletion mutants of HEF1 (Fig1.a) and 6 Myc-tagged Ajuba (5), we found that C-terminal part of HEF (SRR-352-653aa) is involved in interaction with Ajuba, since only constructs with full length HEF1, SRR and p55+ precipitated full length Ajuba from the cells (Fig.4a, b). For Ajuba, we found that the pre-LIM domain of the protein is responsible for interaction with HEF1. The pre-LIM domain of Ajuba (weakly) and full length Ajuba (strongly) precipitated HEF1, SRR and p55(+) (Fig 4 c,d).

We are still analyzing the interaction of HEF1 with AuroraA. We have shown that HEF1 is precipitated by Aurora A, and Aurora A is co-IP-ed with HEF1, but this may be as direct or through Ajuba Fig.5a, b, c). We seek to determine which domains of HEF1 and Aurora A are involved in this interaction, and obtained the mutants defective in this interaction, to evaluate the importance of this interaction for mitotic entry.

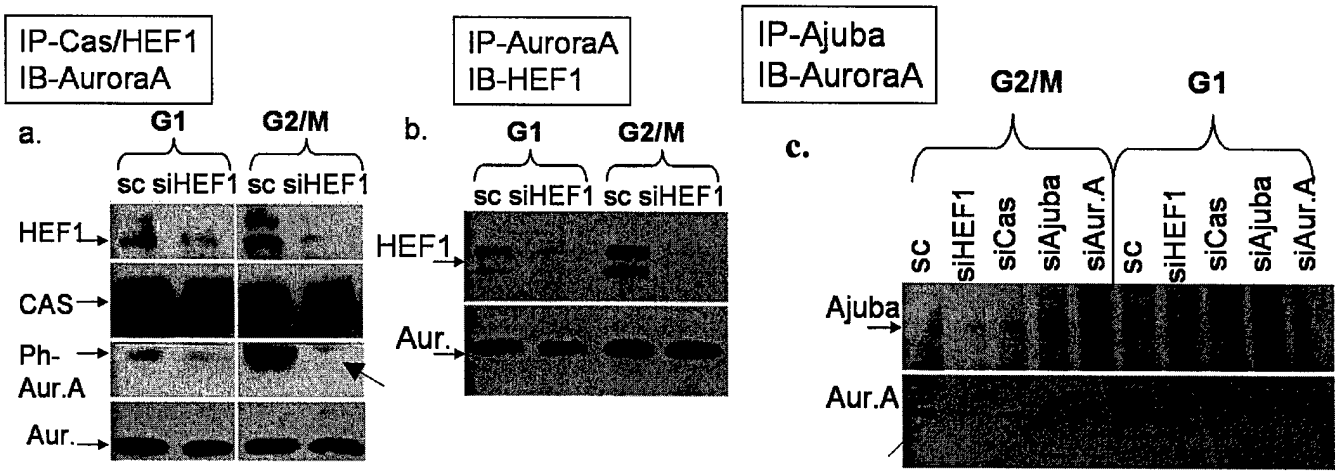

Figure 5. *HEF1 directly interacts with Aurora and Ajuba.* **a.** Western analysis of the immuno-precipitation (IP) of HEF1 by a Cas/HEF1 specific antibody (TL) from siHEF1 or scrambled oligo treated cells with the antibody against phosphorylated active Aurora, Aurora (total) and HEF1. **b.** Western analysis of the immuno-precipitation (IP) of Aurora A (total) from siHEF1 or scrambled oligo treated cells with antibody against Aurora (total) and HEF1. G1 and G2/M marked the cell cycle phases. **c.** Western analysis of the immuno-precipitation (IP) of Ajuba protein from sc-oligo, siHEF1, siCas, siAjuba or siAurora treated cells, using antibody to Aurora A .

As noted above, in *in vitro* kinase assays, we have shown that the SH2BD domain of HEF1 bears phosphorylation sites for AuroraA kinase. Using deletion mutants and mass spectrometry analysis, we have identified two peptides encompassing residues phosphorylated by AuroraA kinase in vitro. Analysis of phosphorylation of HEF1 by Aurora A kinase is ongoing project.

iii. Comparison of HEF1 and p130Cas regulation of centrosome status and AuroraA activation.

The HEF1 protein has been documented as being particularly abundant in epithelial and lymphoid lineages, and less abundant in fibroblasts (6,7). The HEF1-related p130Cas protein is ubiquitously expressed throughout different cell lineages. HEF1 and p130Cas share an 80% similarity at the SH3

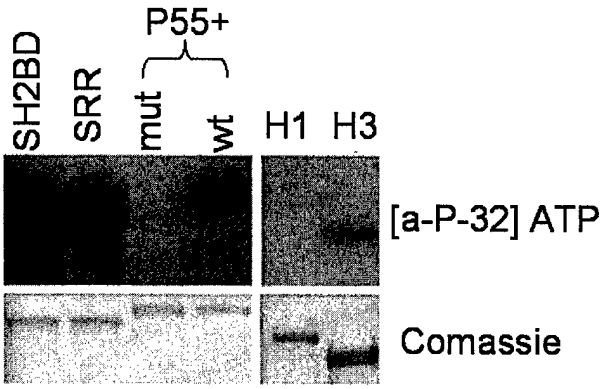

Figure 6.. *HEF1is an AuroraA phosphorylation target.* *In vitro* kinase assay with AuroraA kinase. Substrates were the HEF1 variants presented in Fig1a. Coomassie staining demonstrates the equal loading of protein in the assay.

domain and 52 and 33% at SH2 binding and serine-rich domains, respectively. Nevertheless they produce different phenotypes when over expressed in the epithelial cells. Over-expression of HEF1 causes apoptosis (8). Over expression of p130Cas stimulates cell proliferation and produces drug resistance (9). We investigated the effect of p130Cas on the centrosomal dynamic in several different cell lines: epithelial (MCF7, Hela, HEK293) or fibroblast (FF2425, MCR5-hTERT) lineages derived from tumors, or from normal cells (MCF12F and FF2425). Using a panel of antibodies against p130Cas in immuno-fluorescence assay, we conclude that p130Cas does not translocate to the centrosome (Fig.7a). Moreover, in cell lines over-expressing GFP-tagged p130Cas, GFP was detected in the cytoplasm and partially in the focal adhesions (data not shown), but not apparently at the centrosome or spindle. These data are in agreement with the previously described pattern of localization for p130Cas protein. Nevertheless, depletion of p130Cas in epithelial cells has partial centrosomal phenotypes. In MCF7 cells, depletion of p130Cas produced 40-50% percent of premature centrosomal splitting (Fig.7d), in contrast to the 85% seen with HEF1 depletion. Based on Western analysis (Fig.7b), HEF1 and p130Cas were depleted to a comparable levels in these experiments. p130Cas does not have Aurora A phosphorylation consensuses and was not phosphorylated in an *in vitro* kinase assay similar to that used for HEF1 (data not shown). Depletion of p130Cas in the cells using p130Cas-specific siRNA did not change the normal pattern of activation and localization of Aurora A kinase in mitosis (Fig.7c). Finally, we depleted HEF1 or p130Cas proteins in the fibroblast cells versus epithelial cells (note, HEF1 is almost undetectable in fibroblasts, but p130Cas is highly expressed). In fibroblasts, siRNA treatment for p130Cas or HEF1 did not affect centrosome integrity or splitting in any way. Based on this data we conclude that HEF1 has a specific and critical function in the centrosome cycle in the cells of epithelial lineage, but not fibroblasts.

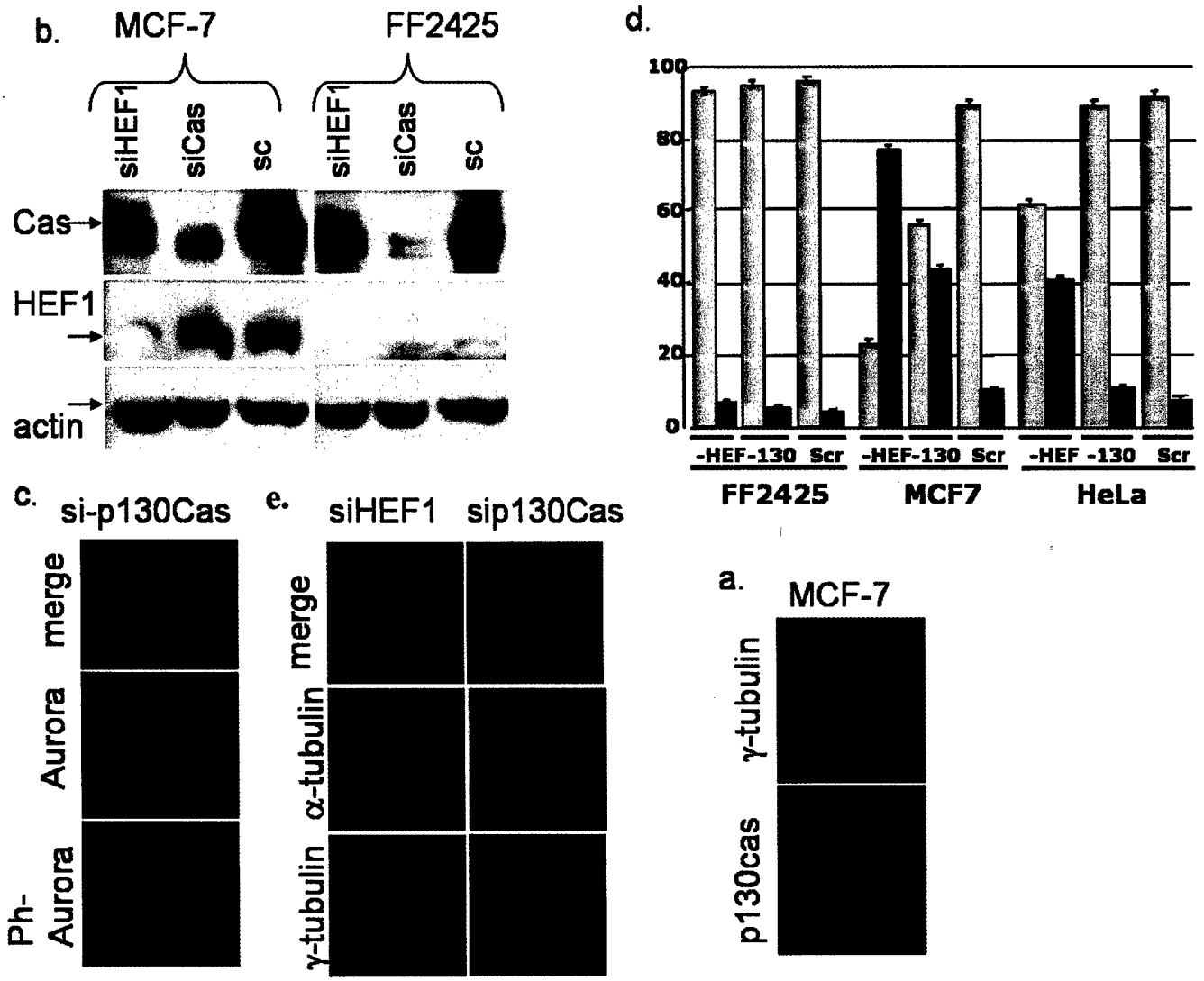

Figure 7. *Comparison of HEF1 and p130Cas regulation of centrosome status and AurA activation* **a.** Immunofluorescence analysis of MCF-7 cells using p130Cas specific antibody (Cas-S from Santa Cruz Biotech.) a (red), and co- stain with γ-tubulin (green). **b.**Western analysis of p130Cas, HEF1 and actin expression level in the MCF-7 and FF2425 cells treated with siHEF1, siCAS or scrambled oligo. **c.** Immunofluorescence analysis of MCF-7 cells treated with siCAS or scrambled oligo (Fig.3a) using antibody against phospho-Aurora (red), Aurora (total-green) and DNA dye (blue). **d.** Statistical analysis of centriole splitting in the MCF-7, Hela (epithelial cells) and FF2425, MRC5-hTERT (not shown) (fibroblast cells) upon treatment with the siRNA. **e.** Immuno-fluorescence analysis of FF2425 cells treated with siHEF1, siCAS or scrambled oligo (not shown) using a-or g-tubulin antibody to investigate centrosome status.

***B-iii-* The codon 47 polymorphism of p53 is functionally significant**

Trainee: Xiaoxian Li, Ph.D.
Mentor: Maureen Murphy, Ph.D.
Period reported: August 1, 2003 – to June 30, 2004

Introduction:

More than one million people are diagnosed with breast cancer every year worldwide (11). It has been generally accepted that breast cancer is the most common malignancy in the female. The mechanism whereas breast cancer forms and develops remains an active area of investigation. Research results have clearly associated the initiation, development and prognosis of breast cancer with different types of genetic alterations of oncogenes and tumor suppressor genes. Among all the altered genes, the p53 gene has the highest frequency of genetic mutation in breast cancer. The mutation of the p53 gene is found in about 20~40% of breast cancer and is often accompanied by loss the wild type allele. Additionally, it is known that germline mutation of the p53 gene is responsible for Li-Fraumeni Syndrome (LFS). LFS patients, at early age, are highly susceptible to the development of several types of cancers, among which breast cancer is the most frequent (12). Several studies have indicated that mutation of the p53 gene is found in ductal carcinoma *in situ* before the development of invasive breast cancer (13-15). Furthermore, the frequency of the p53 gene mutation has been found higher in large and invasive breast cancer (16). Accumulating evidence shows that mutations of the p53 gene is an independent risk factor conferring worse overall survival and some studies indicate the mutations of the p53 gene is the single most significant prognosis indicator (17).

Hormone therapy, chemo- and radio-therapy are the most commonly used clinical regimes in treating breast cancers and have been proved successful. However some patients are more resistant to these clinical treatments and show worse prognosis and higher rate of relapse. Berns et al (18) show that patients with mutated p53 have the poorest response to chemotherapy, such as tamoxifen. Estrogen receptor (ER) is closely related to breast cancer. ER positive breast cancer cells grow more slowly, are better differentiated and tend to have better prognosis. The ER has been shown to interact with and protect the p53 protein from MDM2 mediated degradation (19). The finding the ER prolongs the half life of p53 at least partially explains why ER positive breast cancer is less malignant. Taken together, the available evidence indicates that the p53 tumor suppressor gene has a significant role in the initiation and progression of breast cancer.

p53 is a tumor suppressor protein. Mutation or deletion of p53 is found in about 50% of human cancers. p53 homozygous knock out mice are prone to development of multiple types of cancer. Research shows that over-expression of p53 is sufficient to kill cancer cells. p53 induces apoptosis in tumor cells by its gene regulatory function or its direct effect on mitochondria to release cytochrome-c. The p53 protein transactives pro-apoptotic genes or suppresses anti-apoptotic genes when cells encounter DNA damages. Recently, the mitochondrial pathway through which p53 induces apoptosis has been reported (20).

The p53 tumor suppressor gene contains at least two coding region polymorphisms. A common polymorphism at codon 72 encodes either proline (P72) or arginine (R72). Dumont et al. (20) recently demonstrated that this polymorphism is functionally significant, and that the R72 variant has approximately fifteen-fold increased ability to induce programmed cell death. The mechanistic basis for this increased apoptotic potential was two-fold; the R72 variant demonstrated increased ability to bind to MDM2, which directed p53 for nuclear export and subsequent localization to the

mitochondria, where p53 induced cytochrome-c release. Additionally, we found that the R72 variant has increased ability to transactivate the p53-induced pro-apoptotic target gene PERP (20).

In addition to a polymorphism at codon 72, the p53 gene has a rarer coding region polymorphism at codon 47, encoding serine at this residue instead of proline (S47 and P47, respectively). In the study that initially described this variant, the S47 frequency was found to be 4.7% in African Americans, and undetectable in Caucasians. Preliminary analysis of the possible functional differences in these two proteins failed to reveal such; however, this study was performed over ten years ago, so these analyses did not analyze p53's apoptotic ability. Additionally, at the time this study was performed, *bona fide* p53 target genes were only just beginning to be identified, so the transactivation potential of p53 was only preliminarily analyzed.

Multiple N-terminal and C-terminal phosphorylation events are known to regulate p53 stabilization and activity following genotoxic stress (for review see 21). In particular, phosphorylation at serine 46 has been shown by several groups to be critical for the ability of p53 to induce apoptosis (22-24). Substitution of serine 46 with alanine renders p53 markedly impaired for apoptosis induction, and for transactivation of pro-apoptotic genes, but not for growth arrest genes such as p21/waf1 (24). Consistent with this finding, expression of p53DINP1, which enhances phosphorylation of serine 46, also significantly enhances p53-dependent apoptosis (25). At least one of the responsible kinases for serine 46 phosphorylation is the proline-directed kinase p38. The p38 kinase can directly phosphorylate p53 on serine 46, and can cooperate with p53 to induce apoptosis (26). Chemical inhibitors of p38 can inhibit phosphorylation at serine 46, and also markedly inhibit p53-dependent apoptosis (26). Finally, overexpression of PPM1D, which is a phosphatase that negatively regulates p38 that is subject to gene amplification in breast carcinoma, can inhibit serine 46 phosphorylation of p53, and consequently inhibit p53-mediated apoptosis (27). The combined data from multiple different groups strongly implicate the importance of serine 46 phosphorylation by kinases such as p38 in p53-dependent apoptosis.

At least two effects of serine 46 phosphorylation of p53 have been detected. The first is that this event appears to be important for transactivation of the p53-response gene p53AIP1. In contrast, transactivation of several other p53-response genes appears to be relatively unaffected by this phosphorylation event (24). Additionally, however, it has been reported that phosphorylation of serine 46 facilitates phosphorylation of other N-terminal residues of p53, including serine 20 (22). These latter phosphorylation events have an influence on p53 stability, as well as the recruitment of co-activators for transactivation (28,29).

Kinases in the Map kinase (MAPK) family like p38 require proline residues juxtaposed to the serine or threonine residues that are the targets of phosphorylation. We predicted that the codon 47 polymorphism, which removes this proximal proline residue, might have altered phosphorylation of serine 46; importantly, the proline at amino acid 47 is the only neighboring proline residue in this region. Therefore, we sought to test the hypothesis that, like the codon 72 polymorphism, the codon 47 polymorphism is functionally significant, perhaps due to altered phosphorylation of serine 46. In this report we show that the S47 variant demonstrates 2-fold decreased ability to be phosphorylated on serine 46 by p38 MAPK. In stably-transfected inducible cell lines containing the S47 protein, we show that this protein has 2-3 fold decreased ability to induce programmed cell death. Analysis of the mechanism underlying decreased cell death by the S47 protein revealed that this variant has decreased ability to transactivate a p53 target gene that is known to be critical for apoptosis induction; the BH3-only protein PUMA. Analysis of other N-terminal phosphorylation events likewise indicates a significant decrease in phosphorylation of serine 20, but not serine 15. The decreased phosphorylation of serine 46 and serine 20 at the amino terminus of the S47 variant may

reduce the affinity of this protein for transcriptional co-activators, and hence lead to impaired ability to transactivate a subset of p53 response genes, including PUMA.

Body

The S47 variant shows decreased phosphorylation on serine 46

If the proline at codon 47 is responsible for the phosphorylation of serine 46, the S47 variant should have decreased phosphorylation level compared with the wt p53 (proline 47). Using a serine 46 phospho-specific antibody, we detected significantly decreased binding affinity of the antibody to the S47 p53 (Fig.9A). Because of the amino acid change at codon 47, the decreased affinity of the serine 46 phosphorylation specific antibody could be solely caused by the structural change.

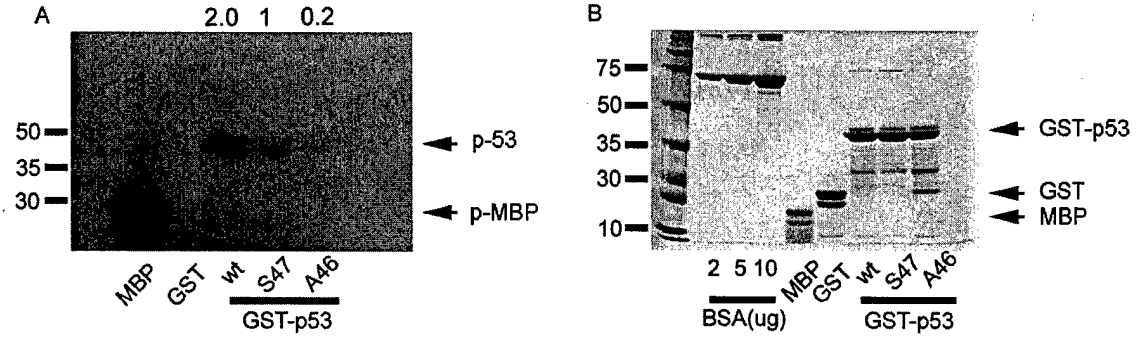

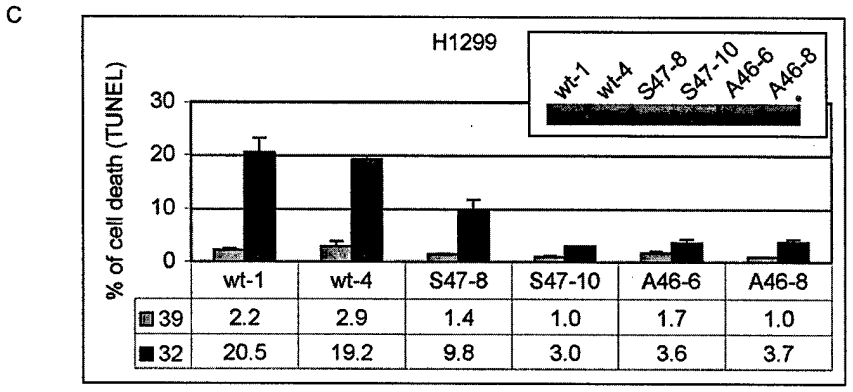

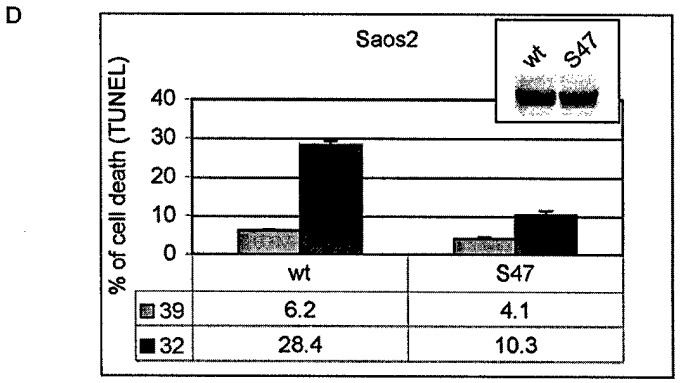

Figure 8. The S47 p53 shows decreased phosphorylation and compromised apoptotic ability.
A. ***The S47 GST-p53 shows 2-fold decrease in phosphorylation of serine 46 by p38 kinase.*** *Equal amount of MBP, GST and GST-p53 were incubated with active p38β2 kinase and [γ-^{32}P]ATP for15 min at 30℃. The reaction was stopped by adding Lithium Dodecyl Sulfate and boiling for 10*

min. Then the samples were loaded on a Nupage Novex 10% Bis-Tris gel (Invitrogen). The gel was dried and exposed to an X-ray film. Phosphorylated GST-p53 and MBP are labeled as p-p53 and p-MBP respectively.

B. Equal amount of GST-p53 was determined using BSA as standard. *GST-conjugated p53 (1-92) was purified using Glutathione-Sepharose 4B beads (Amersham Biosciences) and loaded on a Nupage Novex 10% Bis-Tris gel. Then the gel was stained with 0.025% Coomasic blue to determine the concentration of GST-p53, MBP and GST using BSA as standard.*

C. The S47 p53 shows 2-fold decrease in apoptotic ability than the wt p53 in stable H1229 cells. *The H1299 cells were shifted to 32℃ to activate p53 and then harvested 24 hrs after temperature shift (TS). TUNEL experiments were conducted on two independent clones of each construct (wt, S47 and A46) 24 hrs after TS (32) or maintained at 39 ℃ (39). The bars represent mean± SEM of three independent experiments. The numbers below the figure are the mean values. The p53 expression level of each clone is shown in the inset.*

D. The S47 variant shows 3-fold decrease in apoptotic ability than the wt p53 in stable Saos2 cells. *The Saos2 cells were shifted to 32℃ to activate p53 and then harvested 24 hrs after temperature shift. TUNEL experiments were performed to determine the apoptosis of each clone 24 hrs with (32) or without (39) TS. The bars represent mean± SEM of three independent experiments. The numbers below the figure are the mean values. The p53 protein levels are shown in the inset.*

To confirm the S47 p53 has compromised serine 46 phosphorylation, we performed *in vitro* kinase assay by incubating active p38 kinase (Upstate) with GST-p53 (amino acids 1-92) wt, S47 and A46 (serine 46 was mutated to alanine). It has been reported that the p38 kinase can also phosphorylate p53 at serine 33 (26), which is next to proline 34. To reduce the phosphorylation background, we mutated all three GST-p53 proteins (wt, S47 and A46) by introducing alanine at codon 33. Our results show the S47 p53 has 2-fold decreased phosphorylation level compared with wt p53 (Fig. 8A). The decreased phosphorylation of S47 p53 indicates that the proline 47 is important in the phosphorylation of serine 46. The elimination of phosphorylation of A46 p53 (Fig. 8A) indicates that p38 kinase indeed phosphorylates p53 on serine 46.

The S47 variant of p53 shows compromised apoptotic ability

Since the phosphorylation of serine 46 is important in the apoptotic ability of p53, the compromised serine 46 phosphorylation should decrease the apoptotic ability of the S47 variant. Our results confirm that the H1299 cells stably transfected with the S47 p53 show 2-fold decrease in apoptosis compared with those transfected with wt p53 (Fig.8C). The decreased apoptotic ability of S47 p53 correlates with the 2-fold decreased phosphorylation level in Figure 8B. Consistent with the abolished phosphorylation of amino acid 46 in the *in vitro* kinase assay, the A46 p53 has the least apoptotic ability (Fig.8C). To verify whether the S47 p53 shows decreased apoptotic ability in other cells, we generated stable Saos2 clones expressing wt and S47 p53. Our results show that S47 p53 showed 3-fold compromised apoptosis inducing ability in Saos2 cells (Fig. 8D). The fold deduction of the S47 p53 apoptotic ability in Saos2 cells is again very close to the 2-fold deduction of the phosphorylation level of serine 46. Thus our results confirm the importance of the phosphorylation of serine 46 in the apoptotic function of p53. More importantly, we show that the proline 47 polymorphic variant has descreased ability to induce apoptosis. Therefore, the possibility exists that this polymorphism affects cancer risk, or the efficacy of chemotherapy.

The S47 p53 shows decreased phosphorylation level of serine 20, but not other serine residues.

It has been reported that phosphorylation of serine 46 may affect phosphorylation of other sites (22). We examined the phosphorylation level of the S47 p53 on other N-terminal sites, specifically the nearby phosphorylation sites serine 15 and 20, compared with wt p53. Surprisingly, we found a significant decrease in the serine 20 phosphorylation level of the S47 p53 (Fig. 9A). No significant changes were found in the phosphorylation level of serine 15 and serine 393, however. Our results show that the induction of p21 and MDM2 are not affected by the phosphorylation level of serine 46 (Fig.9B), indicating the S47 p53 has the same general transcriptional activity as wild type p53. Consistent with this, our experiments show that the S47 p53 has the same half-life and ability to induce cell cycle arrest as wt p53 (data not shown). Finally, consistent with our previous results, we found that when the H1299 cell lines were treated with ionizing radiation (IR), the S47 p53 shows decreased apoptotic ability (Fig.9C).

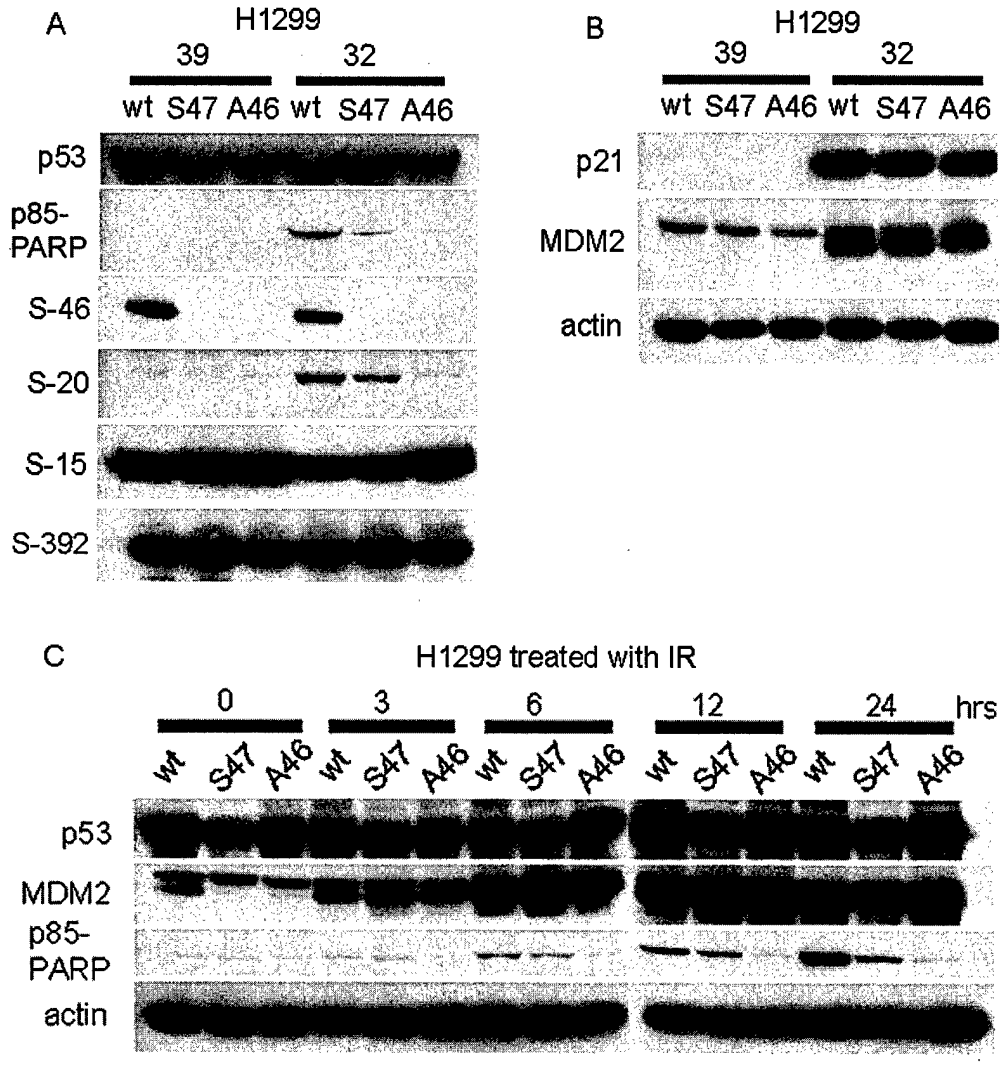

Figure 9. The S47 p53 shows compromised phosphorylation of serine 46 and 20 and decreased apoptotic function after IR.

A. The S47 p53 shows decreased phosphorylation of serine 46 and 20, but not of serine 15 and 392. *H1299 cells were shifted to 32 and harvested 24 hrs after TS. Equal amount of cell lysate was loaded on a Nupage Novex 10% Bis-Tris gel and Western analyzed. The p53 protein was detected with a monoclonal antibody (DO-1 from Oncogene). P85-PARP was detected by an antibody (Promega) specifically recognizes cleaved PARP. The PARP protein is cleaved during apoptosis and*

can be used as an apoptotic marker. Phosphorylation of serine 46, 20, 15 and 392 was detected using phospho-specific antibodies (Cell Signaling). This figure shows results from wt-4, S47-8 and S46-8 clones.

B. The S47 p53 shows the same ability to transactivate p21 and MDM2 as the wt p53. *The same lysates as used in A were loaded on a protein gel and Western analyzed for p21 and MDM2. The expression levels of p21 and MDM2 were detected using monoclonal antibodies (Oncogene).*

C. The S47 p53 shows compromised apoptotic function after IR.. *H1299 cells (wt-4, S47-8 and A46-8) were treated with γ radiation (6 Gy) and harvested at indicated time points after radiation. Then the cell lysates were subjected to Western analysis.*

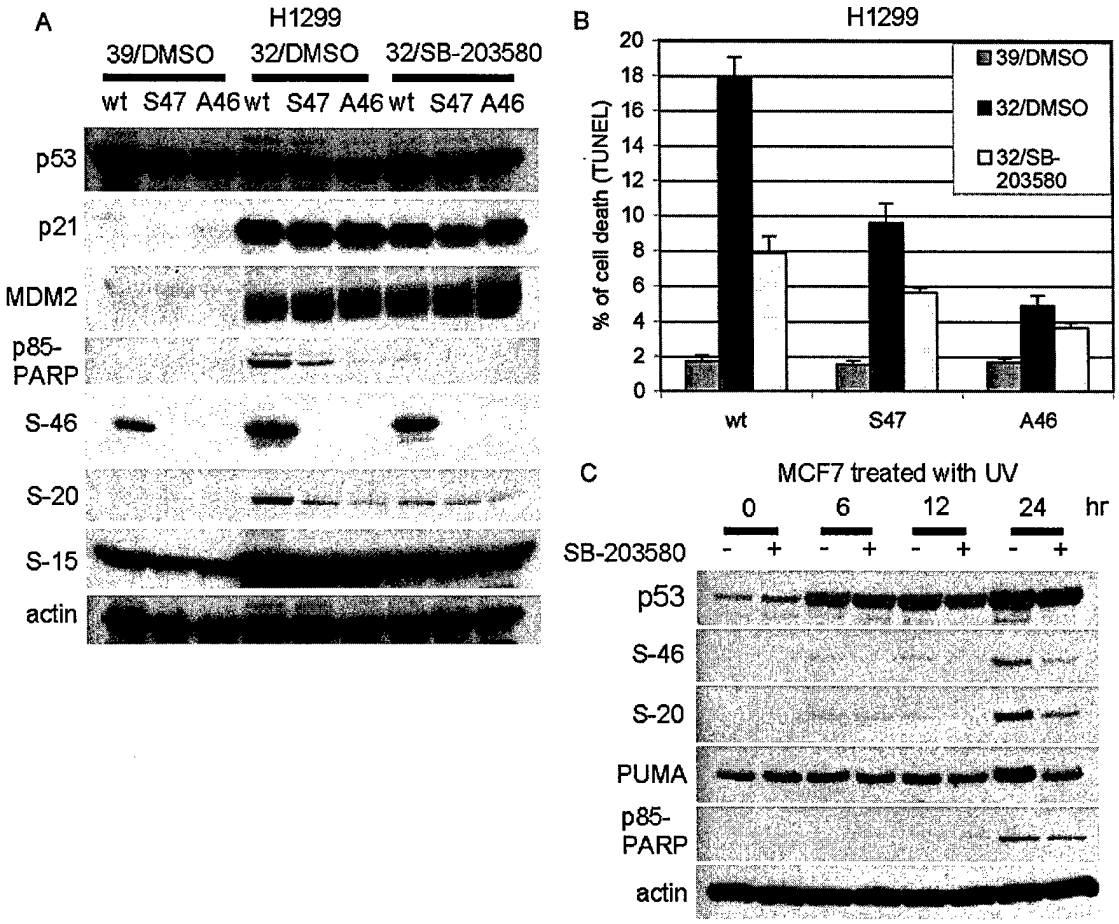

Figure 10. Inhibition of p38 kinase inhibits the phosphorylation of serine 46 and 20 and rescues cells from apoptosis.

A. Inhibition of p38 in H1299 cells inhibits apoptosis and phosphorylation of 46 and 20. *The wt-4, S47-8 and A46-8 clones were incubated with 40 μM of p38 inhibitor SB-203580 (32/SB-203580) or DMSO only (32/DMSO) for 30 min before shifted to 32 ℃. The control cells were maintained at 39 ℃ with DMSO (39/DMSO). Cells were harvested 24 hrs after TS.*

B. TUNEL assay confirms the importance of p38 in the apoptotic ability of p53. *H1299 cells treated as described in figure A were analyzed by TUNEL assay. The bars represents mean±SEM of three independent experiments.*

C. Inhibition of p38 decreases the apoptotic ability and phosphorylation of serine 46 and 20 of endogenous p53. *The breast cancer cell line MCF7 was incubated with 40 μM of p38 inhibitor SB-203580 (+) or DMSO only (-) for 30 min before UV (7.5 J/m^2) treatment. Cells were harvested at indicated time points.*

Inhibition of p38 kinase inhibits the phosphorylation of serine 46 and the apoptotic function of p53

So far, our data clearly show that p38 kinase phosphorylates serine 46 and this phosphorylation is important for the apoptotic function of p53. We then chose to test the phosphorylation of serine 46 and the apoptosis inducing ability of p53 when p38 is inhibited. When we added p38 specific inhibitor SB-203580 to the stably transfected H1299 clones, the phosphorylation of serine 46 was decreased by 2 fold (Fig 10A). The phosphorylation of serine 20, but not serine 15, was also decreased, indicating that phosphorylation of serine 46 may be an upstream event. Not surprisingly, with the presence of SB-203580, the apoptotic ability of both wt and S47 p53 is inhibited, as indicated by both Western analysis (Fig. 10A) and TUNEL assay (Fig. 10B). Consistent with the fact that expression of p21 and MDM2 are not affected by the phosphorylation of serine 46, addition of SB-203580 did not inhibit the expression of p21 and MDM2 (Fig. 10A). To investigate whether inhibition of p38 decreases the phosphorylation of serine 46 and apoptosis in cells with endogenous p53, we conducted experiments on MCF7 cells. The phosphorylation of serine 46 could be detected as early as 6 hrs after UV treatment. When SB-203580 was added, the phosphorylation level of serine 46 was significantly decreased, as was apoptosis (Fig. 10C). The phosphorylation of serine 20 was also decreased (Fig. 10C) as observed in stable H1299 cells. Interestingly, in MCF7 cells, when p38 was inhibited, the expression of the p53 target gene PUMA was also inhibited (Fig. 10C). These data indicate that phosphorylation of serine 46 may be essential for the ability of p53 to transactivate PUMA.

The S47 variant of p53 shows compromised ability to transactivate PUMA

We next examined the mechanism underlying the different apoptotic ability between the wt and S47 p53. Since PUMA has been found to be particularly important in p53-induced apoptosis, we examined whether the S47 p53 has decreased ability to transactivate PUMA. Stable H1299 cells were harvested after temperature shift for p53 induction, and the cell lysates were analyzed by western blot. The S47 p53 shows compromised ability to transactivate PUMA (Fig. 11A). The difference of PUMA expression and apoptosis between wt and S47 clones can be observed as early as 8 hours (Fig. 11A). Luciferase assays using a PUMA reporter construct, containing the PUMA promoter linked to the firefly luciferase gene, confirmed that the wt p53 transactivates the PUMA gene significantly better than the S47 for of p53 (Fig. 11B). However, it remains unclear why the S47 p53 shows compromised transactivation ability to turn on PUMA. Although our results show that the S47 has the same ability to bind to p300 (data not shown), which is a co-activator of p53 (30,31), it may be possible that the S47 p53 has decreased ability to bind to yet unidentified co-activators. The Western analysis of p21 and MDM2 indicates the same general transcriptional ability between wt and S47 p53. Consistently, The Northern analysis shows that the wt and S47 p53 share the same ability to up-regulate Killer/DR5, GADD45, p21 and bax, and down-regulate survivin and cyclin B1 (Fig. 11C).

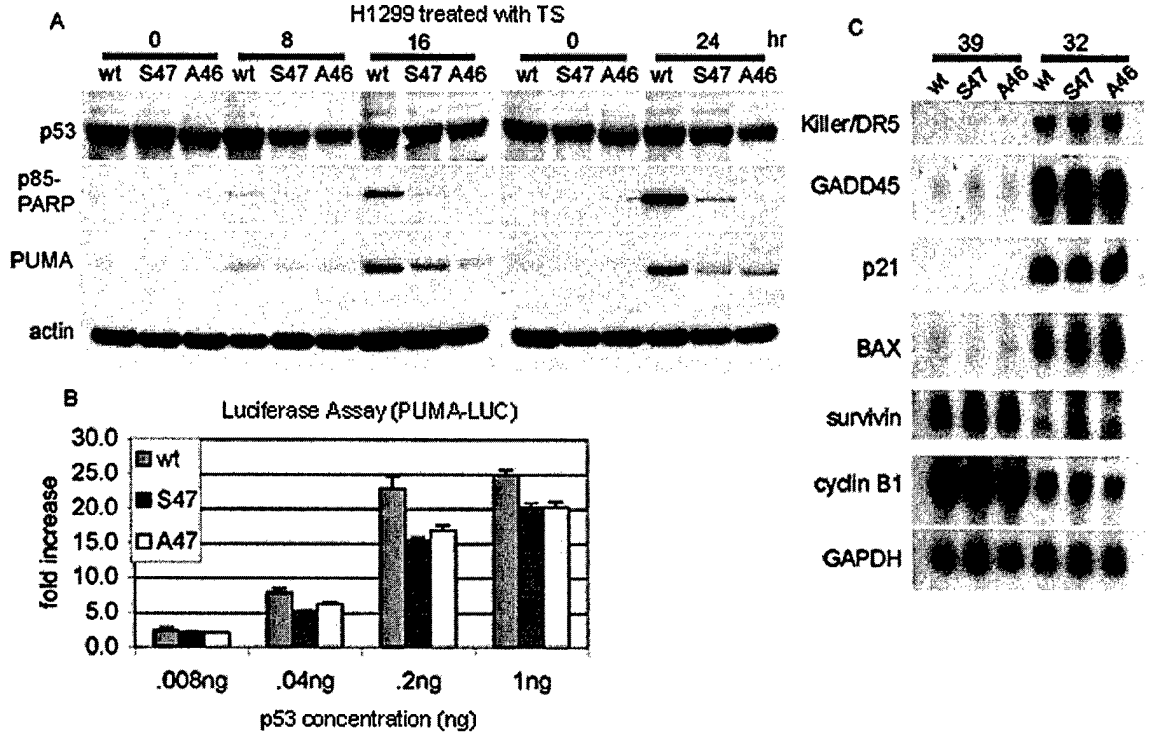

Figure 11. The S47 p53 shows compromised ability to transactivate PUMA.

A. ***The S47 p53 shows compromised ability to transactivate PUMA.*** *The wt-4, S47-8 and A46-8 H1299 clones were shifted to 32 ℃ and harvested at indicated time points after TS. The PUMA was detected using a monoclonal antibody (Oncogene)*

B. ***The S47 p53 shows decreased ability to transactivate PUMA promoter.*** *Different concentrations of wt, S47 and A46 p53 plasmids were co-transfected with luciferase reporter gene with the puma promoter. Luciferase activity was normalized to renilla luciferase activity. The bars represent the mean±SEM of three independent experiments.*

C. ***The S47 variant shows normal general transcriptional ability.*** *H1299 cells (wt-4, S47-8 and A46-8) were harvested 24 hrs after temperature shift. Total RNA was prepared using Trizol (Gibco-BRL). Eight micrograms of total RNA/lane were resolved by denaturing agarose gel electrophoresis and transferred onto a nylon membrane. The membrane was hybridized with probes specifically recognize wanted mRNA.*

B-iv.- Development of a Mouse Model for the Targeted Disruption of the *Appl* Gene in Mammary Gland

Trainee: Huihong You, Ph.D
Mentor: Joseph Testa, Ph.D.
Period reported: August 1, 2003 – to June 30, 2004

Introduction

Like other AKT/protein kinase B (PKB) family members, AKT2 is activated by various growth factors through phosphatidylinositol 3-kinase (PI3K) and thereby mediates signals involved in diverse cellular processes, including apoptosis inhibition, cell proliferation, and insulin signaling. AKT is an integral player in a signal transduction pathway of which many components have been linked to oncogenesis. Activated forms of AKT and its upstream activator, PI3K, are responsible for the transforming activities of certain viruses, and a negative regulator of this pathway, PTEN, is a tumor suppressor.

To facilitate our understanding of the cellular function of AKT2, we had previously used the yeast two-hybrid system to identify two candidate AKT2 partners. Multiple independent isolates of two clones were obtained in a screen of a human fetal brain cDNA library. We have designated one of the putative AKT2 interactors APPL (32). Although a number of important substrates and regulators of AKT/PKB have been identified, our data indicate that APPL is not a substrate but, instead, is an adaptor. To date, APPL is the only adaptor reported to interact with AKT kinases. Moreover, under the conditions tested thus far, this interaction has been strongest with the AKT2 isoform. Since AKT2 appears to play a more prominent role in human neoplasia than other members of the AKT family, the characterization of APPL may provide important insights regarding oncogenic mechanisms involving AKT2.

Recently, APPL(or APPL1, also called DIP13-alpha) has been identified as a Rab5 effector, which resides on a subpopulation of endosomes. APPL1 translocates from the membranes to the nucleus where it interacts with the nucleosome remodeling and histone deacetylase multiprotein complex NuRD/MeCP1 in response to extracellular stimuli (33).

Another study showed that APPL interacts with a region on the cytoplasmic domain of DCC (deleted in colorectal cancer, which is a candidate tumor suppressor gene), which is required for the induction of apoptosis. Co-expression of DCC and DIP13-alpha results in an increase in apoptosis (34).

Apoptosis occurs during normal growth and development of the mammary gland. During involution and remodeling of the breast after lactation, apoptosis is a prominent feature. Most of the secretary epithelium in the lactating breast undergoes apoptosis as the mammary gland regresses and is reorganized for another cycle of lactation. The expression of activated Akt is regulated in this process, such that Akt1 activation peaks in pregnancy and lactation, and decreases during mammary involution (reviewed in reference 35). To provide insights regarding how the loss of *Appl* regulates Akt activation and the normal apoptotic process, and how loss of *Appl* affects mammary development during lactation and involution, we are generating an *Appl* conditional knock-out (KO) mouse model. Since Akt2 and Her2 overexpression or *Pten* deletion play important roles in mammary gland development and mammary tumorigenesis, we propose to elucidate the biochemical significance of Appl in these processes. To address these questions, we intend to cross *Appl* KO mice with MMTV-*Akt*2 or MMTV-*Her*2 transgenic mice, or with *Pten* KO mice.

Body

To date, we have finished Specific Aim 1 and 2. They include: aim1: screen phage libraries derived from 129Sv mouse genomic DNA to identify phage clones containing the *Appl* coding region; and construct a plasmid for gene-targeted disruption of APPL; aim 2: electroporate ES cells with the KO construct and screen the resultant transfected clones for homologous recombination of the gene-targeted construct using Southern blot analysis and PCR.

1) A phage 129Sv mouse genomic library (Stratagene) was screened and clones containing the *Appl* coding region were identified.

Based on the human *APPL* genomic sequence and restriction mapping, we decided to target Exon 5 of the mouse *Appl* gene. We generated a probe specific for Exon 5 of the mouse *Appl* gene, based on mouse EST sequences, and used this probe to screen the library. We identified 5 positive clones, which are about 15.5 kb in length and contain *Appl* genomic sequences that flank exon 2 to 7 or exon 5 to 11.

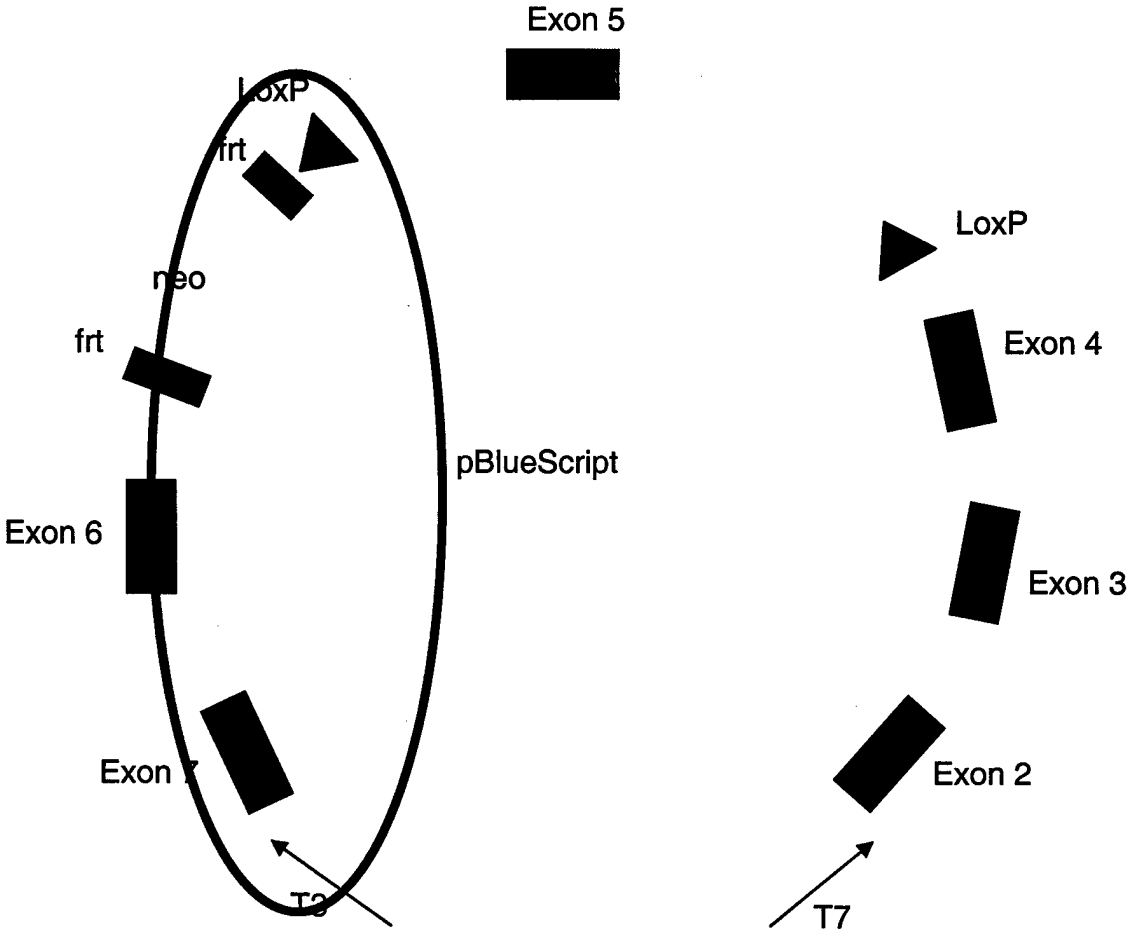

Figure12: KO targeting construct for disruption of Exon 5 of Appl. Processing of the Appl ORF will be disrupted after Exon 4.

2) A construct to conditionally disrupt *Appl* expression/function was synthesized.

The *Appl* gene has 22 exons distributed over ~60 kb. Exon 5 is 88 bp in length and is flanked by two very large introns, which maximize the chance that our engineered cassette will recombine specifically with the *Appl* locus. Disruption of Exon 5 will result in a frame shift in the *Appl* ORF, which is predicted to disrupt endogenous *Appl* gene transcription. We devised a detailed restriction map of the region of interest. With this information, a targeting vector was designed to add one LoxP site upstream of Exon 5 and another LoxP and a selectable neomycin-resistance gene (*neo*) cassette flanked by two FRT sites downstream of Exon 5. Unique restriction fragments have been identified that can distinguish between the wild-type and the LoxP/*neo-Appl* genes by Southern blot and PCR analyses.

Overlapping subclones obtained from the phage genomic library encompass approximately 15.5 kb of sequence. Figure 12 depicts the complete *Appl* KO construct that was constructed for the investigations described. In brief, the 9.3-kb genomic sequence flanking Exon 2 to Exon 7 of mouse *Appl* has been directly excised by restriction enzyme digestion from a subclone derived from a 129Sv mouse genomic library. This 9.3-kb insert was cloned into a pBluescript vector (with mutated KpnI site, XbaI site, SpeI site and BamHI site in its multiple cloning region). An oligo with a LoxP sequence and an EcoRI site has been cloned into the BamHI site of the vector upstream of Exon 5. Another LoxP site with FRT-flanked neo sequence derived from plasmid pK-11/pM-30 (36) has been cloned into the vector downstream of Exon 5, between EcoRV and KpnI sites.

3) Embryonic stem (ES) cell clones containing the conditional *Appl* KO sequence and *Neo* cassette were identified.

We electroporated mouse ES cells with the KO construct and screened the resultant transfected clones for homologous recombination of the gene-targeted construct using Southern blot analysis and PCR and electroporated positively identified gene-targeted ES cells with plasmids, which can express Flp site-specific recombinase to remove the neo selection cassette.

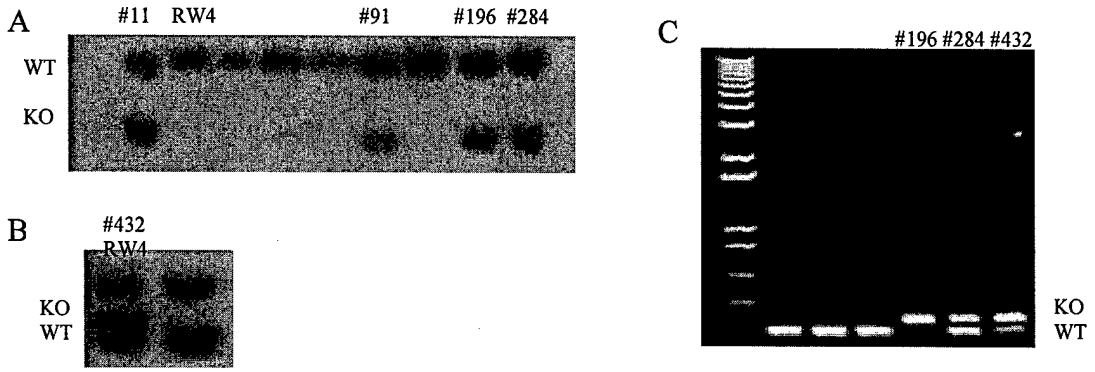

Figure 13. Southern-blot analysis of control and homologous recombined clones after digestion with XbaI (A) or AvaI (B) and hybridization with the 3' (A) or 5'(B) external probe. C: PCR using primers that detect wildtype and loxP containing knockout alleles. WT, wild-type band; KO, knock out band.

a) *ES cell culture and selection:*

A unique XhoI restriction site within the vector itself and near homologous *Appl* intron sequences has been used to linearize the construct prior to transfection of RW4 ES cells. Electroporation and drug selection of ES cells have been performed. Transfected cells were drug-selected (resistance to G418) for 10 days, and then individual stem cell clones were isolated in 24-well plates. Once sufficient cell numbers were obtained, clones were split into two sets of plates (one for freezing of viable cells, the other for generation of DNA). These ES cell clones have been screened for homologous recombination using PCR with specific primers and Southern blot analyses, using restriction enzymes (XbaI for 3' and AvaI for 5') that yield fragments of a predicted molecular weight and genomic probes flanking the targeting sequence. Both 5' and 3' probes and *Neo* probe have been used in order to confirm double homologous recombination and *Neo* insertion. 791 ES cell clones have been screened, and 9 of them were identified as positive homologous recombined clones in this targeting strategy (Figure 13).

b). Karyotyping positive ES clones

After identified the homologous recombined clones, we karyotyped 3 of them in the Cytogenetics Research Facility at Fox Chase Cancer Center (Table1).

Table 1. Karyotype of positive ES clones

Clone number	Normal diploid cells	Abnormal cells
196	18	2
284	19	1
432	19	1

c). Removal of Exon 5 with an adenoviral Cre expression vector:

To test for positive homologous recombination resulting in Exon 5 deletion of *Appl,* clone 284 was infected with an adenoviral Cre expression vector. After infection, 30 clones were picked and screened by PCR and sequencing. One clone was identified that had a deletion of Exon 5 (Figure 14).

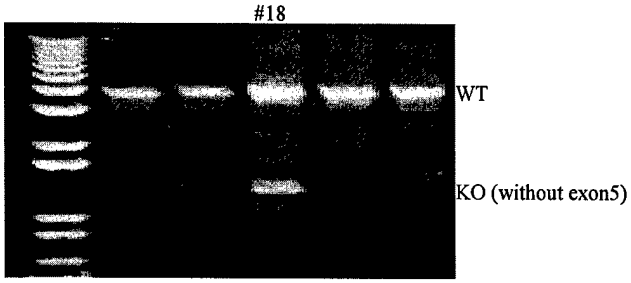

Figure 14. PCR screening Ad-Cre virus infected clones using primers that detect wildtype and knockout alleles. WT, wild-type band; KO, knock out band (without exon5).

d). Removal of the neo selection cassette:

We transiently transfected 2 clones (clone 284 and 432) by electroporating plasmids that express Flp site-specific recombinase in order to remove the Neo selection cassette. After transfection, we used one half of the cells for drug selection to identify clones lacking the Neo cassette. ES clones that are sensitive to G418 were identified and expanded for freezing and screening using Southern blot analysis and PCR. About 1300 clones were picked and drug (G418) selected in two rounds of electroporations, but none of the *Neo*-minus clones retained both loxP sites.

4) Derive mice for future KO studies and breed chimeric mice to obtain germline transmission and mice heterozygous or homozygous for LoxP incorporated *Appl* alleles.

To date, we have injected 3 positive ES clones into 129 mouse blastocysts. Chimeric mice have been obtained and are being mated with B6 female mice. PCR/southern blotting will be used for genotyping of agouti offspring, using mouse tail DNA to see if there is germline transmission of the conditional KO *Appl* sequence.

B-v- **Cloning of a new gene/s in chromosome 17p13.2-13.1 that control apoptosis**

Trainee: Sandra Fernandez, Ph.D *
Mentor: Jose Russo, MD

Period reported: August 1, 2003 – to June 30, 2004

*** The results described below are representing the final report of Dr S. Fernandez. Her training period started on July 1 of 2002 and is ending on June 30, 2004.**

Introduction

Breast cancer is a hormone dependent malignancy whose incidence is steadily increasing in most western societies and in countries that are becoming industrialized (37-41). In United States, breast cancer is the second to lung cancer as a cause of cancer-related deaths (37). Apoptosis (programmed cell death) is a cell suicide process that plays important roles in multiple facets of normal development and physiology (42). Deregulation of apoptosis has been correlated with degenerative diseases, autoimmune disorders and cancer. Apoptosis is caused by caspases, a family of cystein proteases that cleave target proteins at aspartyl residues (43). New studies of the biochemical mechanisms evoked by conventional treatments for neoplastic diseases point to apoptosis as a key process for elimination of unwanted cells (44). Impaired function of apoptosis-related genes is deeply involved in oncogenesis and the progression of cancers (44-48). Our laboratory has recently found a link between apoptosis in chemically transformed human breast epithelial cells and a gene/s located in chromosome 17p13.2 (49), making necessary to identify genes that may regulate apoptosis (50-55). For this purpose we have proposed **to isolate in the precise location in chromosome 17p13.2-p13.1 the gene (s) responsible for the control of apoptosis and to determine the functional role of the isolated gene in the process of neoplastic progression in vivo.**

Body

i- The experimental system.

We have developed an *in vitro* system in which the environmental carcinogen benz(a)pyrene (BP) has been utilized for inducing the transformation of human breast epithelial cells (HBEC) (56-59). For developing this paradigm of human breast cancer, we have capitalized in the availability of the mortal HBEC-MCF-10M or Sample #130, which without viral infection, cellular oncogene transfection, or exposure to carcinogens or radiation became spontaneously immortalized, originating the cell line MCF-10F (60-61). Treatment of MCF-10F cells with chemical carcinogens responded to *in vitro* treatment with BP with the expression of all the phenotypes indicative of neoplastic transformation. BP-treated MCF- 10F cells expressed increased survival and formation of colonies in agar methocel, loss of ductulogenic properties in collagen matrix, invasiveness in a Matrigel *in vitro* system (clones BP-l) and tumorigenesis in severe combined immunodeficient (SCID) mice (BPI-E) (56,59,62).

ii-Background

Because chromosome 17 was involved in both the early and late stages of carcinogenesis we selected it for testing their functional roles in chemically transformed HBEC using a microcell-mediated chromosome transfer (MMCT) technique (63-66). Our study found that seven out of ten clones with

chromosome 17 transferred in to BP1E cells had reverted transformed phenotypes such as advantageous in growth, colony formation in agar-methocel, loss of ductulogenesis and resistant to apoptosis (49). All together the data indicate that 17p13.2 near the marker D17S796 contains one or more gene/s controlling the transformation phenotypes. Allelic imbalance in chromosome 17p13.2 at the microsatellite marker D17S796 has been identified in hepatocellular carcinoma (67) and atypical ductal hyperplasia and in situ ductal carcinoma of breast (68,69).

Microcell-mediated transfer of a human chromosome 17 into BP1E showed a restoration of the lost material in BP1E-17 neo. In the last progress report we suggested the presence of a gene/s that are related to the transformed phenotype in 17p13.2 near the marker D17S796 and a 940 bp of this region was amplified and cloned. Sequences analyzes has shown that cells with transformation phenotype BP1E have lost 10-12 bases consisting in a TG repetition. There is no gene already described in this region although, RT-PCR experiments shown that this region was expressed in MCF-10F, BP1E and BP1E-17 neo. Also we found that the expressed-sequence tag EST 3179739 matches a region that lays 120 bp downstream of the cloned region. The EST 3179739 sequence comes from a cDNA library from lung (tissue type: carcinoid). A 99% identity was found between both sequences using Blast (www.ncbi.nlm.nih.gov/blast/Blast.cgi). The predicted amino acid sequence does not share significant homology with any known protein supporting the idea that this could be a novel protein. In order to cloned the full-length cDNA of this gene, rapid amplification of cDNA ends (RACE) were performed. RACE is a procedure for obtaining full-length cDNA copies of low abundance mRNAs. Although, different cDNAs were obtained, none of them were specific to this region (17p13.2). Furthermore, based on these results we have pursued (i) a detailed analysis using different microsatellite markers lying near D17S796, (ii) studies on the expression of different genes near the marker D17S796 and (iii) assays to measure the functional role of them by determining the apoptotic activity of MCF-10F, BP1E and BP1E-17neo cells after been challenged by an apoptotic inducing agent.

iii- Results.

Karyotype and CGH analysis. The cytogenetic characterization of the human breast cell lines MCF-10F, BP1E and BP1E-17neo were performed using a combination of the standard G-banding and CGH analysis (Figure 15). All the cell lines had extra genetic material on chromosome 1 at band p34 and they presented a balanced translocation between chromosome 3 and chromosome 9 t (3; 9) (p13; p21). The CGH analysis helped to identify the extra genetic material on chromosome arm 1p34 to be from 8q24.

The modal number of chromosomes of the control cell line MCF-10F was 46 and for BP1E transformed cell line was 47. BP1E had an additional isochromosome 10q (Figure 15). DNA losses were not observed in BP1E cell line using CGH. The modal chromosome number for BP1E-17neo was 48. BP1E-17neo has the same chromosomal abnormalities observed in BP1E and in addition has an extra copy of chromosomes 17 (Figure 15). It shows the same gain of chromosome 10q as seen in BP1E. The extra copy of chromosome 17, probably the one that was microinjected appears to be rearranged and it was composed of most of the p arm and a portion of 17q22-ter (Figure 15).

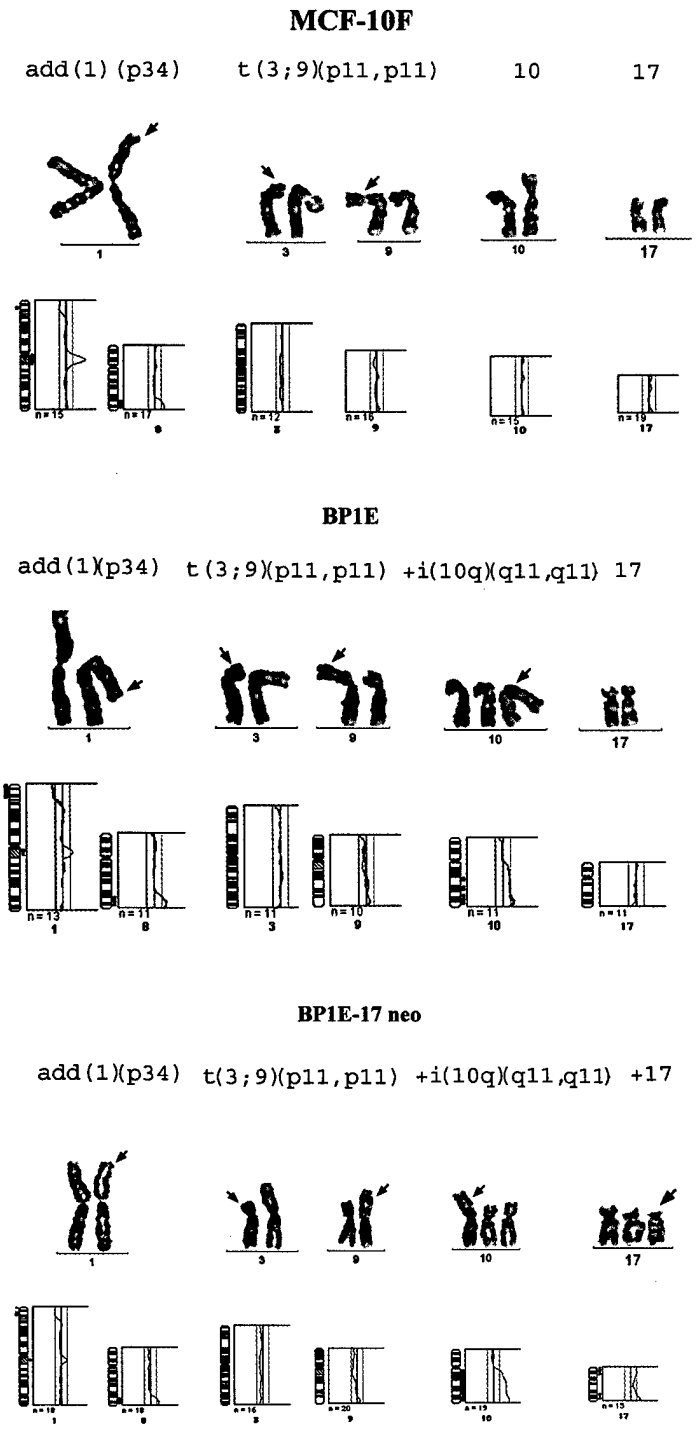

Figure 15. Karyotyping and CGH analysis of MCF-10F, BP1E and BP1E-17neo cells. *The main differences found in the G-banding and CGH analyses are included. In the three cell lines, the arrow on chromosome 1 shows the extra material at 1p34 present in the three cell lines. The arrows on chromosome 3 and chromosome 9 indicated the translocated regions between these chromosomes. The isochromosomes 10 present in BP1E and BP1E-17neo are indicated. The extra chromosome 17 present only in BP1E-17neo is also indicated. Vertical green lines on the right of each chromosome in the CGH analysis represent gains, whereas red vertical lines on the left indicate loss of genetic material.*

Microsatellite analysis. Microsatellite analysis was performed using 25 markers for chromosome 17 lying near D17S796 (Table 2). No differences were found between MCF10F, BP1E and BP1E-17neo. The PCR products obtained using the marker D17S796 were analyzed using capillary electrophoresis (Figure 2) and the only difference between the three cell lines were found with this marker located at 17p13.2 confirming our previous results (Figure 16). BP1E showed allelic imbalance in 17p13.2 using the marker D17S796, whereas, BP1E-17neo showed a pattern similar to

Table 2. Markers used for microsatellite studies

Marker	Primer Reverse (5′ 3′)	Primers Forward (5′ 3′)	Repeat	Location
D17S926	CCGCAGAAGGCTGTTGT	GCAGTGGGCCATCATCA	dinucleotide	17p13.3
D17S1840	TGGGGCAGACTTGGTCCTT	GCCTGGGCGACAGAGTGA	dinucleotide	17p13.3
D17S1528	CAGAGGTGGAGATAAGGG	AGTAGCCAGGAGGTCAAG	dinucleotide	17p13.3
D17S831	GCCAGACGGGACTTGAATTA	CGCCTTTCCTCATACTCCAG	dinucleotide	17p13.3
D17S1810	CCTAGTGAGGGCATGAAAC	TGTCCACTGTAACCCCTG	dinucleotide	17p13.3
D17S1832	TGTGTGACTGTTCAGCCTC	ACGCCTTGACATAGTTGC	dinucleotide	17p13.3
D17S938	ATGCTGCCTCTCCCTACTTA	GGACAGAACATGGTTAAATAGC	dinucleotide	17p13.2
D17S796	AGTCCGATAATGCCAGGATG	CAATGGAACCAAATGTGGTC	dinucleotide	17p13.2
D17S260	CTCCCCAACATGCTTTCTCT	AATGGCTCCAAAAGGAGATATTG	mononucl.	17p13.2
D17S919	GCTTAATTTTCACGAGGTTCAG	AGGCACAGAGTGAGACTTG	tetranucl.	17p13.2
D17S906	TTCTAGCAGAGTGAAACTGTCT	AGCAAGATTCTGTCAAAAGAG	tetranucl.	17p13.2
D17S1149	CGCTGATCTGTCAGGCAGCCCT	AACAAGAGTGAACTCCATAGAGAG	tetranucl.	17p13.2
D17S720	GAATTCTGAGCATATTGTTTGCCTG	CCAGCCTTGGCAACATAGCAAGA	tetranucl.	17p13.2
D17S731	TTTCTGGGGAAATTTTCTTGCTCTTA	CAACCCCAAGGTAACAACATCCAG	trinucleotide	17p13.2
D17S578	CTGGAGTTGAGACTAGCCT	CTATCAATAAGCATTGGCCT	dinucleotide	17p13.2
D17S960	TAGCGACTCTTCTGGCA	TGATGCATATACATGCGTG	dinucleotide	17p13.2
D17S1881	TAGGGCAGTCAGCCTTGTG	CCCAGTTTAAGGAGTTTGGC	dinucleotide	17p13.2
D17S1353	TACTATTCAGCCCGAGGTGC	CTGAGGCACGAGAATTGCAC	dinucleotide	17p13.2
TP53 penta	ACTCCAGCCTGGGCAATAAGAGCT	ACAAAACATCCCCTACCAAACAGC	pentanucl.	17p13.1
TP53 dint	ATCTACAGTCCCCCTTGCCG	GCAACTGACCGTGCAAGTCA	dinucleotide	17p13.1
D17S855	ACACAGACTTGTCCTACTGCC	GGATGGCCTTTTAGAAAGTGG	dinucleotide	17q21.2
D17S579	CAGTTTCATACCAAGTTCCT	AGTCCTGTAGACAAAACCTG	dinucleotide	17q21.31
D17S250	GCTGGCCATATATATATTTAAACC	GGAAGAATCAAATAGACAAT	dinucleotide	17q12
THRA1	CTGCGCTTTGCACTATTGGG	CGGGCAGCATAGCATTGCCT	dinucleotide	17q11.2
GH	TCCAGCCTCGGAGACAGAAT	AGTCCTTTCTCCAGAGCAGGT		17q22.24

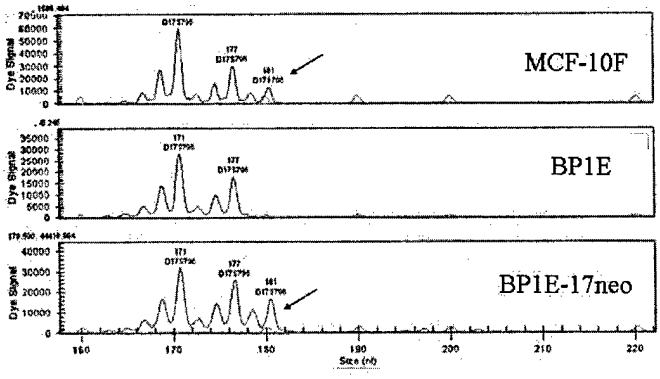

Figure 16. Microsatellite studies with D17S796 marker using capillary electrophoresis.

Growth rates. The doubling time for the different cell lines were study as another parameter of cell transformation. BP1E-17neo grew at slower rate compared with the transformed cell line BP1E (Figure 17). The doubling time for BP1E-17neo was 24h, 1.5-fold longer than the BP1E cell that has a doubling time of 16h and similar to MCF-10F that was 24.6h.

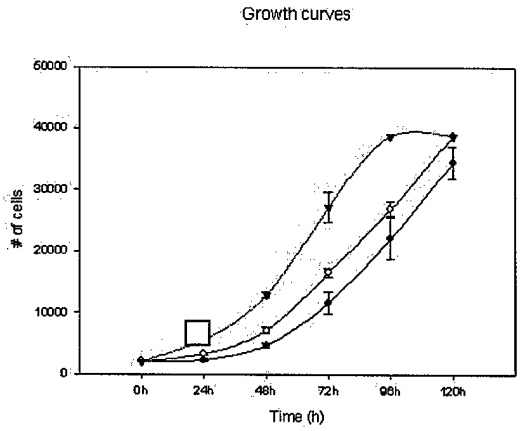

Figure 17. Comparative growth rates in vitro among MCF-10F, BP1E and BP1E-17neo cells. The doubling time, estimated from the growth curves, was significantly higher for BP1E-17neo (24) than for BP1E (16h). The doubling time for BP1E-17neo was similar to MCF10F (24.6h).

Figure 3

Analysis of the expression of DEFCAP and TP53 by RT-PCR. We have found that marker D17S796 is approximately at 1.1cM downstream of the DEFCAP gene (death effector filament-forming Ced-4-like apoptosis protein) and 1.3 cM upstream of the tumor suppressor gene TP53. DEFCAP has two isoforms, DEFCAP-L and DEFCAP-S and they differ in only 44 amino acids (70). We study TP53 and DEFCAP expression in the three cell lines by RT-PCR using the primers indicated in Table 3. We found that DEFCAP-L was downregulated in BP1E compared with MCF-10F and was overexpressed in BP1E-17neo (Figure 18). No differences were found in TP53 expression between the three cell lines (Figure 18).

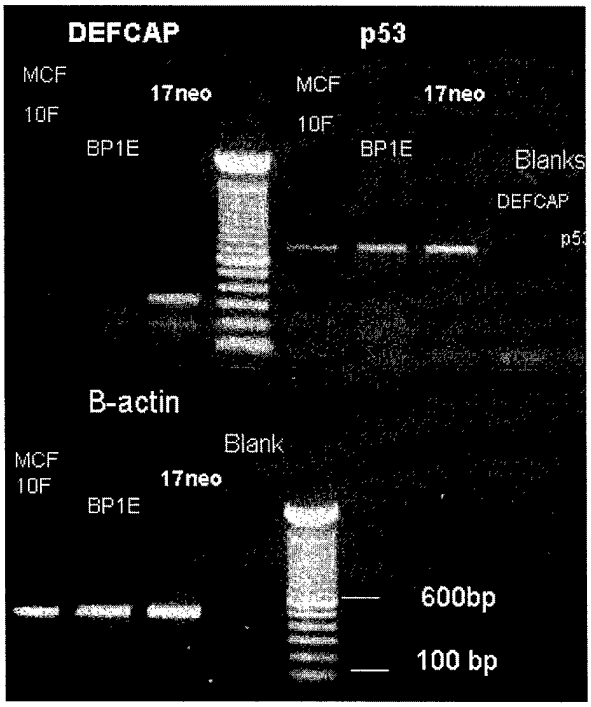

Figure 18. RT-PCR of DEFCAP and TP53 in the different cell lines. *RT-PCR using total RNA from MCF-10F, BP1E and BP1E-17 neo cells. B-actin was used as a control for equal RNA quantity used in the reactions..*

Table 3. Primers used for RT-PCR

Gene	Reverse Primer (5′to 3′)	Forward Primer (5′ to 3′)	Size (bp)
DEFCAP	TCCCCCTTGGGAGTCCTCCTGAAAATGATC	CGAGAACAGCTGGTCTTCTCCAGGGCTTCG	322 and 190
p53	TTCTTGCATTCTGGGACAGCC	GCCTCATTCAGCTCTCGGAAC	703
β-actin	GGGAAATCGTGCGTGACATTAAGG	CTAGAAGCATTTGCGGTGGACGATGGAGGGGCC	520

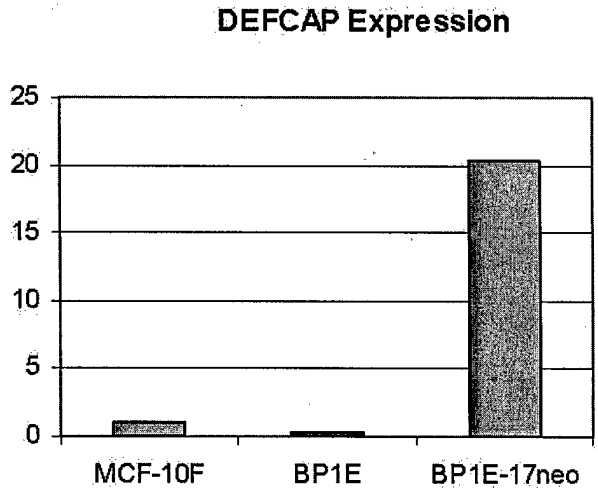

Figure 19: *Quantitation of DEFCAP expression using Real Time RT-PCR in MCF-10F, BP1E and BP1E-17 neo..*

Figure 5

Analysis of the expression of DEFCAP by Real time RT-PCR. We have used real time RT-PCR to quantify the levels of DEFCAP mRNA in MCF-10F, BP1E and BP1E-17neo cells. We found that the expression of DEFCAP in BP1E is 0.4 times less than MCF10F cells, whereas in BP1E- 17neo cells was 20 folds increased (Figure 19). Interestingly DEFCAP expression was significantly low in breast adenocarcinoma when compared with their normal counterpart (Figure 20).

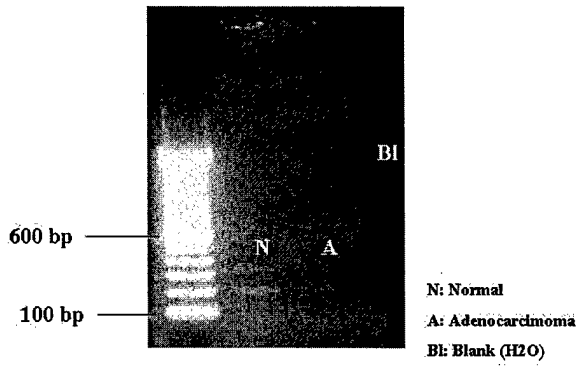

Figure 7.

Figure 20. DEFCAP expression in breast. *RT-PCR of DEFCAP in human normal breast and adenocarcinoma*

Apoptosis. The finding that DEFCAP is a gene controlling apoptosis led us to determine if the level of expression was associated with this function. For this purpose we have studied apoptosis in BP1E and BP1E-17neo using Guava Nexin procedure (Guava Technologies Inc.). This assay utilizes Annexin V –PE to detect phosphatidylserine on the external membrane of apoptotic cells. Annexin V is a calcium dependent phospolipid binding protein with a high affinity for phosphatidylserine (PS), a membrane component normally localized to the internal face of the cell membrane.

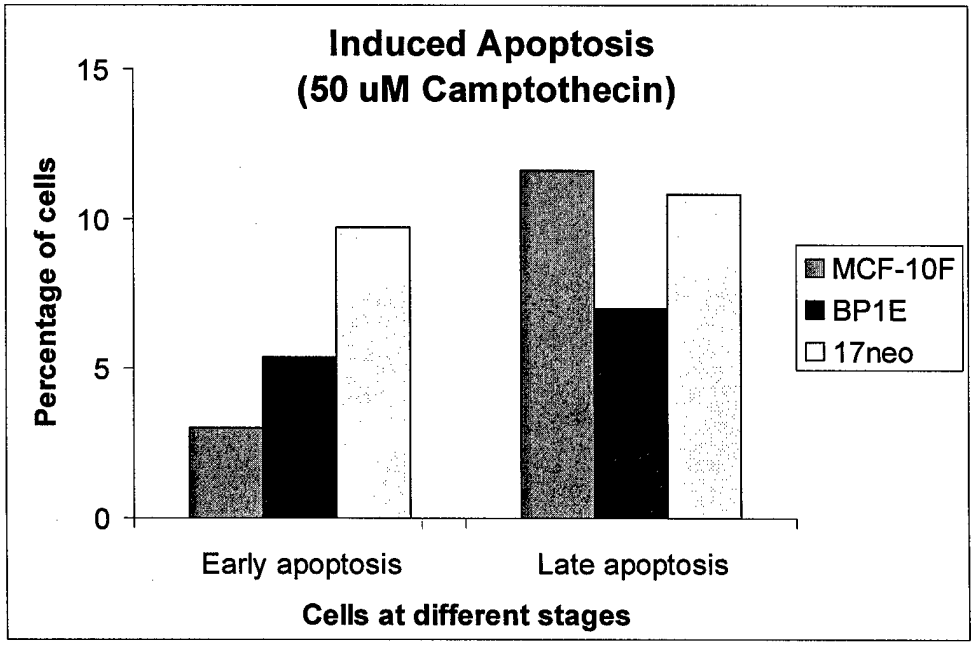

Figure 21. *Apoptosis assay. The cell lines were treated with 50μM Camptothecin for 24h to induce apoptosis. More apoptotic BP1E-17neo cells were observed in early apoptosis.*

Early in apoptosis, PS is translocated to the outer surface of the cell membrane where Annexin V can bind them. Apoptosis was induced using 50 μM Camptothecin and the cells were treated during 20 hs. Differences in early and late apoptosis were found between BP1E and BP1E-17 neo (Figure 21).

.iv-Next proposed Plan of research

Based on the data generated during this training grant we are preparing an RO1 application to NIH for studying further the role of this genes in breast cancer. This plan of study:

a-We will further our understanding in the functional role of DEFCAP by treating the three cell lines under investigation with the apoptotic agent Camptothecin during 6h, 12h, 24h, 36h and 48h. Northern blots and RT-PCR experiments will be performed to study DEFCAP expression. We expect that DEFCAP expression will increase during apoptosis in MCF10F and BP1E-17neo but not in BP1E cells.

b-DEFCAP siRNA experiments will be performed using MCF-10F to check if the silencing of this gene affects the normal phenotype of this cell line. We expect a change in the phenotype of this cell line to a transformed phenotype similar to BP1E.

c-BP1E will be transfected with a plasmid harboring DEFCAP and it is expected that the over-expression of this gene in this cell will revert the transformed phenotype.

d-We will determine if the DEFCAP protein expression follows the same pattern in primary breast cancer than in the neoplastically transformed cells in vitro.

C- KEY RESEARCH ACCOMPLISHMENTS.

C-i- ***Predisposition to genomic instability in breast cancer: Analysis of molecular mechanisms.***

a-Recent work has emphasized the dual activity of centrosomes in contributing to control of cell polarization in interphase cell migration but also in coordinating polarity of the mitotic spindle in M-phase. Centrosomally-associated signaling activities also govern the timing of mitotic Entry.

b-Our work on HEF1 is the first and only study that has clearly indicated an important function of the Cas proteins in profound changes in physical organization during mitosis. We have shown HEF1 is localized to the centrosome throughout cell cycle, but increased significantly at G2/M boundary. Over-expression of full length HEF1 causes the amplification of centrosomes and as a consequence, multipolar spindle formation. Depletion of HEF1 using siRNA approach resulted in premature splitting of the centrioles and malformed spindles. HEF1 is a potential Aurora1 substrate. HEF1 directly interact with Aurora and Ajuba might be involved in Aurora1 activation during mitosis onset. Serine rich region of HEF1 is important for localization to the centrosome.

c-Defects in the integrity of cellular division at mitosis are important predisposing factors to breast cancer, as reflected by the defects in ploidy and over-duplication of centrosomes in many primary breast cancers.

C-ii- ***The codon 47 polymorphism of p53 is functionally significant. By: Xiaoxian Li, Ph.D.***

a-The S47 variant shows significantly decreased phosphorylation of serine 46.

b-The phosphorylation of serine 46 is an upstream event and affects the phosphorylation level of serine 20.

c-The S47 variant shows compromised apoptotic ability.

d-The p38 kinase is a key player in the phosphorylation of serine 46 by interaction with proline 47. When p38 is inhibited, the phosphorylation of serine 46 is inhibited, as well as are the serine 20 and the apoptotic ability of p53.

e-The S47 variant has compromised apoptotic ability because it possesses decreased ability to transactivate PUMA.

C-iii- ***Development of a Mouse Model for the Targeted Disruption of the Appl Gene in Mammary Gland.***

a-We have isolated and characterized genomic fragments of Appl from a phage 129Sv mouse genomic library. A 9.3-kb sequence, flanking exon 2 to exon 7 of Appl, was used to generate a targeting construct containing LoxP sites and neomycin resistance sequence.

b-We are using this homologous construct to electroporate embryonic stem cells that will be selected for resistance to G418 and homologous recombination of the targeting construct.

C-iv- ***Cloning of a new gene/s in chromosome 17p13.2-13.1 that control apoptosis***

a-DEFCAP gene (death effector filament-forming Ced-4-like apoptosis protein) is approximately at 1.1cM downstream of the marker D17S796.

b-DEFCAP also known as NALP1, NAC or CARD7, and it was the first NALP-family protein to be identified on the basis of its sequence homology to APAF-1 (70-73) is down-regulated in BP1E cells and overexpressed in BP1E-neo cells in comparison with MCF10F cells.

c-DEFCAP expression is associated with apoptosis and the abrogation of the neoplastic phenotype. In addition this could be relevant to the human disease since primary breast cancer has lower level of expression of this gene.

d-p53 a gene close to D17S796 is not affected during the neoplastic transformation and is not modified when Ch. 17 was transferred to the transformed cells.

D- REPORTABLE OUTCOMES

1. Pugacheva, E., Golemis, E. The scaffolding protein HEF1 regulates the centrosome division cycle and M-phase progression. Proc. American Society for Cell Biology, Abstract 1847. December 14-18th, 2002. San Francisco, CA.

2. Pugacheva, E. and Golemis, E. Deregulation of HEF 1 expression in breast cancer cells cause severe defects in centrosome and spindle dynamics. Fox Chase Cancer Center Postdoctoral Day, 6 June 2003, Philadelphia, PA (Poster presentation)

3. Pugacheva, E., Serebriisskii , I.G., Finley, R.J. and Golemis, E. Dissection of HEF 1 fubction by aptamer peptides. American Society for Cell Biology Abstract 935. December 14-18th,2003. San Francisco, CA.

4. Serebriiskii, I.G., Mitina, O., Pugacheva, E., Benevolenskaya, E., Kotova, E., Toby, G.G., Khazak, V., Kaelin, W.G., Chernoff, J., and Golemis, E.A. Detection of peptides, proteins, and drugs that selectively interact with protein targets. Genome Res 12: 1785-1791, 2002.

5. Pugacheva, E.N., Longmore, G.D. and Golemis, E. HEF1 regulates chromosomal maturation and spindle formation through control of the Aurora-A kinase. Manuscript in preparation.

6.Li, X., Dumont P., Della Pietra A. and Murphy M. The codon 47 polymorphic variant of p53 is associated with altered phosphorylation pattern and decreased apoptosis. (In Preparation)

7- You, H. and Testa, J.R. Involvement of Akt in vitamin E succinate-induced apoptosis. Graduate and Postdoctoral Day at the Fox Chase Cancer Center. Philadelphia, PA.2004

8- Fernandez, S.V., Lareef, M.H.., Russo, I.H., Balsara, B.B., Testa, J. and Russo, J. Role of 17p13.2 in the neoplastic transformation of human breast epithelial; cells. Proc. Am. Assoc. Cancer Res. 2004.

9- Lareef, M., Fernandez, S.V., Russo, I.H., Balsara, B. and Russo, J. Role of 17p13.2 in the neoplastic transformation of human breast epithelial cells. Submitted for Publication.

E- CONCLUSIONS AND SIGNIFICANCE:

i-The phenotypes we have observed in cells over expressed or depleted of HEF1 is exactly coincident with the cells similarly manipulated for AuroraA kinase or Nek2 kinase and it downstream partner cNAP1. Based on preliminary date we proposed that HEF1 could be a cohesion factor in the centrosome of epithelial cells and play the same role as c-NAP1 in the fibroblast (HEF1 is not expressing in the fibroblasts), i.e., preventing centriolar separation. Alternatively, it could work as activator of Aurora A kinase, bringing his partner Ajuba in complex with Aurora A. In our model, over expression of HEF1 keeps centrioles together and supports over-duplication, but depletion of HEF1 causes centriolar splitting and defects in spindle formation. The regulatory mechanism for the disassociation of HEF1 protein from the centrosome could be phosphorylation of HEF1 by the active Aurora A kinase during earlier stages of cell cycle progression. Our data for the first time suggest an additional model for the function of the Cas proteins in cancer, wherein defective signaling through HEF1 or p130Cas promotes genomic instability, allowing rapid selection for other genetic changes associated with cancer progression, including increased tendency to drug resistance.

ii-Our results clearly show that the proline 47 polymorphic variant is functionally significant, and has impaired ability to induce programmed cell death relative to wild type p53. In the S47 variant, the phosphorylation of serine 46 is decreased by 2 fold. Importantly, the S47 variant has 2-3 fold compromised apoptotic function in both H1299 and Saos2 cells. The phosphorylation of serine 46 does not affect the phosphorylation on other sites except for serine 20. Although our data indicate the phosphorylation level of serine 46 is more important in the apoptotic ability of p53, it remains unclear how much the phosphorylation of serine 20 contributes to the apoptotic function of p53. Consistent with other reports, our results show p38 kinase plays an indispensable role in the

phosphorylation of serine 46. Inhibition of p38 results in a 2-fold deduction of the phosphorylation of serine 46 and 2-fold decreased apoptotic ability of p53. The important role of p38 kinase in phosphorylating serine 46 was confirmed in MCF7 cells with endogenous p53. The S47 p53 shows compromised apoptotic ability because it does not up-regulate PUMA as well as wild type p53. Our observation of the compromised apoptotic ability of S47 p53 may indicate that cancer patients with this variant have worse prognosis upon chemo- or radio-therapy. Thus it may be worthwhile to screen cancer patients at codon 47 of p53 before choosing regime. Significantly, 3 to 5% of African Americans have germline S47 p53. It would be interesting to test whether these people have high risk of developing cancers. Since phosphorylation of S46 is relatively newly shown to be important in apoptosis, not much work has been done to evaluate its role in breast cancer. However, because of the important role of p53 in breast cancer, we would predict patients with decreased phosphorylation of codon 46 of p53 would have worse prognosis. The phosphorylation level of codon 46 may be useful in predicting the progression and outcome of breast cancer. We will focus on finding out whether other pro-apoptotic p53 target genes are affected by the S47 polymorphism. Specifically, micro-array analysis will be performed to screen out the sub-set of apoptotic genes which are less up-regulated by the S47 p53. Chromatin immuno-precipitation is being conducted to test whether wt p53 binds better to the PUMA promoter than the S47 variant. We will also establish breast cancer cell lines to directly confirm the difference of apoptotic ability between wt and S47 p53 in breast cancer cells.

iii- A 9.3-kb DNA genomic sequence, flanking exon 2 to exon 7 of Appl, was isolated and characterized, and was used to generate a targeting construct containing LoxP sites and neomycin resistance sequence. In order to understand the significance of the Appl during cellular processes and the potential interaction with other signaling molecules such as AKT2, it is important to analyze this gene in the context of a living animal. In particular, the generation of Appl mice with targeted disruption of Appl in the mammary gland will elucidate the role of Appl in mammary development. Mating Appl mice with other mouse models of breast cancer will reveal the potential of Appl in contributing to breast tumorigenesis. We will breed chimeric mice to obtain mice heterozygous and homozygous for LoxP incorporated *Appl* alleles. We will breed these mice with MMTV-Cre or WAP-Cre transgenic mice to disrupt the *Appl* gene in mammary gland, delineate the phenotype of *Appl*-targeted disruption in the mammary gland, and elucidate the function of Appl in breast development and during mammary involution. These studies may provide insights regarding *in vivo* mammary-specific apoptotic signaling and potential targets for therapeutic intervention. We also intend to breed floxed *Appl* mice to EIIa-Cre transgenic mice to generate mice with *Appl* deleted during embryogenesis. If disrupting the *Appl* gene during embryogenesis is not lethal, we will breed these mice with *Akt2* KO mice (previously generated by Dr. D. Altomare in our laboratory) to further delineate the role of Appl in mammary gland development, or with *Pten* KO mice (available from our collaborator, Dr. A. Cristofano), MMTV-Akt2, or MMTV-Her2 transgenic mice to study the function of Appl in mammary tumorigenesis. Previous data from our laboratory showed that Akt plays a critical role in mammary gland involution. By breeding *Appl* KO mice with MMTV-*Akt2* transgenic mice or with *Akt2* KO mice, we will determine if Appl can regulate Akt2 function in normal mammary gland development, especially during lactation and involution. About 60% of *Pten*-deficient mice develop breast cancer by 10 months (A. Di Cristofano, personal communication). By breeding *Pten* KO mice or MMTV-*Her2* transgenic mice with *Appl* KO mice, we will be able to investigate whether Appl deficiency can alter the incidence, size, or aggressiveness of mammary tumors. In order to unravel the full spectrum of *Appl* function, it is important to analyze this gene in the context of a living animal. The use of *Appl* conditional KO mice will complement our laboratory's ongoing *in vitro* studies. Gene inactivation through homologous recombination is an unambiguous means to target *Appl,* thereby eliminating its function and establishing a phenotype for Appl loss-of-function. The resulting *Appl* KO mice will be interbred with WAP-Cre or MMTV-Cre

transgenic mice, EIIa-Cre transgenic mice, and other transgenic or knockout mice with genetic defects in the Akt signaling pathway to determine if Appl has an important physiological function in mammary gland development and mammary tumorigenesis.

iv-All together the data indicate that 17p13.2 near the marker D17S796 contains the DEFCAP gene that when inactivated is associated with the expression of cell transformation phenotypes, and that *in vitro* condition are expressed as increase doubling time, colony formation in semisolid media, loss of the ability to from ductules in collagen matrix, loss of the response to apoptosis inducing agent, and *in vivo* has been associated with ductal hyperplasia and carcinoma in situ of the breast (39) that are early stages of breast cancer.

REFERENCES

1. Jiang Y, Zhang Y, Lees E, Seghezzi W. 2003. AuroraA over expression overrides the mitotic spindle checkpoint triggered by nocodazole, a microtubule destabilizer. Oncogene. 2003 Nov 13;22(51):8293-301
2. Sausville EA. Aurora kinases dawn as cancer drug targets. Nat Med. 2004 Mar;10(3):234-5.
3. Hirota T, Kunitoku N, Sasayama T, Marumoto T, Zhang D, Nitta M, Hatakeyama K, Saya H.Aurora-A and an interacting activator, the LIM protein Ajuba, are required for mitotic commitment in human cells. Cell. 2003 Sep 5; 114(5):585-98.
4. Fenteany G, Schreiber SL. Lactacystin, proteasome function, and cell fate. J Biol Chem. 1998 Apr 10;273(15):8545-8.
5. Goyal RK, Lin P, Kanungo J, Payne AS, Muslin AJ, Longmore GD. Ajuba, a novel LIM protein, interacts with Grb2, augments mitogen-activated protein kinase activity in fibroblasts, and promotes meiotic maturation of Xenopus oocytes in a Grb2- and Ras-dependent manner. Mol Cell Biol. 1999 Jun;19(6):4379-89.
6. Law, S. F., J. Estojak, B. Wang, T. Mysliwiec, G. D. Kruh, and E. A. Golemis. 1996. Human Enhancer of Filamentation 1 (HEF1), a novel p130Cas-like docking protein, associates with FAK, and induces pseudohyphal growth in yeast. Mol. Cell. Biol. 16:3327-3337.
7. Bouton, A. H., R. B. Riggins, and P. J. Bruce-Staskal. 2001. Functions of the adapter protein Cas: signal convergence and the determination of cellular responses. Oncogene 20:6448-58.
8. Law SF, O'Neill GM, Fashena SJ, Einarson MB, Golemis EA. The docking protein HEF1 is an apoptotic mediator at focal adhesion sites. Mol Cell Biol. 2000 Jul;20(14):5184-95.
9. Dorssers LC, van Agthoven T, Dekker A, van Agthoven TL, Kok EM. Induction of antiestrogen resistance in human breast cancer cells by random insertional mutagenesis using defective retroviruses: identification of bcar-1, a common integration site. Mol Endocrinol. 1993 Jul;7(7):870-8.
10. Harte MT, Macklem M, Weidow CL, Parsons JT, Bouton AH. Identification of two focal adhesion targeting sequences in the adapter molecule p130(Cas). Biochim Biophys Acta. 2000 Dec 11;1499(1-2):34-48.
11. Ferlay J, Bray F, Pisane P, Parkin DM. 2001. Cancer incidence, mortality and prevalence worldwide. Globocan 2000. IARC Press
12. Malkin D, Li FP, Strong LC, Fraumeni JF Jr, Nelson CE, Kim DH, Kassel J, Gryka MA, Bischoff FZ, Tainsky MA, et al. 1990. Germ line p53 mutations in a familial syndrome of breast cancer, sarcomas, and other neoplasms. Science 250:1233-8.
13. Ho GH, Calvano JE, Bisogna M, Borgen PI, Rosen PP, Tan LK, Van Zee KJ. 2000. In microdissected ductal carcinoma in situ, HER-2/neu amplification, but not p53 mutation, is associated with high nuclear grade and comedo histology. Cancer 89:2153-60..

14. Done SJ, Arneson CR, Ozcelik H, Redston M, Andrulis IL. 2001. P53 protein accumulation in non-invasive lesions surrounding p53 mutation positive invasive breast cancers. Breast Cancer Res Treat 65:111-8.

15. Done SJ, Eskandarian S, Bull S, Redston M, Andrulis IL. 2001. p53 missense mutations in microdissected high-grade ductal carcinoma in situ of the breast. J Natl Cancer Inst. 93:700-4.

16. Norberg T, Klaar S, Karf G, Nordgren H, Holmberg L, Bergh J. 2001. Increased p53 mutation frequency during tumor progression--results from a breast cancer cohort. Cancer Res.61: 8317-21.

17. Borresen-Dale AL. 2003. Genetic profiling of breast cancer: from molecular portraits to clinical utility. Int J Biol Markers.18:54-6.

18. Berns EM, Foekens JA, Vossen R, Look MP, Devilee P, Henzen-Logmans SC, van Staveren IL, van Putten WL, Inganas M, Meijer-van Gelder ME, Cornelisse C, Claassen CJ, Portengen H, Bakker B, Klijn JG. 2000. Complete sequencing of TP53 predicts poor response to systemic therapy of advanced breast cancer. Cancer Res. 60:2155-62.

19. Liu G, Schwartz JA, Brooks SC. 2000. Estrogen receptor protects p53 from deactivation by human double minute-2. Cancer Res.60: 1810-4.

20. Dumont P, Leu JI, Della Pietra AC 3rd, George DL, Murphy M. 2003. The codon 72 polymorphic variants of p53 have markedly different apoptotic potential. Nat Genet. 33:3357-65.

21. Brooks CL and Gu W. 2003. Ubiquitination, phosphorylation and acetylation: the molecular basis for p53 regulation. Curr Opin Cell Biol. 15:164-71.

22. Saito S, Goodarzi AA, Higashimoto Y, Noda Y, Lees-Miller SP, Appella E, Anderson CW. 2002. ATM mediates phosphorylation at multiple p53 sites, including Ser(46), in response to ionizing radiation. J Biol Chem. 277:12491-4.

23. D'Orazi G, Cecchinelli B, Bruno T, Manni I, Higashimoto Y, Saito S, Gostissa M, Coen S, Marchetti A, Del Sal G, Piaggio G, Fanciulli M, Appella E, Soddu S. 2002. Homeodomain-interacting protein kinase-2 phosphorylates p53 at Ser 46 and mediates apoptosis. Nat Cell Biol.4:11-9.

24. Oda K, Arakawa H, Tanaka T, Matsuda K, Tanikawa C, Mori T, Nishimori H, Tamai K, Tokino T, Nakamura Y, Taya Y. 2000. p53AIP1, a potential mediator of p53-dependent apoptosis, and its regulation by Ser-46-phosphorylated p53. Cell. 101: 849-62.

25. Okamura S, Arakawa H, Tanaka T, Nakanishi H, Ng CC, Taya Y, Monden M, Nakamura Y. 2001. p53DINP1, a p53-inducible gene, regulates p53-dependent apoptosis. Mol Cell. 8:85-94.

26. Bulavin DV, Saito S, Hollander MC, Sakaguchi K, Anderson CW, Appella E, Fornace AJ Jr. 1999. Phosphorylation of human p53 by p38 kinase coordinates N-terminal phosphorylation and apoptosis in response to UV radiation. EMBO J.18:6845-54.

27. Bulavin DV, Demidov ON, Saito S, Kauraniemi P, Phillips C, Amundson SA, Ambrosino C, Sauter G, Nebreda AR, Anderson CW, Kallioniemi A, Fornace AJ Jr, Appella E. 2002. Amplification of PPM1D in human tumors abrogates p53 tumor-suppressor activity. Nat Genet.31:210-5.

28. Dornan D, Shimizu H, Perkins ND, Hupp TR. 2003. DNA-dependent acetylation of p53 by the transcription coactivator p300. J Biol Chem. 278:13431-41.

29. Lambert PF, Kashanchi F, Radonovich MF, Shiekhattar R, Brady JN. 1998. Phosphorylation of p53 serine 15 increases interaction with CBP. J Biol Chem.273: 33048-53.

30. Gu W, Roeder RG. 1997. Activation of p53 sequence-specific DNA binding by acetylation of the p53 C-terminal domain. Cell.90:595-606.

31. Ogryzko VV, Schiltz RL, Russanova V, Howard BH, Nakatani Y. 1996. The transcriptional coactivators p300 and CBP are histone acetyltransferases. Cell.87:953-9.

32. Mitsuuchi, Y., Johnson, S. W., Sonoda, G., Tanno, S., Golemis, E. A., and Testa, J. R. Identification of a chromosome 3p14.3-21.1 gene, APPL, encoding an adaptor molecule that interacts with the oncoprotein-serine/threonine kinase AKT2. Oncogene *18:* 4891-4898, 1999.

33. Miaczynska, M., Christoforidis, S., Giner, A., Shevchenko, A., Uttenweiler-Joseph, S., Habermann, B., Wilm, M., Parton, R.G., and Zerial, M. APPL proteins link Rab5 to nuclear signal transduction via an endosomal compartment. Cell. 116(3):445-56, 2004.

34. Liu, J., Yao, F., Wu, R., Morgan, M., Thorburn, A., Finley, R.L. Jr, and Chen, Y.Q., Mediation of the DCC apoptotic signal by DIP13 alpha.
J Biol Chem. 277(29):26281-5, 2002.

35. Strange, R., Metcalfe, T., Thackray, L., and Dang, M. Apoptosis in normal and neoplastic mammary gland development. Microsc. Res. Tech. *52*: 171-181, 2001.

36. Meyers, E.N., Lewandoski, M., and Martin, G.R. An Fgf8 mutant allelic series generated by Cre- and Flp-mediated recombination.
Nat Genet. *18*:136-141, 1998.

37. Cunningham, M.P. Giving life to numbers. C A Cancer J. Clin. 47:3-4,1997.

38. Slamon, D.J., Clark, G.M., Wong, S.G., Levin, W.J., Ullrich, A. and McGuire, W.L. Human breast cancer: Correlation of relapse and survival with amplification of the BER-2/neu oncogene. Science 235:177-182, 1987.

39. Escot, C., Theillet, C., Lidereau,, R., Spyratos, F., Champeme, M.-H., Gest, J. and Callahan, R. Genetic alteration of the c-myc proto-oncogene (MYC) in human primary breast carcinomas. Proc. Natl. Acad. Sci. USA 83-4834-4838, 1986.

40. Ali, l.U., Merlo, G., Callahan, R. and Lidereau, R. The amplification unit on chromosome II q 1 3 in aggressive primary human breast tumors entails the bel-1, int-2 and hst loci. Oncogene 4:89-92, 1989.

41. Theillet, C., Adnane, J., Szepotowski, P., Simon, M, M.P., Jeanateur, P., Bimbaum, D. and Gaudray P. BCL-1 participates in the I lql3 amplification found in breast cancer. Oncogene 5:147-149, 1990.

42. Vaux D and Korsmeyer S, 1999. Cell death in development. Cell 96, 245-254.

43. Thornberry N., and Lazebnik Y 1998. Caspases enemies within. Sciences 281, 1312- 1316.

44. Benjamin CW. Hiebsch RR. Jones DA. Caspase activation in MCF7 cells responding to etoposide treatment. Molecular Pharmacology. 53(3):446-50, 1998.

45. Mor G. Kohen F. Garcia-Velasco J. Nilsen J. Brown W. Song J. Naftolin F. Regulation of fas ligand expression in breast cancer cells by estrogen: functional differences between estradiol and tamoxifen. Journal of Steroid Biochemistry & Molecular Biology. 73(5):185-94, 2000.

46. Mullauer L. Mosberger I. Grusch M. Rudas M. Chott A. Fas ligand is expressed in normal breast epithelial cells and is frequently up-regulated in breast cancer. Journal of Pathology. 190(1):20-30, 2000.

47. Shinoura N. Muramatsu Y. Yoshida Y. Asai A. Kirino T. Hamada H. Adenovirus-mediated transfer of caspase-3 with Fas ligand induces drastic apoptosis in U-373MG glioma cells. Experimental Cell Research. 256(2):423-33, 2000.

48. Buglioni S. Bracalenti C. Cardarelli MA. Ciabocco L. Giannarelli D. Botti C. Natali PG. Concetti A. Venanzi FM. Prognostic relevance of altered Fas (CD95)-system in human. International Journal of Cancer. 89(2): 127-32, 2000.

49. Lareef, M.H., Tahin, Q., Russo, I.H., Mor, G., Song, J., Mihaila, D., Slater, C.M., and Russo, J. Transfer of chromosome 17(p13.1) to chemically transformed human breast epithelial cells induces Fas-mediated apoptosis. Proc. Am. Assoc. Cancer Res. 42:1475a, 2001.

50. Rubinchik S., Ding R., Qiu AJ., Zhang F., Dong J. Adenoviral vector which delivers FasL-GFP fusion protein regulated by the tet-inducible expression system. Gene Therapy. 7(10):875-85, 2000.

51. Owen-Schaub L. Chan H. Cusack JC. Roth J. Hill LL. Fas and Fas ligand interactions in malignant disease. [Review] [116 refs] International Journal of Oncology. 17(1):5-12, 2000 Jul.

52. Bruder JT. Appiah A. Kirkman WM 3rd. Chen P. Tian J. Reddy D. Brough DE. Lizonova A. Kovesdi I. Improved production of adenovirus vectors expressing apoptotic transgenes. Human Gene Therapy. 11(1):139-49, 2000 Jan1.

53. Fan L. Freeman KW. Khan T. Pham E. Spencer DM. Improved artificial death switches based on caspases and FADD.Human Gene Therapy. 10(14):2273-85, 1999Sep 20.

54. Kondo S. Ishizaka Y. Okada T. Kondo Y. Hitomi M. Tanaka Y. Haqqi T. Barnett GH. Barna BP. FADD gene therapy for malignant gliomas in vitro and in vivo Human Gene Therapy. 9(11):1599-608, 1998 Jul 20.

55. Kodaira H. Kume A. Ogasawara Y. Urabe M. Kitano K. Kakizuka A. Ozawa K. Fas and mutant estrogen receptor chimeric gene: a novel suicide vector for tamoxifen-inducible apoptosis. Japanese Journal of Cancer Research. 89(7):741-7, 1998 Jul.

56. Russo, J., Bamabas, N., Zhang, P.L. and Adesina, K. 1996. Molecular Basis of breast cell transformation. Radiat. Oncol. Invest., 3:424429.

57. Russo, J., Calaf, G., Sohl, N., Tahin, Q., Zhang, P.L., Alvarado, M.E., Estrada, S. and Russo, I.H. Critical steps in breast carcinogenesis. The New York Academy of Sciences 698:1-20, 1993.

58. Russo, J., Russo, I.H. 1987 Biological and molecular basis of mammary carcinogenesis. Lab. Invest. 57: 112-137.

59. Russo, J., Calaf, G., and Russo, I.H. 1993. A critical approach to the malignant transformation of human breast epithelial cells. CRC Critical Reviews in Oncogenesis, 4:403-417.

60. Soule, H.D., Maloney, T.M., Wolman, S.R., Peterson, N.D., Brenz, R., McGrath, C.M., Russo, J., Pauley, R.J., Jones, R.F. and Brooks, S.C. Isolation and characterization of a spontaneously immortalized human breast epithelial cell line, MCF-10. Cancer Research, 50:6075-6086, 1990.

61. Tait, L., Soule, H., Russo, J. 1990. Ultrastructural and immunocytochemical characterization of an immortalized human breast epithelial cell line MCF-10. Cancer Res., 50:6087-6099.

62. Calaf, G., and Russo, J. 1993. Transformation of human breast epithelial cells by chemical carcinogens. Carcinogenesis, 14: 483-492.

63. Foumier, R.E.K., and Ruddle, F.H. Microcell-mediated transfer of murine chromosomes into mouse, Chinese hamster, and human somatic cells. Proc Natl Acad Sci USA 74:319-323, 1977.

64. Stanbridge, E.J. Functional evidence for human tumor suppressor genes- chromosome and molecular genetic studies. Cancer Surveys 12:5-24, 1992.

65. Hunt J.D. Evaluation of phenotypic alteration by microcell- mediated chromosome transfer. Analytical Blochem 2338:107-116, 1996.

66. Koi M, Umar A, Chauhan DP, Chen'an SP, Carethers JM, Kunkel TA, and Boland CR (1994) Human chromosome 3 corrects mismatch repair deficiency and microsatellite instability and reduces N- methyl- N'- nitroN-nitrosoguanidine tolerance in colon tumor cells with homozygous hMLH1 mutation. Cancer Res 54:43084312.

67. Suzuki K., Hirooka Y., Tsujitani S., Yammane Y., Ikeguchi M., Kaibara N. Relationship between loss of heterozygosity at microsatellite loci and computerized nuclear morphometry in hepatocellular carcinoma. Anticancer Res. 20 (20B), 1257-62 (2000).

68. Lakhani, SR; Collins, N.; Stratton, M.R.; Sloane, J.P. Atypical ductal hyperplasia of the breast: clonal proliferation with loss of heterozygosity on chromosomes 16q and 17p. J. Clin. Pathol 48:611-615, 1995.

69. Johnson S.M., Shaw J.A., Walker R.A. Sporadic breast cancer in young women: prevalence

of loss of heterozygosity at p53, BRCA1 and BRCA2. Int. J. Cancer 98 (2):205-209 (2002).

70. Hlaing T., Guo RF, Dilley KA, Loussia JM, Morrish TA, Shi MM, Vincenz C. and Ward PA, 2001. Molecular cloning and characterization of DEFCAP-L and –S, two isoforms of a novel member of the mammalian Ced-4 family of apoptosis protein. J Biol Chem 276: 9230- 9238.

71. Chu Z., et al., 2001. A novel enhancer of the Apaf1 apoptosome involved in cytochrome c dependent caspase activation and apoptosis. J. Biol. Chem. 276, 9239-9245.

72. Martinon F., Hofmann K and Tschopp J. 2001. The Pyrin domain: a possible member of the death domain-fold family implicated in apoptosis and inflammation. Curr. Biol. 10, R118-R120 (2001).

73. Tschopp J, Martinon F and Burns K. 2003. NALPS: a novel protein family involved in inflammation. Nature Rev. Vol 4: 95- 106.

Appendices

JOSE RUSSO, M.D., F.C.A.P., FASCP

Publications:

1. Pugacheva, E., Golemis, E. The scaffolding protein HEF1 regulates the centrosome division cycle and M-phase progression. Proc. American Society for Cell Biology, Abstract 1847. December 14-18th, 2002. San Francisco, CA.

2. Pugacheva, E. and Golemis, E. Deregulation of HEF 1 expression in breast cancer cells cause severe defects in centrosome and spindle dynamics. Fox Chase Cancer Center Postdoctoral Day, 6 June 2003, Philadelphia, PA (Poster presentation)

3. Pugacheva, E., Serebriisskii , I.G., Finley, R.J. and Golemis, E. Dissection of HEF 1 fubction by aptamer peptides. American Society for Cell Biology Abstract 935. December 14-18th,2003. San Francisco, CA.

4. Serebriiskii, I.G., Mitina, O., Pugacheva, E., Benevolenskaya, E., Kotova, E., Toby, G.G., Khazak, V., Kaelin, W.G., Chernoff, J., and Golemis, E.A. Detection of peptides, proteins, and drugs that selectively interact with protein targets. Genome Res 12: 1785-1791, 2002.

5. Pugacheva, E.N., Longmore, G.D. and Golemis, E. HEF1 regulates centrosomal maturation and spindle formation through control of the Aurora-A kinase. Manuscript in preparation.

6.Li, X., Dumont P., Della Pietra A. and Murphy M. The codon 47 polymorphic variant of p53 is associated with altered phosphorylation pattern and decreased apoptosis. (In Preparation)

7- You, H. and Testa, J.R. Involvement of Akt in vitamin E succinate-induced apoptosis. Graduate and Postdoctoral Day at the Fox Chase Cancer Center. Philadelphia, PA.2004

8- Fernandez, S.V., Lareef, M.H.., Russo, I.H., Balsara, B.B., Testa, J. and Russo, J. Role of 17p13.2 in the neoplastic transformation of human breast epithelial; cells. Proc. Am. Assoc. Cancer Res. 2004.

9- Lareef, M., Fernandez, S.V., Russo, I.H., Balsara, B. and Russo, J. Role of 17p13.2 in the neoplastic transformation of human breast epithelial cells. Submitted for Publication.

Russo, Jose

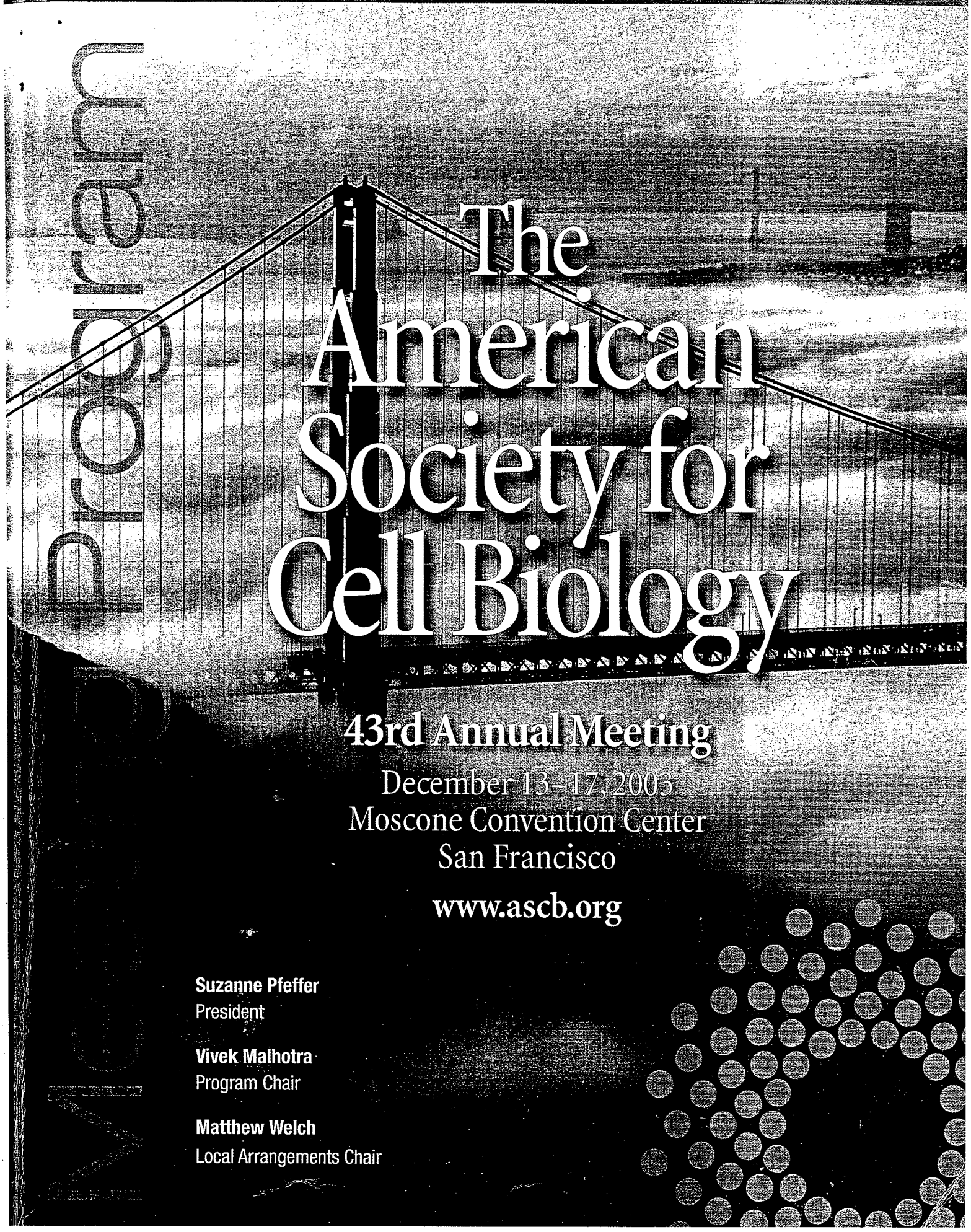

The American Society for Cell Biology

43rd Annual Meeting

December 13–17, 2003
Moscone Convention Center
San Francisco

www.ascb.org

Suzanne Pfeffer
President

Vivek Malhotra
Program Chair

Matthew Welch
Local Arrangements Chair

1841 B309 **A novel regulation mechanism couples DNA damage-repair and the centrosome duplication cycle.** J. L. Salisbury, K. Suino, R. Busby, A. Dorin, S. Bullock, G. Almodovar-Mercado, A. D'Assoro; Tumor Biology Program, Mayo Clinic, Rochester, MN

1842 B310 **Analysis of centrosome endo-replication cycles during S-phase arrest.** E. S. Halpin, E. H. Hinchcliffe; Biological Sciences, Notre Dame, South Bend, IN

1843 B311 **Error correction during centriole inheritance: stability and robustness of organelle copy number.** W. F. Marshall; Biochemistry & Biophysics, UCSF, San Francisco, CA

1844 B312 **3D Analysis of APC and EB1 Localization to the Mother Centriole.** S. Bahmanyar, w. Nelson, A. I. Barth; Molecular and Cellular Physiology, Stanford University, Stanford, CA

1845 B313 **bnd1p is a novel component of the MTOCs in the fission yeast S. pombe.** T. Gangi-Setty, P. T. Tran; Cell and Developmental Biology, University of Pennsylvania, Philadelphia, PA

1846 B314 **Novel centrosome proteins required for the final stages of cytokinesis.** A. Gromley, S. Doxsey; UMASS Medical School, Worcester, MA

1847 B315 **The scaffolding protein HEF1 regulates the centrosome division cycle and M-phase progression.** E. N. Pugacheva, E. A. Golemis; Fox Chase Cancer Center, Philadelphia, PA

1848 B316 **Centrosome Maturation and Spindle Assembly in C. elegans Requires SPD-2, a Coiled-Coil Domain Protein.** K. F. O'Connell,[1] K. R. Kopish,[1] J. Ahringer,[2] C. A. Kemp[1]; [1]Lbg, NIDDK/NIH, Bethesda, MD, [2]Wellcome CRC Institute and Department of Genetics, University of Cambridge, Cambridge, United Kingdom

1849 B317 **Interaction of Aurora-A and Centrosomin at the Microtubule-nucleating Site in Drosophila and Mammalian Cells.** Y. Terada, Y. Uetake, R. Kuriyama; Genetics, Cell Biology, and Development, University of Minnesota, Minneapolis, MN

1850 B318 **D-PLP in centrosome and centriole function.** M. Martinez Campos,[1] R. Basto,[1] J. Baker,[2] M. Kernan,[2] J. W. Raff[1]; [1]Wellcome/Cancer Research UK Institute, Cambridge, United Kingdom, [2]Department of Neurobiology and Behaviour, S.U.N.Y., Stony Brook, NY

1851 B319 **Mapping interactions at the centrosome.** S. Elliott, T. Stearns; Biological Sciences, Stanford University, Stanford, CA

Intracellular Movement

1852 B321 **BicaudalD and the regulation of intracellular transport in Drosophila embryogenesis.** K. S. Larsen, S. P. Gross; Developmental and Cellular Biology, University of California, Irvine, Irvine, CA

1853 B322 **A determinant for directionality of organelle transport in Drosophila embryos.** M. A. Welte,[1] Y. Guo,[1] J. E. Martinez,[2] S. P. Gross[3,2]; [1]Rosenstiel Center, Brandeis University, Waltham, MA, [2]Department of Biomedical Engineering, University of California Irvine, Irvine, CA, [3]Department of Developmental and Cell Biology, University of California Irvine, Irvine, CA

1854 B323 **Intracellular Bidirectional Transport: Dissecting the Transport Complex.** J. E. Martínez,[1] S. Varma,[2] S. P. Gross[1,3]; [1]Biomedical Engineering, University of California Irvine, Irvine, CA, [2]Department of Physics, University of California Irvine, Irvine, CA, [3]Department of Developmental and Cell Biology, University of California Irvine, Irvine, CA

1855 B324 **Signaling Molecules Form a Complex with Molecular Motors That is Essential for Regulation of Organelle Transport.** A. Kashina, E. Potekhina, I. Semenova, V. Rodionov; Physiology, University of Connecticut Health Center, Farmington, CT

1856 B325 **A Role for Spectrin in Transport of Melanosomes in Melanophores.** S. Aspengren, M. Wallin; Zoology, Göteborg University, Göteborg, Sweden

1857 B326 **Blebbistatin, a Myosin II Inhibitor, Blocks Melanosome Aggregation but not Dispersion in Fish Retinal Pigment Epithelial (RPE) Cells.** I. B. Barsoum, C. King-Smith; Biology, Saint Joseph's University, Philadelphia, PA

1858 B327 **Melanosome Motility and Identification of the Small GTPase, Rab27a, in Retinal Pigment Epithelial (RPE) Cells of Sunfish (Lepomis spp.) and Zebrafish (Danio rerio).** C. D. Fox, P. Damiani, R. V. Williams, B. M. Biallas, D. M. Tacelosky, C. King-Smith; Department of Biology, Saint Joseph's University, Philadelphia, PA

1859 B328 **Characterization of Zebrafish Melanophores for Genetic and Functional Studies of Melanosome Motility.** L. Sheets, B. Schnapp; Cell and Developmental Biology, Oregon Health & Science University, Portland, OR

1860 B329 **Actin-linked Bulk Transport in the Distal Axon Alters Growth Cone Size.** K. E. Miller, M. P. Sheetz; Biology, Columbia University, New York, NY

1861 B330 **Actin-based Motility of Listeria monocytogenes as a Probe for Intracellular Architecture.** C. I. Lacayo, J. A. Theriot; Biochemistry, Stanford University, Stanford, CA

1862 B331 **Correlation of Nikkomycin Z hypersensitivity in myo1 strains of Saccharomyces cerevisiae with changes in Chs3p cellular distribution and protein stability.** F. E. Rivera Molina, S. Gonzalez Crespo, J. R. Rodríguez-Medina; Biochemistry, University of Puerto Rico, School of Medicine, San Juan, PR

1863 B332 **Stable Metaphase Centromere Orientation and Replication Specific Cse4p Incorporation in budding yeast.** C. G. Pearson, E. Yeh, E. D. Salmon, K. Bloom; Dept of Biology, UNC at Chapel Hill, Chapel Hill, NC

1864 B333 **The Hepatocyte Growth Factor acts through the Ras, PI 3-Kinase and MAPK Signaling Pathways to Stimulate E-Cadherin Internalization, Peripheral Lysosome Redistribution and Invasion of Prostate Cancer Cells.** C. Yu, E. Harris, D. Duhon, J. Williams, J. Cardelli; Microbiology, LSU Health Sciences Center, Shreveport, LA

1865 B334 **cappuccino and spire encode novel actin-associated proteins that regulate yolk protein endocytosis.** S. Balasundaram,[1] B. P. James,[1] A. J. Wellington,[1] L. J. Manseau,[1] M. Ramaswami[2]; [1]Molecular and Cellular Biology, University of Arizona, Tucson, AZ, [2]Molecular and Cellular Biology and ARL Division of Neurobiology, University of Arizona, Tucson, AZ

1866 B335 **Macromolecule and organelle trafficking is normal in dystonia musculorum sensory neurons in culture.** M. Pool,[1,2] H. McBride,[3,4] R. Kothary[1,2]; [1]Molecular Medicine Program, Ottawa Health Research Institute, Ottawa, ON, Canada, [2]Cellular and Molecular Medicine, University of Ottawa, Ottawa, ON, Canada, [3]University of Ottawa Heart Institute, Ottawa, ON, Canada, [4]Biochemistry, Molecular Biology and Immunology & Pathology and Laboratory Medicine, University of Ottawa, Ottawa, ON, Canada

functions in the organization of discrete multiple iMTOCs during interphase and in the nucleation of eMTOC microtubules during cytokinesis. Mutant *bnd1δ* cells fail to form multiple bundles of iMTOC microtubules, and instead have a single aggregated bundle of microtubules during interphase. The defective iMTOC microtubule organization leads to bent-shaped instead of the normal rod-shaped cell morphology. During mitosis, mutant *bnd1δ* cells fail to nucleate the eMTOC microtubules. bnd1-GFP localizes to the SPB, eMTOC, and iMTOCs, and also appears as dynamic "dots" along the interphase microtubule bundles. Our findings suggest a model where bnd1p is a common component of the three types of MTOCs, yet plays distinct roles in nucleation and organization of microtubules throughout the cell cycle.

1846

Novel centrosome proteins required for the final stages of cytokinesis

A. Gromley, S. Doxsey; UMASS Medical School, Worcester, MA

Centrosomes have been implicated in cytokinesis and cell cycle progression in vertebrate cells, although the molecular components that regulate these processes have not been identified. Recently we have described a novel centriolar protein called centriolin, which functions in both processes. Centriolin shares homology with the budding and fission yeast spindle pole body component Nud1p/Cdc11p, which anchors regulatory pathways involved in mitotic exit/cytokinesis. Altering centriolin protein levels induces a unique cytokinesis phenotype characterized by the persistence of a thin intracellular bridge between two daughter cells. These defects suggest a function of centriolin in the late stages of cytokinesis, which may involve membrane delivery and fusion as well as midzone microtubule stability. To identify proteins which interact with centriolin, a yeast two-hybrid screen was conducted using the Nud1-like domain as bait. Results of this screen identified several proteins including a novel GTPase Activating Protein (GAP), referred to here as agGAP. Similar to the centriolin phenotype, silencing of agGAP results in cytokinesis defects indistinguishable from those observed upon centriolin silencing. Based on its interaction with centriolin as well as its phenotypic similarities, we propose that agGAP represents an additional member of a cytokinesis signaling pathway in vertebrate cells.

1847

The scaffolding protein HEF1 regulates the centrosome division cycle and M-phase progression.

E. N. Pugacheva, E. A. Golemis; Fox Chase Cancer Center, Philadelphia, PA

HEF1, p130Cas, and Efs/Sin define the Cas (Crk-associated substrate) family of scaffolding proteins. The best-studied role of these proteins is as intermediates in integrin-dependent signaling, contributing to regulation of cell adhesion, cell migration, and cell survival. We here report a completely unexpected function for the HEF1 protein in control of progression through mitosis. Beyond its well-established localization at focal adhesions in interphase cells, we find that endogenous HEF1 localizes to the centrosome during the S and G2 phases of cell cycle, to the mitotic spindle in early M-phase, and proximal to the midbody at cytokinesis. We have manipulated HEF1 by use of peptide aptamers targeted to stabilize full length endogenous HEF1; by overexpression of full length HEF1; and by siRNA depletion. Increases the level of HEF1, whether in asynchronous cultures or specifically at the G2/M boundary, result in defects in cleavage furrow progression and abscission in cytokinesis, frequently accompanied by development of supernumerary centrosomes and a multipolar spindle. Conversely, depletion of HEF1 results in premature centrosomal splitting, frequent appearance of monoastral spindles, and defects in progress through early stages of mitosis. These defects are similar to those seen with deregulation of centrosomally-associated regulatory proteins required for M-phase progression, including the Cdc14a phosphatase and the AuroraA-BTAK-STK15. Work in progress also indicates that HEF1 association with the centrosome is controlled by post-translational modification by centrosomally active cell cycle regulatory kinases. We postulate that HEF1 at the centrosome serves as a scaffold to promote the activity of signaling complexes required for centrosomal maturation and movement, thereby providing an important input to the regulation of mitotic progression, and we propose that long term deregulation of HEF1 may contribute to genomic instability.

1848

Centrosome Maturation and Spindle Assembly in *C. elegans* Requires SPD-2, a Coiled-Coil Domain Protein.

K. F. O'Connell,[1] K. R. Kopish,[1] J. Ahringer,[2] C. A. Kemp[1] ; [1] Lbg, NIDDK/NIH, Bethesda, MD, [2] Wellcome CRC Institute and Department of Genetics, University of Cambridge, Cambridge, United Kingdom

Centrosomes play a critical role in assembly of the mitotic spindle but the composition of these dynamic organelles and the mechanisms that regulate their activity remain poorly understood. The *spd-2* gene of *C. elegans* is required for maturation of the centrosome and spindle assembly. In the absence of *spd-2* activity, astral microtubules are poorly organized and centrosome components such as gamma-tubulin fail to localize. We have cloned *spd-2* and found that it encodes a phosphoprotein with several predicted coiled-coil domains. Using both antibodies and a SPD-2::GFP fusion construct, we find that SPD-2 protein localizes to interphase nuclei, centrioles, and pericentriolar material. In early embryos, SPD-2 gradually accumulates at the centrosome concomitant with an increase in microtubule organizing activity. Association of SPD-2 with the centrosome does not require microtubules, cytoplasmic dynein, aurora-A kinase, or ZYG-9, an XMAP215 homolog. Interestingly, SPD-2 interacts genetically with dynein heavy chain and SPD-5, another coiled-coil protein required for centrosome function. SPD-2 and SPD-5 are dependent on one another for localization to the pericentriolar region but SPD-2 localizes to centrioles independently of SPD-5. These data indicate that SPD-2, SPD-5, and dynein heavy chain function in a common pathway to regulate microtubule nucleation.

1849

Interaction of Aurora-A and Centrosomin at the Microtubule-nucleating Site in *Drosophila* and Mammalian Cells

Y. Terada, Y. Uetake, R. Kuriyama; Genetics, Cell Biology, and Development, University of Minnesota, Minneapolis, MN

A mitosis-specific Aurora-A kinase has been implicated in microtubule organization and spindle assembly in diverse organisms. However, exactly how Aurora-A controls the microtubule nucleation onto centrosomes is unknown. Here we show that Aurora-A specifically binds to the C-terminal domain of a *Drosophila* centrosomal protein, centrosomin (CNN), which has been shown to be important for assembly of mitotic spindles and spindle poles. Aurora-A and CNN are mutually dependent for localization at spindle poles, which is required for proper targeting of γ-tubulin and other centrosomal components to the centrosome. The N-terminal half of CNN interacts with γ-tubulin/γ-tubulin containing protein complexes and induces cytoplasmic foci that can initiate microtubule nucleation in vivo and in vitro in both *Drosophila* and mammalian cells. These results suggest that Aurora-A regulates centrosome assembly by controlling the CNN's ability to targeting and/or anchoring γ-tubulin/γ-tubulin complex to the centrosome and organizing microtubule-nucleating sites via its interaction with the C-terminal sequence of CNN.#

1850

D-PLP in centrosome and centriole function

M. Martinez Campos,[1] R. Basto,[1] J. Baker,[2] M. Kernan,[2] J. W. Raff[1] ; [1] Wellcome/Cancer Research UK Institute, Cambridge, United Kingdom, [2] Department of Neurobiology and Behaviour, S.U.N.Y., Stony Brook, NY

Proteins that contain a pericentrin/AKAP450 centrosomal-targeting (PACT) domain have been implicated in recruiting other proteins to the centrosome. We show that the *Drosophila* pericentrin-like protein (D-PLP) is concentrated both in centrioles and in the pericentriolar material (PCM). The centrosomal recruitment of all the centrosomal proteins that we tested (γ-tubulin, Centrosomin, D-TACC, Msps, CP190, and CP60) is impaired in *D-plp* mutant cells, but cell division occurs relatively normally, and homozygous *D-plp* mutant flies are viable. Mutant flies, however, are severely uncoordinated, and we show that the formation of ciliated structures is abnormal; as a result, mutant sperm cells and sensory neurons are defective. We conclude that D-PLP is required for both centrosome and centriole function, and we propose that D-PLP serves as a structural link between the centrioles and the PCM.

1851

Mapping interactions at the centrosome

S. Elliott, T. Stearns; Biological Sciences, Stanford University, Stanford, CA

The centrosome is the major microtubule organizing center of the cell. Centrosomes are central to cytoplasmic organization, chromosome segregation and cell division. Defects in centrosome behavior can lead to missegregation of chromosomes during cell division resulting in genomic instability and aneuploidy. One of the problems with studying the centrosome is that little is known about its protein composition or how its components interact with each other to carry out essential centrosomal functions. Therefore, it is important to increase understanding of the centrosome not just by identifying more centrosomal proteins, but also by studying their interactions at the centrosome. For example, centrin and members of the tubulin family are required for centrosome duplication. We can use these proteins to search for interacting proteins that may also play crucial roles in centrosome function. Numerous detailed studies on the budding yeast centrosome, the spindle pole body (SPB), have allowed the construction of an interaction map of all the known SPB components. We aim to construct a similar interaction map for the mammalian centrosome. This map will be an important tool for the future of centrosome research. In order to develop this interaction map, we take advantage of well established techniques, such as the yeast two-hybrid interaction trap and immunoprecipitation. We also have the ability to study alternative centrosome-like structures that form at the center of microtubule asters in frog egg extract and the basal bodies at the base of sperm tails, which can give valuable information about centrosomal substructures.

Intracellular Movement (1852-1868)

1852

BicaudalD and the regulation of intracellular transport in Drosophila embryogenesis

K. S. Larsen, S. P. Gross; Developmental and Cellular Biology, University of California, Irvine, Irvine, CA

BicaudalD (BicD) is known to be involved in the dynein-dynactin mediated transport of nuclei, mRNA particles, and golgi, however its exact function is unclear. Here we report a new regulatory role for BicD in the transport of

Russo, Jose

The 8th Annual

Postdoctoral and Graduate Student Research Conference

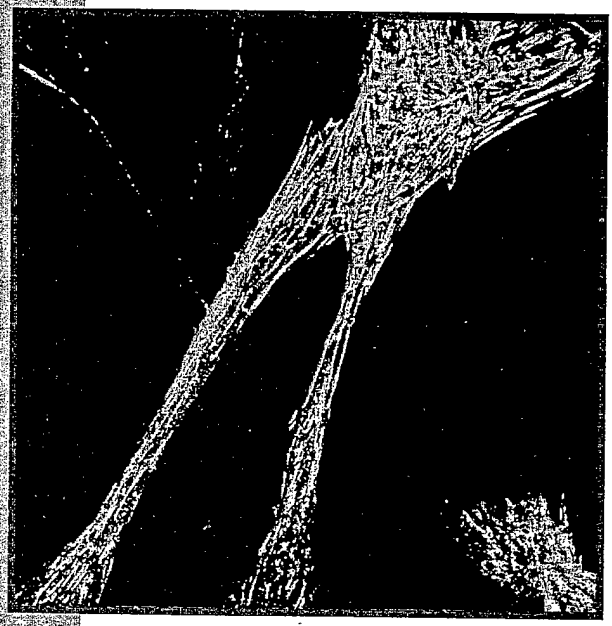

Friday, June 6, 2003

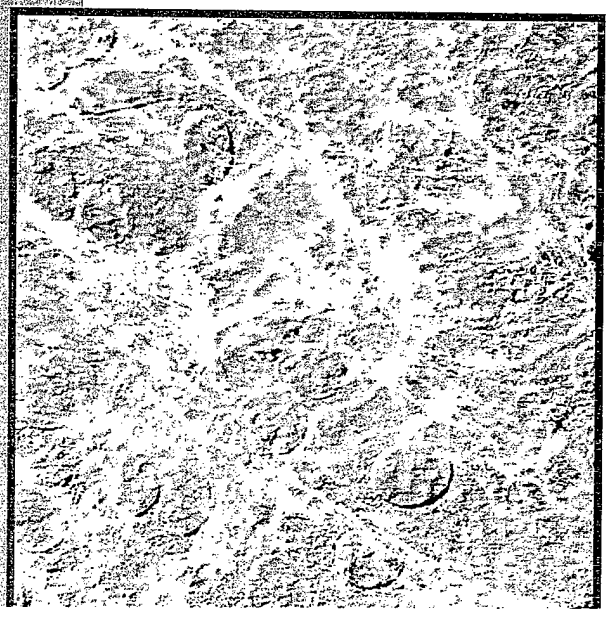

FOX CHASE
CANCER CENTER

DEREGULATION OF HEF1 EXPRESSION IN BREAST CANCER CELLS CAUSES SEVERE DEFECTS IN CENTROSOME AND SPINDLE DYNAMICS

Elena Pugacheva and Erica Golemis
Fox Chase Cancer Center, Philadelphia, PA 19111

The Cas proteins are central components of integrin-dependent signaling networks. Cas proteins are docking molecules containing many protein interaction domains. HEF1 is one of the most well-studied Cas family members. HEF1 is present in many cell lines, but is most abundant in epithelial cells of the breast and lung, and in aggressive breast and lung carcinoma cell lines.

HEF1 protein relocalizes from focal adhesions to the mitotic apparatus during the M phase of cell cycle, but the significance of this localization change had not been clear. To clarify the function of HEF1 protein in mitosis we first analyzed the distribution of HEF1 throughout the cell cycle. Using high resolution confocal analysis, and two distinct antibodies specific for HEF1 in immunofluorescence, we have now determined that a population of endogenous HEF1 associates with the centrosome throughout cell cycle in MCF7 and Hela cells. As a separate control, we have determined that overexpressed GFP-HEF1 also localizes to the centrosome. Overexpression of HEF1, either by transient transfection or through use of a set of stable, tetracycline-repressible cell lines in an MCF-7 parental background, or stabilization of endogenous HEF1, using of a set of specific peptide "aptamers", resulted in centrosomal amplification, with cells containing in excess of 4 centrosomes. Based on this failure rate, populations over-expressing HEF1 accumulated binucleate (polyploid) cells.

In contrast, depletion of HEF1 by siRNA resulted in the premature splitting of the centrosomes in more than 70% of the cell population and monoastral spindle formation. Intriguingly, the two phenotypes associated with over- versus under-expressed HEF1 are very similar to the recently reported phenotypes for under- versus over-expressed Cdc14A. Cdc14A is a human phosphatase that has been shown to be a crucial, centrosome-associated regulator of cell division. Taken together, these data strongly support the hypothesis that HEF1 has an active function in the regulation of cell division at mitosis through the centrosomal apparatus. Investigations into the mechanistic basis for this function are in progress.

Molecular Biology of the Cell

ASCB

Supplement to Molecular Biology of the Cell Volume 13 Nov 2002

Abstracts

42nd American Society for Cell Biology Annual Meeting
December 14–18, 2002, San Francisco, CA

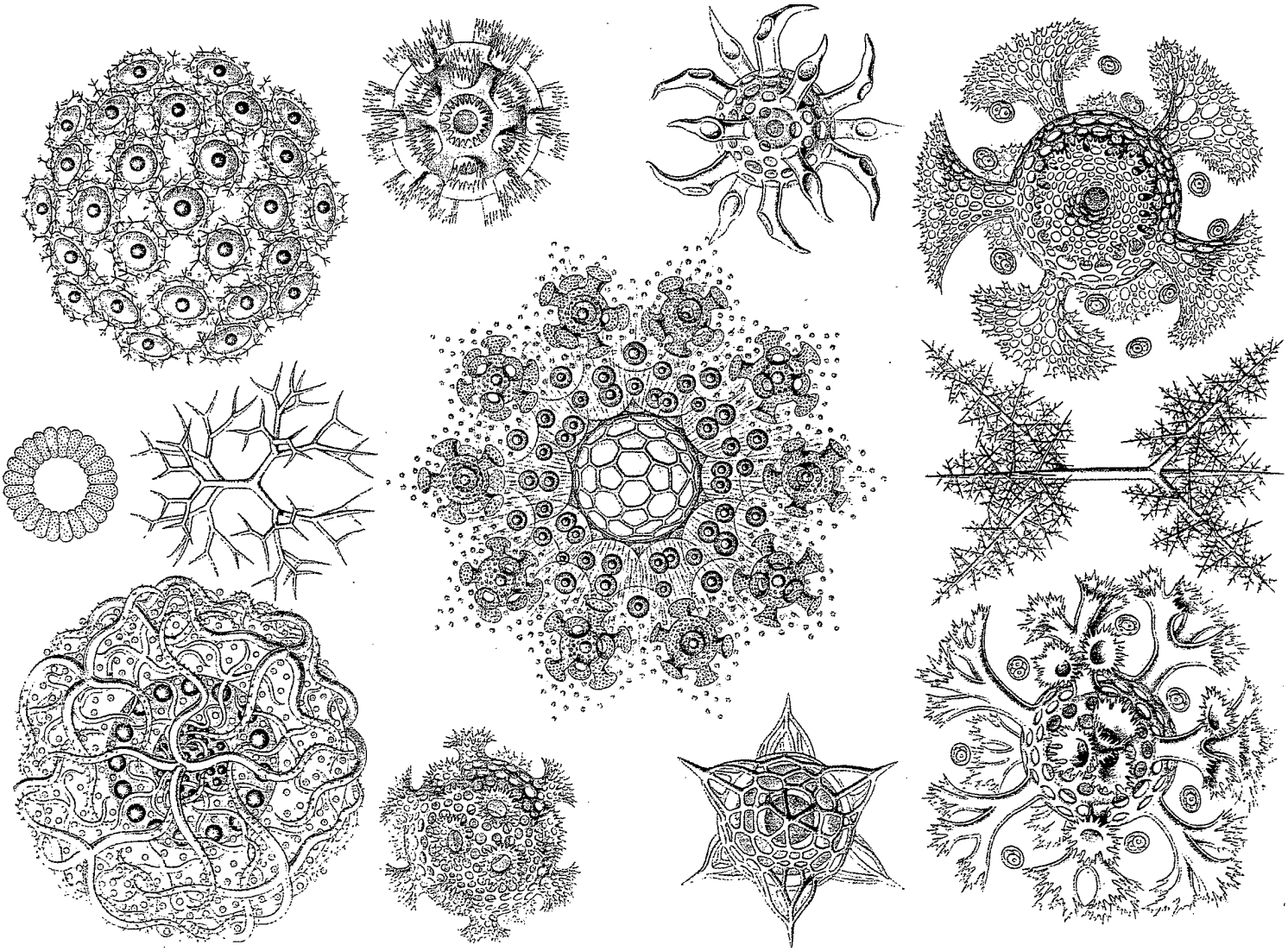

multiple mitotic checkpoints and suggest that γ-tubulin plays an important role in the regulation of mitotic progression. Supported by grant GM31837 from the NIH.

934

Cell Cycle Dependent Properties of the Novel Spindle Protein Astrin

G. J. Mack,[1] B. K. Kaiser,[2] P. K. Jackson,[2] D. A. Compton[1] ; [1] Biochemistry, Dartmouth Medical School, Hanover, NH, [2] Pathology, Microbiology and Immunology, Stanford University School of Medicine, Palo Alto, CA

Astrin is a novel mitotic spindle and kinetochore-associated protein that was identified from in vitro assembled microtubule asters using mass spectrometry (PNAS, 2001, 98:14434-39). Astrin possesses no known functional motifs other than two regions of predicted coiled-coil and has no known function.Here we characterize the cell cycle properties of astrin. Astrin is phosphorylated in a mitosis specific manner as judged by a reduction in its molecular weight when isolated from mitotic cells followed by treatment with lambda phosphatase. Upon fractionating cell extracts by sucrose gradient centrifugation or gel filtration, astrin is found to be present in a large mitosis-specific complex. Assembly of astrin into this complex is phosphorylation dependent as dephosphorylation with lambda phosphatase results in the release of astrin. Yeast two hybrid analysis has also shown that the centrosomal phosphatase Cdc14A interacts with astrin and is capable of its dephosphorylation. Astrin also undergoes significant changes in abundance during the cell cycle due to ubiquitin-mediated proteolysis. Both astrin antibody injection and RNAi appear to cause cells to be delayed in progression through prometaphase. However, once past this delay cells form normal bipolar spindles, align chromosomes correctly and enter anaphase. These data suggest that astrin plays a functional role in mitotic progression, but that redundantly acting factors compensate when it is perturbed.

935

Dissection of HEF1 function by aptamer peptides

E. N. Pugacheva,[1] I. G. Serebriiskii,[1] R. J. Finley,[2] E. A. Golemis[1] ; [1] Basic Sciences, Fox Chase Cancer Center, Philadelphia, PA, [2] Center for Molecular Medicine and Genetics, Wayne State University School of Medicine, Detroit, MI

Integrin-mediated cell adhesion to extracellular matrix (ECM) is crucial for many cell activities including proliferation, migration and survival. Cas-protein family, including p130Cas and HEF1 has been shown to be important in control of cell migration and decisions between survival and apoptosis. The full-length HEF1 protein (115 and 105 kD) contains an N-terminal SH3 domain, substrate domain and conserved C-terminal domain. Post-translational modifications of HEF1 produce multiple HEF1 isoforms. Cleavage of the full length HEF1 at two caspase consensus sites, DLVD (aa360 – 363) and DDYD (aa627 – 630) produce a stable p55kD N-terminal isoform, and rapidly degraded C-terminal fragments. Following this processing, the p55 isoform tightly associates with the mitotic spindle during mitosis, then is degraded at the return to G1. To probe the function of p55 in mitosis we have sought to selectively block DLVD cleavage in vivo using a peptide aptamer approach. Peptide aptamers can disrupt or otherwise modulate specific protein interactions, and thus allow manipulation of protein function in vivo. Using a dual-bait two-hybrid system developed in our laboratory and a random peptide aptamer library, we have identified peptides that specifically interact with HEF1 protein bearing a wild type cleavage site (DLVD) versus non-cleavable HEF1 (DLVA) mutant. We have demonstrated that bacterially expressed GST-fused peptides specifically pull down the DLVD, but not DLVA form of HEF1 protein from cell lysates. Transduction of peptides specifically targeting DLVD/HEF1 into mammalian cells increases the amount of full-length HEF1 and reduces levels of p55/HEF1 from 2 to 3 times in comparison with control peptides, and has no effect on DLVA/HEF1. Transfection of DLVD-specific peptides into the MCF-7 cells outcome with serious mitotic spindle defects, accumulation of cells with several spindles and getting population of polyploid cells.

936

Simulation of XKCM1 activity by a novel component of the inner centromere

R. Ohi,[1] M. L. Coughlin,[1] W. S. Lane,[2] T. J. Mitchison[1,3] ; [1] Cell Biology, Harvard Medical School, Boston, MA, [2] Harvard Microchemistry Facility, Harvard University, Cambridge, MA, [3] Institute for Chemistry and Cell Biology, Harvard Medical School, Boston, MA

Spindle assembly and chromosome segregation require an exquisitely orchestrated interplay between microtubules and mitotic chromatin. To identify novel proteins which participate in these processes, we developed a method to isolate microtubule-associated proteins from mitotic *Xenopus* egg extracts (XMAPs) with the aim of discovering new microtubule dynamics regulators. Using this approach, we identified a coiled-coil protein of unknown function which we designate XSKI-A (Stimulator of KinI). During spindle assembly reactions in frog egg extracts, XSKI-A is located at discrete pericentromeric foci, a localization pattern which is reminiscent of the inner centromere proteins. Antibody blocking and immunodepletion experiments demonstrate that XSKI-A function is required for both spindle assembly and maintenance of spindle architecture. Structures assembled in XSKI-A-deficient extracts contain abnormally long microtubules, similar to those formed in XKCM1-compromised extracts. These results suggest that XSKI-A positively regulates the microtubule depolymerizing activity of the KinI kinesin XKCM1. Consistent with a role in regulating XKCM1. XSKI-A and XKCM1 co-immunoprecipitate from mitotic egg extracts and co-localize in mitotic spindles assembled *in vitro*. Finally, we demonstrate that recombinant XSKI-A purified from insect cells stimulates the activity of XKCM1 on pure microtubules *in vitro*. Our data indicate that the microtubule depolymerizing activity of XKCM1 can governed directly by additional protein factors. We are currently exploring the function that XSKI-A performs at the inner centromere and how it may contribute to chromosome behavior during mitotic spindle assembly.

937

Human Enhancer of Invasion-Cluster (HEI-C): a Novel Coiled-Coil Protein which Functions at the Mitotic Spindle

M. B. Einarson,[1] D. A. Compton,[2] E. A. Golemis[1] ; [1] Division of Basic Science, Fox Chase Cancer Center, Philadelphia, PA, [2] Department of Biochemistry, Dartmouth Medical School, Hanover, NH

In a cross-species overexpression approach, we have utilized the pseudohyphal transition of *Saccharomyces cerevisiae* as a model system to identify human genes which regulate cell morphology and the cell cycle. A gene we have termed Human Enhancer of Invasion-Cluster (HEI-C), encoding an evolutionarily conserved coiled-coil protein, was isolated in a screen for human genes which when overexpressed induce agar invasion in yeast. Immunocytochemical analysis of mammalian cells indicates that during mitosis HEI-C localizes primarily to the spindle while in interphase the protein localizes to the cytoplasm, the centrosome and to regions of cell-cell contact. Depletion of HEI-C *in vivo* using short interfering RNAs results in aberrant mitotic spindle morphology and apoptosis. HEI-C is found in mitotic asters formed *in vitro*, although immunodepletion of HEI-C does not affect aster formation. Further, HEI-C is shuttled between the nucleus and the cytoplasm by a CRM1-dependent mechanism. These results indicate that HEI-C is required for spindle function while its complex subcellular localization, coupled with its isolation in a screen for invasive yeast, suggest it may link events of the cell cycle with the cell periphery.

938

Cloning and Characterization of *Drosophila* Polo Kinase Kinase, DPlkk

S. A. Godinho,[1] P. Alves,[1] V. Parelho,[1] A. Tavares[1,2] ; [1] Cell Division Group, Instituto Gulbenkian de Ciência, Oeiras, Portugal, [2] Dept. Chemical Engineering, Instituto Superior Técnico, Lisboa, Portugal

The polo-like kinases (Plks) are a conserved family of enzymes that play different roles during mitosis. The Drosophila polo protein kinase, like other Plks, has a peak of activity during mitosis and is largely inactive during interphase. Although the mechanisms of regulation of polo activity remain to be elucidated, phosphorylation is clearly important. Two Polo-like kinase kinases have been recently described: xPlkk, and the mammalian Slk have been proved to phosphorylate and activate Plx1 and Plk1, respectively. We have now cloned the gene dPlkk, a likely homologue of Xenopus xPlkk. dPlkk has the typical motifs of a serine-threonine protein kinase, with a N-terminal catalytic domain and a long coiled-coil C-terminal. The two kinases share 60% identity over the catalytic domain and 38% identity over the non-catalytic C-terminal. We could detect an association between Polo and dPlkk proteins. When dPlkk is immunoprecipitated from extracts derived from either S2 cells or embryo extracts Polo protein is pulled down, and that dPlkk is present in Polo immunoprecipitates. Furthermore, the two proteins co-sediment in sucrose gradients. We confirmed by kinase assays that dPlkk obtained either from Drosophila embryo or S2 cell extracts is an active kinase, capable of phosphorylating and activating Polo protein. We have isolated a Drosophila mutant, obtained by insertion of a P-element in the first exon of the dPlkk gene. Homozygous embryos show severe defects during the first syncitial mitotic divisons, and the majority never reach celularisation. Further analysis is required to determine if polo is not phosphorylated in the dPlkk1 mutant embryos. Simultaneously, in order to further investigate Polo phosphorylation by dPlkk and its biological significance, we are on the process of doing RNAi experiments of dPlkk in Drosophila S2 cells.

939

Reorganization of the Microtubule Array in Prophase/Prometaphase Requires Cytoplasmic Dynein Dependent Microtubule Transport

N. M. Rusan, U. S. Tulu, C. J. Fagerstrom, P. Wadsworth; Biology, University of Massachusetts, Amherst, MA

When mammalian somatic cells enter mitosis, a fundamental reorganization of the Mt cytoskeleton occurs that is characterized by the loss of the extensive interphase MT array and the formation of a bipolar mitotic spindle. Microtubules in cells stably expressing GFP-alpha tubulin were directly observed from prophase to just after NEBD in early prometaphase. Our results demonstrate a transient stimulation of individual Mt dynamic turnover and the formation and inward motion of microtubule bundles in these cells. Motion of microtubule bundles was halted following antibody mediated inhibition of cytoplasmic dynein/dynactin, but was not perturbed following inhibition of the kinesin related motor Eg5 or myosin II. In metaphase cells, assembly of small foci of Mts was detected at sites distant from the spindle; these Mts were also moved inward. We propose that cytoplasmic dynein-dependent inward motion of Mts functions to remove Mts from the cytoplasm at prophase and from the peripheral cytoplasm

Detection of Peptides, Proteins, and Drugs That Selectively Interact With Protein Targets

Ilya G. Serebriiskii,[1] Olga Mitina,[1,2] Elena N. Pugacheva,[1] Elizaveta Benevolenskaya,[3] Elena Kotova,[1] Garabet G. Toby,[1,4] Vladimir Khazak,[5] William G. Kaelin,[3] Jonathan Chernoff,[1] and Erica A. Golemis[1,6]

[1]Division of Basic Science, Fox Chase Cancer Center, Philadelphia, Pennsylvania 19111, USA; [2]Department of Molecular Biology and Medical Biotechnology, Russian State Medical University, Moscow, Russia; [3]Dana-Farber Cancer Institute, Boston, Massachusetts 02115, USA; [4]Cell and Molecular Biology Group, University of Pennsylvania School of Medicine, Philadelphia, Pennsylvania 19104, USA; [5]Morphochem, Inc., Monmouth Junction, New Jersey 08852, USA

Genome sequencing has been completed for multiple organisms, and pilot proteomic analyses reported for yeast and higher eukaryotes. This work has emphasized the facts that proteins are frequently engaged in multiple interactions, and that governance of protein interaction specificity is a primary means of regulating biological systems. In particular, the ability to deconvolute complex protein interaction networks to identify which interactions govern specific signaling pathways requires the generation of biological tools that allow the distinction of critical from noncritical interactions. We report the application of an enhanced Dual Bait two-hybrid system to allow detection and manipulation of highly specific protein–protein interactions. We summarize the use of this system to detect proteins and peptides that target well-defined specific motifs in larger protein structures, to facilitate rapid identification of specific interactors from a pool of putative interacting proteins obtained in a library screen, and to score specific drug-mediated disruption of protein–protein interaction.

[Supplemental material is available online at http://www.genome.org. The following individuals kindly provided reagents, samples, or unpublished information as indicated in the paper: A. Taliana, M. Russell, M. Berman, and R. Finley.]

Since its inception (Fields and Song 1989), the two-hybrid system has been utilized in increasingly complex strategies to analyze interactions between proteins of biological interest and known or novel cognate partners including other proteins, RNA sequences, pharmacological agents, and peptides (for review, see Serebriiskii et al. 2001). More recently, a number of groups have exploited the potential of two-hybrid systems as a tool for understanding protein interactions on a genome-level scale, with pilot studies involving elucidation of large sets of protein interactions developed in *Saccharomyces cerevisiae* (Schwikowski et al. 2000; Ito et al. 2001) providing a model for ongoing work in higher eukaryotes. Given the increasing realization that protein interaction networks involve the interaction of discrete signaling molecules with multiple partner proteins in different biological circumstances, accurate description of the function of a given protein now implicitly involves dissection of its interaction domains, ranking of its interaction affinity with each of its partners, and determination of physiological conditions under which each pair of proteins preferentially interacts. These determinations pose significant technological hurdles in high-throughput efforts.

We have described previously a proof-of-concept experiment for a two-hybrid Dual Bait system that provides internal controls for interaction specificity, and could theoretically be used to selectively compare the interaction of a protein with more than one partner molecule (Serebriiskii et al. 1999). Building from this preliminary study, we have now developed a complete system of reagents that can be used to score interaction of one transcriptional activation domain (AD)-fused prey protein with either of two DNA-binding domain (DBD)-fused bait proteins over a range of different interaction affinities. In three different library screening applications, we demonstrate that these reagents can be used to identify proteins or peptides that target short sequence elements of biological importance within a larger protein structure. We further demonstrate that the system can be used in a bait swap application for rapid secondary screening to sort multiple library hits into subgroups most likely to be reproducible and physiologically relevant. Finally, we describe the use of the reagents in a subtractive two-color visualization procedure that can discriminate specific from nonspecific drug-induced inhibition of protein interactions. These studies, together with our other work involving use of the system to build enhanced specificity derivatives of signaling proteins engaged in complex interactions, indicate the Dual Bait is a useful tool in dissection of complex cellular regulatory machinery.

[6]Corresponding author.
E-MAIL EA_Golemis@fccc.edu; FAX (215) 728-3616.
Article and publication are at http://www.genome.org/cgi/doi/10.1101/gr.450702.

RESULTS AND DISCUSSION

In the Dual Bait two-hybrid system (Fig. 1), the use of two parallel bait-reporter systems allows simultaneous and com-

Table 1. Summary of New Dual Bait-Compatible Reagents

cI Fusion plasmids

Plasmid name (frames)	Selection in yeast/in *E. coli*		Comment/Description
pGKS3# AB pGKS4* AB	*HIS3*	Ap^R Km^R	ADH1 promoter expresses cI followed by polylinker
pGKS6# ABC pGKS7* AB			ADH1 promoter expresses cI followed by polylinker Modified ADH1 promoter expresses ~5× higher level of expression of cI bait
pGKS8# AB		Zeo^R	Dual purpose vector. ADH1 promoter expresses cI followed by polylinker, whereas cI-responsive *gusA* reporter cassette (with 3 *cI ops*) is integrated into the same plasmid backbone
pGBS9* AB pGBS10* AB	$G418^R$	Km^R	ADH1 promoter expresses cI followed by polylinker Modified ADH1 promoter ensures higher level of expression of cI
pGMS11* A		Zeo^R	GAL1 promoter expresses cI followed by polylinker; for
pGMS12* B	$G418^R$	Km^R	use with baits whose continuous presence is toxic to yeast

Reporter Plasmids

Plasmid name	Selection in yeast/in *E. coli*		No. of operators	
pRG64* pRG62*			4 cI 2 cI	cI operators direct transcription of the *gusA* gene: sensitivity to transcriptional activation is a function of operator number
pRG61* pDR8*	*URA3*	Km^R	1 cI 8 lexA 3 cI	LexA-responsive *lacZ* reporter is comparable with pMW112, whereas cI-responsive *gusA* reporter has sensitivity comparable to pRG62

***LEU2/LYS2* Selection Strains**

Strain name	Genotype	No. of operators	
SKY48	MATα *trp1, his3, ura3, lexAop-LEU2, cIop-LYS2*	6 lexA 3 cI	Stringent selection for interaction partners of cI-fused baits; most sensitive LexA-responsive *LEU2* reporter
SKY191		2 lexA 3 cI	Most stringent LexA-responsive *LEU2* reporter, and more sensitive cI-responsive *LYS2* reporter versus SKY48
SKY473*	MAT*a his3, leu2, trp1, ura3, lexAop-LEU2 cIop-LYS2*	4 lexA 3 cI	Sensitivity of *LEU2* reporter is intermediate between sensitivity of *LEU2* in SKY48 and SKY191. Sensitivity of *LYS2* reporter is the same as sensitivity of *LYS2* in SKY191. Can be used as mating partner for SKY48 and SKY19 strains.

Reagents newly constructed (*) or modified (#) (change of reading frame and/or sequence of polylinker) in this work are indicated. SKY48 and SKY191 have been described previously (Serebriiskii et al. 1999), but are noted here to provide context for SKY473. A complete listing of dual bait-compatible reagents is provided at http://www.fccc.edu/researchy/labs/golemis/InteractionTrapInWork.html, as are links to detailed protocols for system use. The newly described cI plasmids provide options to regulate expression levels of baits using either constitutive or galactose inducible promoters (useful for toxic baits), and to use *HIS3*, Zeo^R or $G418^R$ as selectable markers in yeast, and either Ap^R or Km^R as selectable markers in *E. coli*, to maximize compatibility with other yeast two-hybrid systems. A newly developed DR8 dual reporter contains both *lacZ* and *gusA* genes, simplifying transformations, whereas the pRG reporter series allows variation of sensitivity levels for gauging cI-responsive transcription. Finally, the SKY473 reporter strain is an extremely robust MATa reporter strain that is optimal as an interaction mating partner with pre-existing Dual Bait or other two hybrid strains.

Screen Step	Description	Fetal Liver	Fetal Brain/ B42	Fetal Brain/ GAL4
1	LEU+LacZ+	49	84	20
2	LEU+LacZ+GusA-	47	67	20
3	# genes	7	6	20
4	post-swap LEU-LacZ-GusA+	20	56	1
5	# genes	5	2	1
6	# final validated genes	4	2*	1*

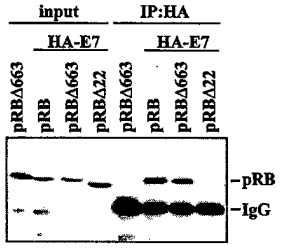

Figure 3 Use of Dual Bait reagents to reduce false positive background. (*Top*) The RBΔ663 and RBΔex22 mutants of pRB are described in Sellers et al. (1998), and were expressed in the context of a large pocket domain of pRB containing amino acids from 379 to 928. SKY48 yeast expressing LexA-RBΔ663 and cI-RBΔex22 baits were used to screen three different libraries. (Lines *1,2*) Numbers of clones positive for LexA-RBΔ663-responsive (*LEU2*, *lacZ*) but negative for cI-RBΔex22-responsive (*gusA*) reporters. (Line *3*) Number of discrete genes represented among the clones. (Line *4*) Number of clones positive for cI-RBΔ663-responsive (*GusA*), but not LexA-RBΔex22-responsive (LEU, *lacZ*) reporters; note, this reduction from line *2* values was not observed with retransformation testing with the original LexA-RBΔ663 and cI-RBΔex22 baits. (Line *5*) Number of genes represented in line *4* set of clones. (Line *6*) Number of surviving genes that were validated by coimmunoprecipiation and other techniques. (*) Note, papillomavirus E7 was identified from two different fetal brain libraries with B42 or GAL4 as activation domains. Although a legitimate pRB interactor, as E7 is not normally expressed in brain, it may represent an artifact of the libraries' construction. (*Bottom*) HA-tagged E7 and pRB derivatives were overexpressed in Saos-2 (*Rb−/−*) osteosarcoma cells and their interaction was determined by immunoprecipitation with anti-HA antibody (HA 11, BAbCO). The precipitated proteins pRB, pRBΔ663, and RBΔex22 (RBΔ22 in figure) were detected by immunoblotting with anti-RB antibody (XZ56). Input proteins are 10% of that used in immunoprecipitation.

papilloma virus HPV-18 was isolated from two different libraries by this approach. E7, a known wild-type pRB interactor (Munger et al. 1989), was, for the first time, shown to interact with the low pentetrant RBΔ663 but not the high-penetrant Δex22 mutant.

As in Application 1, this is a demonstration of the capacity of the system to identify interactors with specific requirement for a binding motif in a larger protein. However, whereas in some libraries, positives represented multiple hits on a small number of genes, in others (fetal brain, GAL4), unique isolates of a large number of genes were obtained, suggesting specific interactions (Serebriiskii and Golemis 2001). To further improve specificity of the screen, we performed a bait swap, now expressing LexA-RBΔex22 and cI-RBΔ663 rather than LexA-RBΔ663 and cI-RBΔex22. Simultaneous retransformation of initially isolated preys with yeast containing swapped DBD fusions in parallel with the original baits eliminated a substantial number of the originally isolated clones, which were presumptively binding to a unique but artifactual configuration of the original baits (Fig. 3, top).

For the fetal brain/GAL4 library, this single step reduced the number of possible specific interacting clones from 20 to 1. With a single exception, all of the clones that interacted selectively with both LexA- and cI-RBΔ663 were confirmed by additional assays including coimmunoprecipitation (Fig. 3, bottom). The ease of swapping the two baits while remaining in the same reporter strain background, and using the same precalibrated reporter genes, is not matched by any other two hybrid-based system.

Application 4

Scoring Specific Disruption of Protein Interactions by Small Molecule Inhibitors

It has been of interest to try to develop small molecule inhibitors of specific protein–protein interactions as an intelligent

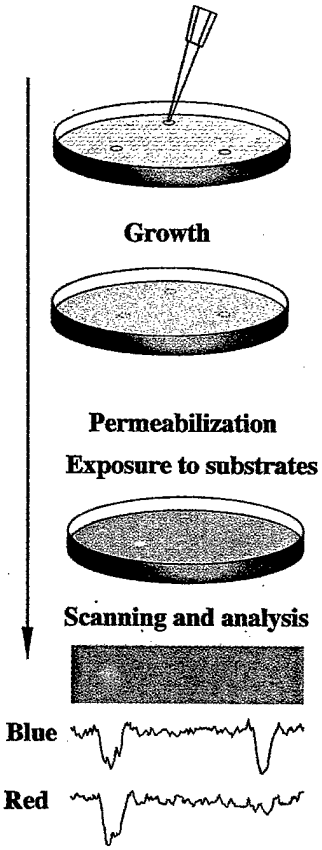

Figure 4 Drug disruption of protein–protein interactions. (*Top*) Yeast containing baits and preys are mixed with low-melt agarose and poured over appropriate dropout growth medium. After agarose is set, 1 μL of each compound to be tested or solvent negative control is dropped on the plate. Yeast are incubated for 1–2 d, then permeabilized and overlaid with Z-buffer, Magenta-Gal (a red colorimetric substrate for LacZ) and X-Gluc (a blue colorimetric substrate for GusA). (*Bottom*) The result shown derives from a mixed population of yeast strains containing LexA-Ras and AD-Raf or cI-Ras and AD-RalGDS. In this example, only the colorimetric (*lacZ* and *gusA*) reporters are being assessed. Fungicide (*left*) inhibits both *lacZ* and *gusA* signal, whereas a specific Ras–Raf interaction inhibitor reduces only *gusA* (blue) output, leaving a red spot; solvent control produced no spots (data not shown). Shown below the spots are results obtained following a scan of plate, import of image into NIH Image, and performance of densitometry for signal intensity in blue versus red across the spot midline.

Biol. **10:** 111–119.
Pirone, D.M., Fukuhara, S., Gutkind, J.S., and Burbelo, P.D. 2000. SPECs, small binding proteins for Cdc42. *J. Biol. Chem.* **275:** 22650–22656.
Schwikowski, B., Uetz, P., and Fields, S. 2000. A network of protein–protein interactions in yeast. *Nat. Biotechnol.* **18:** 1257–1261.
Sellers, W.R., Novitch, B.G., Miyake, S., Heith, A., Otterson, G.A., Kaye, F.J., Lassar, A.B., and Kaelin, Jr., W.G. 1998. Stable binding to E2F is not required for the retinoblastoma protein to activate transcription, promote differentiation, and suppress tumor cell growth. *Genes & Dev.* **12:** 95–106.
Sells, M.A., Knaus, U.G., Bagrodia, S., Ambrose, D.M., Bokoch, G.M., and Chernoff, J. 1997. Human p21-activated kinase (Pak1) regulates actin organization in mammalian cells. *Curr. Biol.* **7:** 202–210.
Serebriiskii, I.G. and Golemis, E.A. 2001. Two hybrid system false positives, and approaches to their detection and elimination. In *Two-hybrid systems, methods and protocols.* (ed. P.N. MacDonald), pp. 123–134. Humana Press, Totowa, NJ.
Serebriiskii, I., Khazak, V., and Golemis, E.A. 1999. A two-hybrid dual bait system to discriminate specificity of protein interactions. *J. Biol. Chem.* **274:** 17080–17087.
Serebriiskii, I.G., Khazak, V., and Golemis, E.A. 2001. Redefinition of the yeast two-hybrid system in dialogue with changing priorities in biological research. *BioTechniques* **30:** 634–655.
Thapar, R., Karnoub, A.E., and Campbell, S.L. 2002. Structural and biophysical insights into the role of the insert region in rac1 function. *Biochemistry* **41:** 3875–3883.
Vidal, M. and Endoh, H. 1999. Prospects for drug screening using the reverse two-hybrid system. *Trends Biotechnol.* **17:** 374–381.
Wu, W.J., Lin, R., Cerione, R.A., and Manor, D. 1998. Transformation activity of Cdc42 requires a region unique to Rho-related proteins. *J. Biol. Chem.* **273:** 16655–16658.

WEB SITE REFERENCE

http://www.fccc.edu/research/labs/golemis/InteractionTrapInWork.html; Web site for this project.

Received May 22, 2002; accepted in revised form August 30, 2002.

HEF1 regulates centrosomal maturation and spindle formation through control of the Aurora-A kinase.

Elena N. Pugacheva[1], Gregory D. Longmore[2], and Erica A. Golemis[1,*]

Division of Basic Science, Fox Chase Cancer Center, 7701 Burholme Ave., Philadelphia, PA 19111.

Running Title: HEF1 regulates centrosomes through Aurora-A

Key words: HEF1, centrosome, spindle, mitosis, Aurora-A, Ajuba

Number of Characters: xxxxxxxxxx

* corresponding author:
Erica Golemis, W406
Fox Chase Cancer Center
333 Cottman Ave.
Philadelphia, PA 19111
Phone: 215-728-2860
Fax: 215-728-3616
Email: EA_Golemis@fccc.edu

Abstract.

The HEF1 scaffolding protein has a well-defined role in mediating integrin-dependent attachment signaling at focal adhesions. We had previously shown that HEF1 relocalizes to the spindle asters at mitosis, but the significance of this migration was unclear. We here report that HEF1 status controls mitotic spindle formation through action at centrosomes in the G2 phase of cell cycle. Increased levels of HEF1 cause the development of supernumerary centrosomes, and a multipolar spindle. Conversely, depletion of HEF1, or overexpression of a dominant-negative HEF1 derivative, results in premature centrosomal splitting, monoastral and malformed spindles, and transient appearance of >4N populations. HEF1 association with the centrosome peaks in late G2, and is followed by HEF1 movement from the centrosome to the spindle, similar to the Aurora-A kinase (AurA). Further, positive and negative regulation of AurA causes defects of the centrosome and spindle similar to those seen with HEF1. We show that HEF1 interacts with AurA, controls activation of AurA at the centrosome, and is itself an AurA substrate. These interactions may be mediated in part through HEF1 interactions with the AurA-associated protein Ajuba. These results suggest a novel mechanism for the coordination of cell attachment status with cell division in mitosis, and may provide insight into the induction of genomic instability in cancer.

Introduction.

Organismal development requires the synchronized interaction of cell differentiation, polarization, and division controls to enable the creation of highly organized structures from an isolated oocyte. At present, although the mechanisms by which these different processes are coordinated are not well understood, studies predominantly in *C. elegans* and *D. melanogaster* have led to the identification of a number of proteins that act at cell-cell or cell-substrate interfaces in interphase, and at the mitotic machinery in M-phase. The complex functions of these proteins allow the direct specification of cleavage plane to be coordinated with the establishment or maintenance of a polarized cellular identity (e.g., (1-3). Some, including the PAR family of proteins in *C. elegans*, play critical roles in early embryogenesis. In one an elegant recent example, the fly Adenomatous Polyposis Coli (APC) ortholog was shown to organize a bridge between cell cortex and the centrosome in male germline cells that oriented the mitotic spindle and subsequent division plane, thus specifying the differentiation status of daughter cells based on their post-cleavage proximity to a divisional "hub" (4). A number of the proteins identified in these studies have homologs with presumably orthologous functions in higher eukaryotes. However, studies of mammalian signaling proteins typically have not focused on very early development, but rather emphasize the study of cell processes and protein function in 2-dimensional cell culture models, where the coordination of cell division polarity with cellular attachment status is less readily perceived and analyzed.

It has long been known that loss of basal cell adhesion can cause mitotic defects in mammalian cells, most notably by causing failure of cytokinesis (5, 6). This failure is not simply due to the loss of traction forces that cells use to physically separate, as it has been documented that the presence of too high a level of cell attachment can similarly reduce cytokinetic efficiency (7). These results imply crosstalk between the cell division machinery and the focal adhesions that provide basal cell attachment. However, because cell adhesion is most readily observable in interphase cells, and focal adhesions tend to minimize or disappear in mitotic cells, accompanied by the downregulation of some key focal adhesion-associated signaling proteins (8-10), little work has investigated a possible requirement or alternative roles for focal adhesion-associated proteins in M-phase. Notably, in the past several years, investigations of the nuclear cell cycle

have also documented the coordination of nuclear signaling events in time and space during M-phase progression in higher eukaryotes, emphasizing the roles of proteins associated with structures such as the centrosome, the contractile ring, the central spindle, and the midbody, in controlling the timing of progression through different cell cycle stages (e.g. (11); reviewed in (12)). These structures exist in close contact with or are derived from the actin and tubulin cytoskeletons. An economical view of cellular function would suggest that the re-use of proteins which govern cytoskeletal dynamics in interphase cells might not only be efficient, but might also provide a means to synchronize changes in cell contacts during the mitotic process.

Of all the mitotic structures, a number of recent studies suggest that the centrosome might be a primary signal integration point. Recent work has emphasized the dual activity of centrosomes in contributing to control of cell polarization in interphase cell migration (13, 14), but also in coordinating polarity of the mitotic spindle in M-phase (15). Centrosomally-associated signaling activities also govern the timing of mitotic entry (16). Mechanistically, the initial activation of cyclin B1 at mitosis has been proposed to depend on an initial recruitment of activated AurA kinase to the centrosome in late G2, following AurA interaction with the LIM domain protein Ajuba (17). The subsequent destruction of cyclin B later in M-phase, required for the metaphase-anaphase transition, is also regulated from the centrosome, based on the initial assembly and activation of the anaphase promoting complex/cyclosome (APC/C) at this structure (11). Finally, some studies have also indicated that the centrosome performs a key licensing function at the point of cytokinesis (7).

HEF1 is a member of a group of scaffolding proteins that includes p130Cas and Efs/Sin (18, 19). This group of Cas proteins localizes to focal adhesions in interphase cells, and acts as intermediates in a variety of integrin-dependent signaling processes, including establishment of cell attachments, migration, and cell survival signaling. In 1998, our group first raised the possibility that HEF1 might have a previously unsuspected function in mitosis (10). This was based on two observations. First, a significant part of the endogenous population of HEF1 was cleaved at a central DLVD cleavage motif at the G2/M boundary. Subsequent processing of the protein by the proteasome eliminated C-terminal fragments, leaving behind a mixed population of full length HEF1 and a p55, amino-terminal, fragment. Second, the HEF1 protein relocalized

from focal adhesions to the mitotic spindle asters in M-phase. Since that time, reports have appeared suggesting of the association of other focal adhesion-associated proteins, such as zyxin (20), paxillin (21), FAK, and Pyk2 (22) with mitotic spindle or other relevant structures such as the microtubule organizing center (MTOC) or centrosome. One question that has not been well addressed for any of these proteins is whether these changes have any functional significance for spindle function, or are simply reflections of the considerably changed signaling landscape that accompanies focal adhesion disassembly in mitotic versus interphase cells.

In this study, we have specifically tested the hypothesis that HEF1 localization to the mitotic spindle reflects an active role for this protein in M-phase. We have found that HEF1 association with the spindle follows an initial HEF1 localization to the centrosome that peaks in late G2 phase. A detailed analysis of the consequences of positively or negatively deregulating the activity of HEF1 indicates that HEF1 function is essential for centrosomal maturation and mitotic spindle formation in epithelial cells. HEF1 interacts with and controls the activation of AurA, suggesting a mechanism for its activity. Interestingly, the functions we have identified for HEF1 are not completely shared with its well-studied family member p130Cas. These and other results, in the context of prior studies, indicate that HEF1 provides a crucial bridge coordinating attachment and cell division processes at M-phase in mammals.

Results.

HEF1 localization to the centrosome in G2 precedes HEF1 spindle localization in M-phase. The initial goal of this study was to analyze potential consequences of deregulated HEF1 signaling for formation and function of the mitotic spindle. Mitotic spindles generally are nucleated from centrosomes, and defective signaling by centrosomally associated proteins is frequently associated with aberrant spindle formation and/or progression through mitosis (e.g. (23, 24)). Moreover, in many cases, spindle-associated signaling proteins first associate with and become activated at the centrosome, prior to propagation of signals to the spindle (e.g.(11)). Therefore, as a prelude to this work, we first examined whether HEF1 localizes only to the spindle, or also to the centrosome. Immunofluorescence analysis with antibodies to HEF1 and to the centrosomal protein gamma-tubulin indicates that HEF1 is detectable at the centrosome in late G2, (Figure 1A), prior to the release of most or all HEF1 to the spindle in mitosis (Figure 1B). This endogenous HEF1 signal is blocked by peptide against which the HEF1 antibody was raised, supporting signal specificity (not shown). Further, transient over-expression of GFP-fused HEF1 reveals similar centrosomal and spindle localizations (Figure 1C). HEF1 association with the centrosome is cell cycle regulated. In experiments using cells synchronized at different stages of the cell cycle (Figure 1D, E), endogenous HEF1 is only weakly visible at the centrosomes in G1- and S-phases, but is prominently detected at this structure in the G2-phase. This corresponds with a general increase in levels of HEF1 as cell cycle progresses from G1 to mitosis (Figure 1E, bottom). Using GFP-fused HEF1 derivatives (Figure 1F), we have performed preliminary mapping of sequence determinants necessary for localization of HEF1 to the mitotic spindle. Based on this analysis, we have identified a minimal sequence of amino acids 1-398 required for association with the centrosome, with sequences between 363-398 an essential localization determinant.

To establish a functional requirement for HEF1 at the centrosome and the mitotic spindle, we established three independent systems for manipulation of HEF1 in MCF7 cells. First, we overexpressed the full length HEF1 protein under control of a tetracycline-repressible promoter (Figure 2A). Second, based on prior data indicating HEF1 cleavage and proteolysis at mitosis ((10); discussed further below), we utilized peptide aptamers targeted to the primary mapped cleavage site (25) to stabilize the full length endogenous HEF1 (Figure 2B). Third and

reciprocally, we used a siRNA approach to deplete HEF1 (Figure 2C). For each class of manipulation, a matching negative control set was used, corresponding to tetracycline-regulated GFP (for overexpression), use of non-specific peptides, and use of a scrambled siRNA (for depletion).

Up- or down-regulation of HEF1 expression causes centrosomal and spindle abnormalities. Both overexpression of exogenous HEF1 and peptide stabilization of endogenous HEF1 induce a high frequency of cells with spindle defects by 48 hours following cell treatment (Figure 3A, B). Most notable is the increase in the number of cells with multipolar spindles, which represent 12% of the population with overexpression, and >16% with specific HEF1-targeted peptides, as compared to 2-3% for all negative controls. In other cells, while no multipolar spindles are observed, nevertheless the spindle is defective. The observed defects are likely to arise from a primary defect at the centrosome, as for every cell with multipolar spindles, each spindle originated from a supernumerary centrosome (Figure 3A). Overexpression of full length HEF1, or introduction of HEF1-stabilizing peptides, was found to consistently induce centrosomal amplification, with >10% of cells containing in excess of 4 centrosomes within 48 hours following treatment (Figures 3B).

In contrast, depletion of HEF1 using siRNA induced a distinct mitotic phenotype, marked by high percentages of cells with monoastral spindles (Figure 3C, center panels), or with malformed or asymmetric spindles (Figure 3C, right panels). SiRNA depletion is not completely homogenous among cells in a population; using antibodies to HEF1, we determined that cells with monoastral or deformed spindles consistently represented cells with the most complete HEF1 depletion, whereas those cells with apparently normal bipolar spindles had detectable HEF1 signal (data not shown) We can make a panel of representative mitosis's I have HEF1 and a-tubulin co-stain). In examining the centrosomes of mitotic HEF1-depleted cells, two abnormalities were observed. First, the centrosomes of cells with defective spindles showed weaker reactivity with antibody to gamma-tubulin than did cells with higher HEF1 levels, and apparently normal spindles. Second, although two distinct gamma-tubulin or GFP-centrin centrosomal structures were observed in all mitotic cells with depleted HEF1, there was invariably asymmetry in the ability of the two centrosomal structures to nucleate spindle

formation. Gamma-tubulin is known to accumulate during centrosomal maturation in the G2 phase of cell cycle (26-28): our observations suggested that HEF1 depletion might be interfering with this maturation process, rendering one centrosomal daughter incompetent to act as a microtubule organizing center.

We therefore also inspected the status of centrosomes in non-mitotic cells. Notably, two distinct, widely separated, GFP-centrin-positive structures (Figure 3D) were observed in >80% of HEF1-depleted cells (>500 cells counted in 5 separate experiments), but in less than 10% of cells treated with a scrambled siRNA. In the normal centrosomal duplication cycle, the single "mother" centrosome remaining in a cell after cytokinesis undergoes duplication in S-phase, with the two centrosomes remaining linked while the "daughter" matures through G2: Normally, two widely separated centrosomes are not observed until the G2/M transition (26, 27). FACS analysis of HEF1-depleted cells versus scramble-treated controls confirms that their cell cycle profile is very similar (results not shown), with no enrichment of the G2 compartment. Hence, the primary defect is likely one of centrosome cohesion, rather than a secondary consequence of altered cell cycle compartmentalization.

HEF1 interacts with Ajuba and is required for the activation of AurA kinase at the centrosome. The premature splitting phenotype observed with HEF1 depletion is similar to that reported for inhibition of other proteins known to exert a key role in centrosomal maturation, including notably the AurA kinase (24, 29). AurA activation at the centrosome has recently been reported to require interaction with the LIM domain/scaffolding protein Ajuba, which had previously been thought to function primarily at cell junctions and in the nucleus. The most well defined function of HEF1 is as a scaffolding protein mediating the association of critical signaling complexes at focal adhesions (19). Based on the congruence of HEF1 and Aurora phenotypes, we examined whether HEF1 might also contribute to AurA signaling by providing a scaffolding function at the centrosome.

In HEF1-depleted MCF7 cells in the G2 phase of cell cycle, total levels of AurA at the centrosome are similar to those found in MCF7 cells treated with a matched scrambled siRNA (Figure 4A). In contrast, levels of phospho-AurA, indicative of kinase activation (17), are

greatly reduced or absent under conditions of HEF1 depletion (Figure 4A, B), implying that HEF1 plays an important role in the activation process. This role could be direct, with HEF1 physically a component of an AurA activation complex, or it might be indirect, with HEF1 causing defects at an early stage of the centrosomal cycle so that AurA is subsequently unable to be activated in association with an immature centrosomal structure. Several lines of evidence indicate that role of HEF1 in regulating AurA activation is direct. Antibody directed at HEF1 co-immunoprecipitates endogenous AurA, while antibody to AurA precipitates HEF1 (Figure 4C). Further, in a two-hybrid system approach in yeast, an Ajuba bait used in a library screen directly isolated the carboxy terminal two-thirds (amino acids 365-834) of HEF1 (results not shown). This last finding indicated the interaction is likely to involve at minimum a direct interaction between HEF1 and Ajuba, rather than involving indirect association of HEF1, AurA, and Ajuba as parts of a multi-component complex in mammalian cells.

We therefore further probed the interaction between HEF1, AurA, and Ajuba. We demonstrated above that amino acids 1-398 (p55+) are a minimum determinant of HEF1 association with the centrosome, with a critical localization determinant located in the serine-rich 35 amino acids from 363-398 (Figure 1). Using antibody to GFP for co-immunoprecipitation, we find that GFP-p55+ is also sufficient to interact with AurA, while GFP-p55 is not (Figure 5A). Given the interaction between HEF1 and AurA, we asked if HEF1 might be an AurA substrate. Purified activated AurA was incubated with equal quantities (Figure 5B, top) of GST-fused domains of HEF1, with the AurA substrate histone H3 as a positive control, and GST and histone H1 as negative controls. AurA efficiently phosphorylated both the p55 and p55+ HEF1-derived proteins to a degree comparable to or exceeding the histone H3 positive control, while not phosphorylating either of the negative controls (Figure 5B). These results indicated that AurA phosphorylation does not contribute HEF1 recruitment to the centrosome (as predicted based on the accumulation of HEF1 at the centrosome prior to AurA activation at G2/M transition), but may otherwise regulate HEF1 activity. Interestingly, siRNA depletion of AurA (Figure 5C) markedly depressed the steady state levels of HEF1. Both AurA (30) and HEF1 (31) have been shown to bind proteins that promote their degradation by the proteasome. We suggest loss of association between AurA and HEF1 may render them more susceptible to proteolysis, as treatment of AurA- or scrambled-siRNA depleted cells with the proteasome inhibitor

significantly stabilized the levels not only of AurA, but also of HEF1 (Figure 5C). This stabilization was seen both in nocodazole- and thymidine-arrested cells, so is not cell cycle-stage specific.

We have analyzed the sequence determinants conferring HEF1 interaction with Ajuba. First, cells were transfected with FLAG-tagged HEF1, and N- and C-terminal derivatives; and Myc-tagged full length Ajuba, Ajuba pre-LIM domain, or a negative control (GFP) (Figure 6A). Immunoprecipation with FLAG demonstrated strong association of full length HEF1 with full length Ajuba, weak association of the N-terminal domain of HEF1 with full length Ajuba, and strong association between the C-terminal fragment of HEF1 and both the full length Ajuba, and the pre-LIM domain of Ajuba (Figure 6A). In a reciprocal experiment, full length Ajuba, and to a lesser degree the isolated Ajuba LIM domain, co-immunoprecipitated HEF1 (Figure 6B): full length Ajuba also weakly co-immunoprecipitated the HEF1 N-terminus (Figure 6C). Combining these results with the earlier observation that the carboxy-terminal domain of HEF1 was sufficient to interact with Ajuba in a two-hybrid screen, we propose that the Ajuba LIM domain interacts with the HEF1 N-terminus, whereas the Ajuba pre-LIM domain has the potential to interact with the HEF1 C-terminus, but this is masked in the context of full length HEF1 sequences. Finally, Ajuba is a member of a sub-group of closely related LIM domain proteins with functions in cell attachment, cell division, and oncogenesis, including TRIP6 (32), zyxin (20, 33), LPP (34, 35), and LIMD1 (36). Two other members of this family, Trip6 and zyxin, have been shown to interact with HEF1 and p130Cas through their LIM domains (37). To probe the specificity of HEF1 interactions with this family, we compared co-immunoprecipitation of HEF1 with Ajuba, LIMD1, LPP, and zyxin (Figure 6D). HEF1 interacted most strongly with Ajuba and LIMD1, and to a lesser degree with LPP and zyxin.

Comparison of HEF1 and p130Cas regulation of centrosome status and AurA activation. The HEF1 protein has been documented as being particularly abundant in epithelial and lymphoid lineages, and less abundant in fibroblasts (10, 38), while a second Cas family member, p130Cas, is more ubiquitously expressed. We investigated whether the requirement for HEF1 for centrosome maturation were specific to cells of epithelial lineages, and whether p130Cas had similar activities. FF2425 fibroblasts (Figure 7A, 7B) and other human fibroblast lines (MCR5-

hTERT, results not shown) express minimal levels of HEF1. Treatment of FF2425 or MCR5-TERT fibroblasts with siRNA to HEF1 produced no phenotype under conditions where centrosomal splitting was observed in 41% of centrosomes in HeLa and 78% in MCF7 cells (Figure 7A). This result confirmed the specificity of the HEF1-directed siRNA in the experiments described above – i.e., in a cell type in which no HEF1 is detected by Western blot or immunoflurescence, the HEF1-directed siRNAs have no effect. In MCF7 cells, and HeLa cells, depletion of p130Cas produced 45% and 12% percent splitting, respectively (Figure 7A), in contrast to the much greater effect seen with HEF1 depletion. Based on Western analysis (Figure 7B, and results not shown), p130Cas was effectively depleted, excluding limited depletion of p130Cas as an explanation for the more limited phenotype.

Interestingly, p130Cas depletion did not cause centrosomal splitting in FF2425 cells or MCR5-hTERT cells (Figure 7A, 7B and results not shown). Antibodies to p130Cas do not reveal localization of this protein to centrosomes. However, comparison of cells transfected with plasmids overexpressing p130Cas and HEF1 suggest that the two proteins can localize to centrosomes with comparable efficiency under conditions of overexpression,whether in either fibroblasts or epithelial cells (Figure 7C). One speculative explanation for these differing results is that p130Cas is known to exist as numerous differentially phosphorylated isoforms within different cellular compartments (39): it may be that endogenous p130Cas localized to the centrosome is not well recognized by antibodies to the protein. Finally, we compared levels of AurA and phospho-AurA at the centrosome in p130Cas- versus HEF1-depleted cells. Phospho-AurA activation was not notably diminished following p130Cas depletion, (Figure 7D), in contrast to the results seen with HEF1 (Figure 4), again suggesting a less important function for centrosome maturation.

Depletion of HEF1 may provide a stimulus towards genomic instability. Based on the phenotypes described above, a long-term consequence of HEF1-dependent defects in centrosomal and spindle dynamics might be predicted to be the development of aneuploid population of cells. FACS analysis of a total population of MCF7 or MCF12F epithelial cells depleted for HEF1 for 48 hours did not reveal a large number of such aneuploid cells. However, elutriation of a population of cells treated with HEF1-directed or control siRNAs, followed by

FACS analysis, clearly indicated the presence of distinct 6N and 8N populations in some fractions (Figure 8, top two panels). The elutriated fractions containing significant levels of 6N and 8N cells were returned to culture, propagated for an additional 24 hours, then re-assayed by FACS. Over 24 hours, these >4N cell populations were lost (Figure 8, bottom two panels), and cells adapted a more normal cell cycle distribution. These observations could be most readily explained as clearance of the hyperploid cells by the spindle checkpoint surveillance machinery, suggesting loss of HEF1 from epithelial cells predisposes to, but is insufficient for, genomic instability.

Discussion.

The summed data in this study indicate that the HEF1 protein is a novel and important regulator of centrosomal function. In particular, depletion studies reveal a requirement for HEF1 in centriolar cohesion in interphase cells; centrosomal maturation, as marked by the recruitment of gamma-tubulin and ability to act as a microtubule-organizing center in mitosis; and centrosomal signaling, reflected by loss of ability to activate AurA at mitotic entry. We find that HEF1, AurA, and Ajuba physically interact, and HEF1 is itself phosphorylated by AurA kinase, and present at reduced levels in the absence of AurA. The general similarity between HEF1 and AurA depletion and overexpression phenotypes (40-42) is striking, and implies that HEF1 and AurA functions are closely linked. Although there appears to be less of a requirement for the HEF1-related protein p130Cas for centrosomal activity, depletion of p130Cas nevertheless induced some centrosomal defects. Together, these results support the idea that the focal-adhesion associated Cas proteins function in a distinct sphere to control mitotic entry.

This study complements other recent work in our laboratory demonstrating HEF1 regulation of mitotic entry, cleavage furrow formation, and cytokinesis (Dadke et al., submitted). Besides the centrosome and spindle defects described here, we found that deregulated HEF1 expression also results in changes in processes governed by regulation of cortical actin, with this actin regulation dependent of HEF1 regulation of the activation cycle of the RhoA GTPase (Dadke et al., submitted). In the present study, we found that overexpression of HEF1 induced supernumerary centrosomes and multipolar spindles. An ongoing debate in the field is whether centrosomal amplification is a primary event regulated at the level of the centrosomal duplication cycle, or whether it results from failed cytokinesis (26, 40, 43). In previous studies of AurA overexpression, failed cytokinesis has been suggested as a contributing factor to the centrosomal amplification observed (24, 26, 44). In our work, HEF1 overexpression does not induce centrosomal amplification over background in cells arrested by thymidine in G1/S for 16 hours, but such amplification becomes apparent at 48 hours after HEF1 induction (data not shown). These results cells must undergo a round of mitosis to generate enhanced numbers of centrosomes, implying centrosomal amplification is a secondary defect. In contrast, the HEF1 depletion phenotypes appear likely to be primary for several reasons, including the localization

of HEF1 to the centrosome, and HEF1 regulation of proteins such as AurA and Ajuba that play a role in centrosomal maturation and action as an MTOC.

The most well defined function of HEF1 is as a scaffolding protein mediating the association of critical signaling complexes at focal adhesions (19). Our data indicate that HEF1 may similarly contribute to the interactions of AurA and Ajuba at the centrosomes. Based on two-hybrid and co-immunoprecipitation results, the carboxy-terminal domain of HEF1 interacts with the amino-terminal, non-LIM domain of Ajuba, while the carboxy-terminal, LIM domain of Ajuba has been reported to interact with AurA (17). HEF1 is phosphorylated in its amino-terminal region by AurA. This phosphorylation occurs within a fragment, p55 (aa 1-353) that is not sufficient to bring HEF1 to the centrosome: however, a slightly larger fragment of HEF1 (p55+, aa 1-398) associates with the centrosome, interacts with AurA in vivo, and induces a centrosomal splitting phenotype similar to HEF1 depletion, suggesting action as a dominant negative. The presence of a key localization determinant at aa 353-398 is interesting. We have previously reported that endogenous HEF1 is proteolytically cleaved at amino acid 353 during apoptosis (45, 46), and mitosis (10), resulting in the separation of different domains used for protein interaction. In subsequent work, we have used multiple techniques to examine pure populations of cells in M-phase, and we now revise our conclusion to indicate that M-phase HEF1 comprises a mixed pool of full length and cleaved HEF1 in which full length HEF1 substantially predominates, with the earlier more complete cleavage observed in a mixed population of mitotic and apoptotic cells (results not shown). We have shown here that HEF1 moves out from the centrosome at mitotic entry: speculatively, one model consistent with our data is that phosphorylation by AurA promotes cleavage of centrosomal HEF1 to p55, separation of p55 from the carboxy-terminal centrosomal localization sequences, and removal of HEF1 scaffolding activities at the centrosome. A precedent for such a mitosis-specific regulatory cleavage has recently been published for the MEK1 kinase (47). The nature of the localization sequence between aa 353-398 is not known, but based on the very high serine/threonine content of this region (18 out of 35 residues) is likely to involve a phosphorylation-regulated event. The identity of the putative regulatory kinase, and the role of HEF1 cleavage *in vivo*, is under investigation in our laboratory.

Our data suggest a more important role for HEF1 than Cas in maintaining centrosomal integrity, and imply that epithelial cells are more prone to centrosomal dysfunction than fibroblasts following Cas protein depletion. Indeed, an essential function for p130Cas at the centrosome is incompatible with the observation that p130Cas knockout mice die only at embryonal day 11.5 (48), and that fibroblasts from these cells are viable (49). Our data are congruent with an increasing number of studies that note a cell-type specific component to centrosomal regulation (14) and AurA function. AurA is most commonly upregulated in epithelial cancers (50). The tumor suppressor adenomatous polyposis coli (APC) and its partner beta-catenin, proteins that are predominantly expressed in epithelial cells and associate with epithelial-specific structures, have been shown to also interact directly or indirectly with the centrosome, controlling its organization and function (4, 13, 51). Elegant genetic studies in lower eukaryotic models for development such as C. elegans (reviewed in (52, 53)) have begun to elucidate a model in which dynamic interconnections between the centrosome and structures at the cell cortex controls the plane of mitotic spindle orientation, and cleavage furrow formation. Control of cleavage plane direction is of critical importance in developing organisms, because of the necessity to program growth in specific directions. Speculatively, it is reasonable to propose that control of cleavage plane is more importance in epithelial cells than in fibroblasts in higher eukaryotes, because the intrinsic function of epithelial cells in vivo is to maintain polarized structures that serve barrier functions. In this context, the association an epithelially-enriched protein such as HEF1 with mitotic structures may contribute to coordination of centrosomal orientiation with the focal structures at the basolateral surface of epithelial cells.

Finally, the results presented here have interesting implications for the process of cancer development. A first study by Lingle et al. in 1998 demonstrated that the centrosomes of breast adenocarcinoma cells generally were characterized by abnormal structure, and increased microtubule nucleating capacity in comparison to centrosomes of normal breast epithelial and stromal tissues (54). A number of subsequent studies have firmly documented the association between over-amplification of centrosomes, multipolar mitoses, genomic instability characterized by frequent aneuploidy, and development of aggressive breast cancer (e.g. (43, 55-61)). Some proteins that have well-established signaling roles in breast cancer have been found to take part in the normal centrosomal duplication cycle. For example, the tumor suppressor

BRCA1 normally associates with the centrosome, and interacts with the central centrosomal protein gamma-tubulin. Through interactions at the centrosome with gamma-tubulin and other proteins, BRCA1 restricts centrosomal replication to once per cell cycle; in BRCA1-deficient cells, centrosome amplification is common (58, 61). Overexpression of AurA (also known as BTAK, for breast tumor amplified kinase) has been shown to occur early in breast cancer development, and induce centrosome amplification and aneuploidy (41, 42). However, in many tumors, the provenance of centrosomal defects is not known. Intriguingly, a previous study has associated upregulated expression of a Cas family member in breast cancers as associated with increased malignancy and poor prognosis (62). Our data raise the possibility that deregulated Cas proteins may not only impact cancer development based on their functions in cell migration (metastasis) and resistance to apoptosis, but also in the acquisition of genome instability.

Methods.

Plasmids and constructs. The generation of full length, GFP-tagged HEF1 (45), GST-HEF1 (63). FLAG-tagged HEF1 and deletion mutants: p55 (1-363aa), p55+ (1-406 aa), SH2BDall (82-398aa), 3/4HEF1 (1-652), SRR (352-653) were subcloned into the pCatch–FLAG vector (a gift of Dr. Jonathan Chernoff) to produce FLAG fusion proteins in eukaryotic cells. GFP-p55, GFP-p55+, GST-p55 and GST-p55+ were produced by subcloning this HEF1 deletion fragments into the pEGFP-C4 (Clontech) and pGST (57) plasmids respectively. A full length cDNA of the human p130Cas protein was produced by RT-PCR using a cDNA library from MCF7 cells and specific primers to human p130Cas. The p130Cas cDNA was cloned into the pEGFP-C4 vector and pCatch-FLAG to produce GFP and FLAG–tagged proteins, respectively. HEF1 specific and non-specific peptides (25) were cloned in the retroviral vector pUP (a gift of Dr.Alexey Ivanov) and introduced into MCF-7 cells by infection. To create tet-repressible expression of HEF1 in MCF7, full length HEF1 cDNA was cloned into retroviral vector pUST-4 (A.Ivanov unpublished data). GP-293 cells were used as a packaging cell line to produce retrovirus for infection of the MCF-7-tTa cells (Clontech). To achieve 100% of infection in MCF7 cells the GFP-p55 and GFP-p55+ were cloned in the lentiviral vector pLV-GFP (a gift of Dr. I. Verma). For immunoprecipitation studies of Ajuba and HEF1 interactions we used the following plasmids: pCMV-6-myc-Ajuba, pCMV-6-myc-PreLim-Ajuba, pCMV-6-myc-Lim-Ajuba (64) and pCMV-EGFP as a control.

Cell culture. The human MCF7 (breast adenocarcinoma), HeLa (cervical carcinoma) and FF2425 (normal fibroblast) and MCR5-hTERT (immortalized fibroblasts) cell lines were grown in DMEM supplemented with 10% fetal calf serum at 37°C in a 5% CO_2 atmosphere. The human MCF-12F (normal breast epithelial) cell line was grown in F12/DMEM media supplemented with 5% horse serum, EGFR, insulin, cholera toxin and hydrocortisone (as recommended by the ATCC). The MCF7-GFP-centrin2 and HeLa-GFP-centrin2 stable cell lines were obtained by transfection of the pEGFP-centrin2 plasmid ((65), a gift of Dr. Jeffrey Salisbury) into the MCF7 and HeLa cells, and subsequent G418 selection. Tetracycline-regulated MCF-tTa-HEF1 stable cell lines were obtained by first infecting the parental MCF7-tTa cell line (Clontech) with the pUST-4-HEF1 retroviral vector, then selecting with G418 and puromycin to produce a mass

culture of MCF7-tTa-HEF1 cells. For selection, G418 was used at 500 μg/ml, and puromycin at 1 μg/ml. For lentivirus, 293T cells were used as a packaging cell line, and and irecipient cells MCF-7 treated with the supernatant of 293T transfected cells within 24-48 hours post-transfection. MCF7 cells were lysed at 48 hours post-infection and used for immunoprecipitation assays.

Protein expression, Western blotting, immunoprecipitation (IP) and associated antibodies. Recombinant proteins used for pulldown and IP were expressed in BL21 (DE3) bacteria, induced with 300 μM IPTG, and purified using the MicroSpin GST Purification module (Amersham Biotech.). For Western blotting and immunoprecipitation (IP), mammalian cells were disrupted by M-PER lysis buffer (PIERCE) or NET2 buffer (50mM Tris-HCl pH7.5, 150mM NaCl, 0.05% Triton-X100) in the presence of complete protease inhibitors cocktail, and equivalent protein loads of whole cell lysates used either directly for SDS-polyacrylamide gel electophoresis (SDS-PAGE), or for IP. IP samples were incubated overnight with antibody at 4°C, subsequently incubated for 2 hours with protein A/G-sepharose (Sigma), washed 3 times in lysis buffer supplemented with protease inhibitors, and resolved by SDS-PAGE. Western blotting was done using standard procedures and developed by chemoluminescence using the West-Pico system (Pierce Co.), following the manufacturer's recommendations.

Transiently transfected cells were analyzed for protein expression at 24 or 48 hours hours post-transfection. Transfection procedures were carried out by 5 hour incubation in Lipofectamine 2000 reagent (Invitrogen) for plasmid transfection, or Oligofectamine (Invitrogen) for siRNA oligonucleotide transfection. Antibodies used for Western assay were the following: rabbit polyclonal antibody to HEF1 (10), at a 1:100 dilution, anti-α-tubulin-mouse monoclonal (Sigma; 1:10,000), mouse monoclonal anti-γ-tubulin (GTU-88, Sigma; 1:5,000), anti-p130Cas (Transduction Labs, 1:2000), anti-AuroraA (Pharmingen, 1:1,000), anti-Phospho-AuroraA (Cell Signaling, 1:1000), mouse monoclonal anti-Myc tag E910 (Santa Cruz: for IP), rabbit polyclonal anti-Myc (A14, Santa Cruz: for Western), and mouse monoclonal anti-FLAG (Sigma). The secondary anti-mouse or anti-rabbit HPR conjugated antibody were supplied by Amersham Biotech and used at a dilution of 1:10000 or 1:20000.

siRNA experiments RNA oligonucleotides duplexes were synthesized targeted to HEF1, to p130CAS, Ajuba, and Aurora A. These and a negative control scrambled siRNA were obtained from (Dharmacon). After transfection of siRNAs, degree of depletion of target proteins was determined by Western blot.

Preparation of cells and synchronization procedures. For observation of cells initially synchronized at the G1/S boundary, cells were initially incubated for 16-18 hours in the presence of 2mM Thymidine (Sigma). Some cells were then washed 2 times in PBS, then returned to fresh medium and allowed to grow for 9-12 hours to observe synchronized progression to mitosis. For synchronization at G2/M boundary, cells were incubated in 1μM nocodazole for 14 hours, and collected by shake-off. Collected cells were washed 3 times in PBS, then either replated in fresh medium on the glass cover slips and cultured at 37°C for up to 90 minutes, then fixed for immunofluorescence analysis; or lysed for Western and IP analysis. As an alternative drug-free synchronization approach, in some cases an elutriating centrifuge (Beckman J) was used to enrich for G1 or mitotic populations. For elutriation of MCF7 cells the following conditions were used: speed 1800 rpm, 4°C, and a starting flow rate of 5.5 ml/min. Flow rate was stepped up by increments of 0.5 ml/min, with fractions collected at each step. In a typical experiment, G1 cells were found in fractions 1 and 2, while fractions 5 and 6 were enriched for cells in G2/M. For all the synchronization procedures, the predicted cell cycle compartmentalization was confirmed by use of fluorescence-activated cell sorter (FACS) analysis.

Immunofluorescence (IF). For IF, cells growing on cover slips were fixed with 4% paraformaldehyde for 10 minutes, washed with 1xPBS, then incubated with cold (-20°C) methanol for 2-3 minutes. They were permeabilized with 1% Triton X-100 in 1xPBS for 10 minutes, then blocked in 3% BSA, 0.1% Triton X-100 in 1xPBS for 1 hour. Cover slips were incubated with a primary antibody for 1 hour, washed 3 times with PBS, 0.1% Triton X-100, then incubated with secondary, fluorochrome-conjugated, antibody for 1hour, and mounted in Vector shield mounting media (Vector). Primary antibodies included mouse monoclonal anti-AuroraA (Pharmingen, dilution 1:300), rabbit polyclonal anti-phospho-AuroraA Cell Signaling, 1:200), rabbit polyclonal anti-HEF1 1:100, rat monoclonal anti-α-tubulin (Abcam, 1:200), rabbit

polyclonal anti-γ-tubulin (Abcam, 1:200), mouse monoclonal anti-pericentrin (Transduction Labs, 1:250), mouse monoclonal anti-phosphohistone 3 (Upstate). Secondary antibodies were anti-mouse-Alexa-488, anti-rabbit-Alexa488, anti- mouse-Alexa-568, anti-mouse-Alexa-633, anti-rabbit-Alexa 633 (Molecular Probes, Inc.). DNA was stained by TOTO-3 dye (Molecular Probes.) . Confocal microscopy was performed using a Radiance 2000 laser scanning confocal microscope (Bio-Rad laboratories, Hercules, CA) coupled to a Nikon Eclipse E800 upright microscope (Carl Zeiss, Thornwood, NY). Images were obtained separately by independent excitation at 488/568/633 nm to minimize overlapping signals. All optical sectioning was carried out in 0.5 μm increments.

Kinase assay. An in vitro kinase assay was performed using the GST-fused HEF1 deletion mutants prepared as described above for pulldowns. Histone H3 and H1 were used as positive and negative controls for Aurora A phosphorylation. 0.5 μg of recombinant proteins were treated at 30°C for 20 minutes in a 20 μl reaction with 5 ng AuroraA kinase (Upstate) in supplied buffer plus 250 μM ATP and 10 μCi of γ-(^{32}P)ATP. An aliquot without ^{32}P was processed for Coomassie staining in SDS-PAGE.

Acknowledgments. Jeff Salisbury. Jon, Lisa Henske, Maureen Murphy. *Russ for peptides,* Komen and NIH grant to EG, DOD to ENP. Dr.Chumakov and Dr.Ivanov for the pUST and pUP vectors. and Jon for comments, plasmids. Other reagents?

References.

1. Knust, E. & Bossinger, O. (2002) *Science* **298,** 1955-9.
2. Nance, J., Munro, E. M. & Priess, J. R. (2003) *Development* **130,** 5339-50.
3. Severson, A. F. & Bowerman, B. (2003) *J Cell Biol* **161,** 21-6.
4. Yamashita, Y. M., Jones, D. L. & Fuller, M. T. (2003) *Science* **301,** 1547-50.
5. Orly, J. & Sato, G. (1979) *Cell* **17,** 295-305.
6. Ben-Ze'ev, A. & Raz, A. (1981) *Cell* **26,** 107-15.
7. Piel, M., Nordberg, J., Euteneuer, U. & Bornens, M. (2001) *Science* **291,** 1550-3.
8. Yamaguchi, R., Mazaki, Y., Hirota, K., Hashimoto, S. & Sabe, H. (1997) *Oncogene* **15,** 1753-61.
9. Yamakita, Y., Totsukawa, G., Yamashiro, S., Fry, D., Zhang, X., Hanks, S. K. & Matsumura, F. (1999) *J Cell Biol* **144,** 315-24.
10. Law, S. F., Zhang, Y.-Z., Klein-Szanto, A. & Golemis, E. A. (1998) *Mol. Cell. Biol.* **18,** 3540-3551.
11. Raff, J. W., Jeffers, K. & Huang, J. Y. (2002) *J Cell Biol* **157,** 1139-49.
12. Glotzer, M. (2001) *Annu Rev Cell Dev Biol* **17,** 351-86.
13. Etienne-Manneville, S. & Hall, A. (2003) *Nature* **421,** 753-6.
14. Yvon, A. M., Walker, J. W., Danowski, B., Fagerstrom, C., Khodjakov, A. & Wadsworth, P. (2002) *Mol Biol Cell* **13,** 1871-80.
15. Segal, M. & Bloom, K. (2001) *Trends Cell Biol* **11,** 160-6.
16. Jackman, M., Lindon, C., Nigg, E. A. & Pines, J. (2003) *Nat Cell Biol* **5,** 143-8.
17. Hirota, T., Kunitoku, N., Sasayama, T., Marumoto, T., Zhang, D., Nitta, M., Hatakeyama, K. & Saya, H. (2003) *Cell* **114,** 585-98.
18. Bouton, A. H., Riggins, R. B. & Bruce-Staskal, P. J. (2001) *Oncogene* **20,** 6448-58.
19. O'Neill, G. M., Fashena, S. J. & Golemis, E. A. (2000) *Trends Cell Biol.* **10,** 111-119.
20. Hirota, T., Morisaki, T., Nishiyama, Y., Marumoto, T., Tada, K., Hara, T., Masuko, N., Inagaki, M., Hatakeyama, K. & Saya, H. (2000) *J Cell Biol* **149,** 1073-86.
21. Herreros, L., Rodriguez-Fernandez, J. L., Brown, M. C., Alonso-Lebrero, J. L., Cabanas, C., Sanchez-Madrid, F., Longo, N., Turner, C. E. & Sanchez-Mateos, P. (2000) *J Biol Chem* **275,** 26436-40.
22. Rodriguez-Fernandez, J. L., Gomez, M., Luque, A., Hogg, N., Sanchez-Madrid, F. & Cabanas, C. (1999) *Mol Biol Cell* **10,** 1891-907.
23. Mailand, N., Lukas, C., Kaiser, B. K., Jackson, P. K., Bartek, J. & Lukas, J. (2002) *Nat Cell Biol* **4,** 317-22.
24. Marumoto, T., Honda, S., Hara, T., Nitta, M., Hirota, T., Kohmura, E. & Saya, H. (2003) *J Biol Chem.*
25. Serebriiskii, I. G., Mitina, O., Pugacheva, E., Benevolenskaya, E., Kotova, E., Toby, G. G., Khazak, V., Kaelin, W. G., Chernoff, J. & Golemis, E. A. (2002) *Genome Res.* **12,** 1785-91.
26. Meraldi, P. & Nigg, E. A. (2002) *FEBS Lett* **521,** 9-13.
27. Bornens, M. (2002) *Curr Opin Cell Biol* **14,** 25-34.
28. Rieder, C. L., Faruki, S. & Khodjakov, A. (2001) *Trends Cell Biol* **11,** 413-9.
29. Hannak, E., Kirkham, M., Hyman, A. A. & Oegema, K. (2001) *J Cell Biol* **155,** 1109-16.
30. Kiat, L. S., Hui, K. M. & Gopalan, G. (2002) *J Biol Chem* **277,** 45558-65.

31. Liu, X., Elia, A. E. H., Law, S. F., Golemis, E. A., Farley, J. & Wang, T. (2000) *EMBO J.* **19,** 6759-6769.
32. Yi, J. & Beckerle, M. C. (1998) *Genomics* **49,** 314-6.
33. Sadler, I., Crawford, A. W., Michelsen, J. W. & Beckerle, M. C. (1992) *J Cell Biol* **119,** 1573-87.
34. Petit, M. M., Meulemans, S. M. & Van de Ven, W. J. (2003) *J Biol Chem* **278,** 2157-68.
35. Petit, M. M., Mols, R., Schoenmakers, E. F., Mandahl, N. & Van de Ven, W. J. (1996) *Genomics* **36,** 118-29.
36. Kiss, H., Kedra, D., Yang, Y., Kost-Alimova, M., Kiss, C., O'Brien, K. P., Fransson, I., Klein, G., Imreh, S. & Dumanski, J. P. (1999) *Hum Genet* **105,** 552-9.
37. Yi, J., Kloeker, S., Jensen, C. C., Bockholt, S., Honda, H., Hirai, H. & Beckerle, M. C. (2002) *J Biol Chem* **8,** 8.
38. Minegishi, M., Tachibana, K., Sato, T., Iwata, S., Nojima, Y. & Morimoto, C. (1996) *J. Exp. Med.* **184,** 1365-1375.
39. Polte, T. R. & Hanks, S. K. (1997) *J. Biol. Chem.* **272,** 5501-5509.
40. Dutertre, S., Descamps, S. & Prigent, C. (2002) *Oncogene* **21,** 6175-83.
41. Goepfert, T. M., Adigun, Y. E., Zhong, L., Gay, J., Medina, D. & Brinkley, W. R. (2002) *Cancer Res* **62,** 4115-22.
42. Zhou, H., Kuang, J., Zhong, L., Kuo, W. L., Gray, J. W., Sahin, A., Brinkley, B. R. & Sen, S. (1998) *Nat Genet* **20,** 189-93.
43. Kramer, A., Neben, K. & Ho, A. D. (2002) *Leukemia* **16,** 767-75.
44. Meraldi, P., Honda, R. & Nigg, E. A. (2002) *Embo J* **21,** 483-92.
45. O'Neill, G. M. & Golemis, E. A. (2001) *Mol. Cell. Biol.* **21,** 5094-5108.
46. Law, S. F., O'Neill, G. M., Fashena, S. J., Einarson, M. B. & Golemis, E. A. (2000) *Mol. Cell. Biol.* **20,** 5184-5195.
47. Harding, A., Giles, N., Burgess, A., Hancock, J. F. & Gabrielli, B. G. (2003) *J Biol Chem* **278,** 16747-54.
48. Honda, H., Oda, H., Nakamoto, T., Honda, Z., Sakai, R., Suzuki, T., Saito, T., Nakamura, K., Nakao, K., Ishikawa, T., Katsuki, M., Yazaki, Y. & Hirai, H. (1998) *Nat Genet* **19,** 361-365.
49. Honda, H., Nakamoto, T., Sakai, R. & Hirai, H. (1999) *Biochem Biophys Res Commun* **262,** 25-30.
50. Anand, S., Penrhyn-Lowe, S. & Venkitaraman, A. R. (2003) *Cancer Cell* **3,** 51-62.
51. Ligon, L. A., Karki, S., Tokito, M. & Holzbaur, E. L. (2001) *Nat Cell Biol* **3,** 913-7.
52. Schneider, S. Q. & Bowerman, B. (2003) *Annu Rev Genet* **37,** 221-49.
53. Salisbury, J. L. (2003) *Curr Biol* **13,** R88-90.
54. Lingle, W. L., Lutz, W. H., Ingle, J. N., Maihle, N. J. & Salisbury, J. L. (1998) *Proc Natl Acad Sci U S A* **95,** 2950-5.
55. Duesberg, P., Stindl, R. & Hehlmann, R. (2000) *Proc Natl Acad Sci U S A* **97,** 14295-300.
56. Brinkley, B. R. (2001) *Trends Cell Biol* **11,** 18-21.
57. D'Assoro, A. B., Barrett, S. L., Folk, C., Negron, V. C., Boeneman, K., Busby, R., Whitehead, C., Stivala, F., Lingle, W. L. & Salisbury, J. L. (2002) *Breast Cancer Res Treat* **75,** 25-34.
58. Deng, C. X. (2002) *Oncogene* **21,** 6222-7.
59. Hollander, M. C. & Fornace, A. J., Jr. (2002) *Oncogene* **21,** 6228-33.

60. Lingle, W. L., Barrett, S. L., Negron, V. C., D'Assoro, A. B., Boeneman, K., Liu, W., Whitehead, C. M., Reynolds, C. & Salisbury, J. L. (2002) *Proc Natl Acad Sci U S A* **99,** 1978-83.
61. Weaver, Z., Montagna, C., Xu, X., Howard, T., Gadina, M., Brodie, S. G., Deng, C. X. & Ried, T. (2002) *Oncogene* **21,** 5097-107.
62. van der Flier, S., Brinkman, A., Look, M. P., Kok, E. M., Meijer-Van Gelder, M. E., Klijn, J. G., Dorssers, L. C. & Foekens, J. A. (2000) *J Natl Cancer Inst* **92,** 120-7.
63. Law, S. F., Estojak, J., Wang, B., Mysliwiec, T., Kruh, G. D. & Golemis, E. A. (1996) *Mol. Cell. Biol.* **16,** 3327-3337.
64. Kanungo, J., Pratt, S. J., Marie, H. & Longmore, G. D. (2000) *Mol Biol Cell* **11,** 3299-313.
65. D'Assoro, A. B., Stivala, F., Barrett, S., Ferrigno, G. & Salisbury, J. L. (2001) *Ital J Anat Embryol* **106,** 103-10.

Figure Legends.

Figure 1. HEF1 localization to the centrosome peaks in G2. A, B. Nocodazole block and mitotic shake-off of MCF7 cells, followed by re-plating for 0 (**A**) or 30 (**B**) minutes was used to enrich for G2/M cells. γ-tubulin marks centrosomes; phosphorylated histone H3 (P-H3-His) marks mitotic entry. **C.** GFP-HEF1 fusion protein confirms GFP-HEF1 localization at the centrosome in late G2 (arrows), and at the spindle in mitosis. **D.** Cells were synchronized with thymidine, released, and harvested at set timepoints to obtain G1/S, S, and G2/M populations. Shown, phospho-histone H3 (P-H3), HEF1, and centrin staining at indicated phases of cell cycle. **E.** Top, FACS analysis of cells shown in **D**. Bottom, Western analysis of HEF1 levels in the indicated phases of cell cycle and beta-actine as loading control.**F.** Cells transfected with plasmids expressing GFP-p55 or GFP-p55+, and gamma-tubulin.

Figure 2. Overexpression, stabilization, and depletion of HEF1. A. MCF7 cells with tetracycline-repressed expression of stably integrated HEF1 or GFP in the presence (+) or absence (-) of tetracycline, measured at 24 or 48 hours after medium change. Western analysis with antibody to HEF1 demonstrates induction following tetracycline removal: the beta-actin protein was used as a loading control. **B.** Western blot analysis of MCF7 cells infected retroviruses expressing HA-tagged thioredoxin (TRX)-peptide fusion proteins. Levels of HEF1 are stabilized by specific HA-TRX peptides (P1-HEF1, P2-HEF1), but not by non-specific HA-TRX peptides (P1-NS), or by HA-TRX with no peptide inserted (NP). HA shows comparable expression of HA-TRX fusions in all lanes. **C.** Western blot analysis of MCF7 cells treated with siRNAs to HEF1 (siHEF1) or a scrambled control (Scr) shows efficient and specific HEF1 depletion.

Figure 3. Overexpression, stabilization, and depletion of HEF1 induce defects in the centrosomes and the mitotic spindle. A. MCF7 cells with tet-repressed HEF1 were uninduced (left panel) or induced by tetracycline removal (+HEF1, right 4 panels). Cells were treated to visualize DNA (blue) alpha-tubulin (green) and gamma-tubulin (red) for immunofluorescence; 4 representative mitoses are shown. **B.** Quantitation of multipolar spindles scored in cells with induced indicates the percentage of cells with multipolar spindles in the presence (+) or absence

(-) of overexpressed HEF1, an overexpressed GFP control, or following treatment with HEF1-specific (H) or non-specific (NS) peptide, or negative control (NP) HA-TRX fusions. 3 independent experiments were performed, resulting in the assessment of 150 mitoses in total for each condition. **C.** MCF7 cells were transfected with either a control scrambled (left panels), or an siRNA specific for HEF1(-HEF1; center and right panels) for 48 hours, then processed for immunofluorescence using markers to gamma-tubulin (red), alpha-tubulin (green), and DNA (blue). Shown, representative mitoses: top panels are a merged image. **D.** Immunofluorescence analysis of MCF7 cells with stably expressed GFP-centrin2 (green) 48 hours post-transfection of scrambled (Scr) or HEF1-directed (-HEF1) siRNAs was used to calculate the frequency of split (top panel, -HEF1) versus closely paired (bottom panel -Scr) centrioles. For quantification (discussed in Results), data were collected from at least three independent experiments, and 150 cells were counted for HEF1-depleted or control cells.

Figure 4. HEF1 associates with AurA and control AurA activation. **A.** MCF7 cells were depleted with HEF1-directed siRNA (-HEF1) or a scrambled control (Scr). Mitotic cells stained with antibodies directed at AurA (green), phospho-AurA (P-AurA, red), and DNA (blue) are shown. **B.** MCF7 cells were transfected with scrambled control (Scr) or HEF1-directed (-HEF1) siRNA for 48 hours, then collected and part of the sample elutriated. Non-elutriated (Asyn.), G1/S, or G2-M enriched populations were used for Western blot analysis using the antibodies indicated (left). **C.** MCF7 cells prepared as in **B** were used for co-immunoprecipitation. Top, immunoprecipitation with control IgG (left lane only) or Cas antibody (cross-reactive with p130Cas and HEF1), and Western blot using antibodies as indicated to left. Bottom, immunoprecipitation with control IgG or AurA antibody, and Western blot as indicated.

Figure 5. Delineation of the HEF1-AurA interaction. **A.** MCF7 cells were mock-infected or infected with a pLV- plasmid encoding GFP-p55+ or GFP-p55, immunoprecipitated with either control IgG (left lane) or antibody to GFP (right two lanes), and Western blot visualization with antibodies to GFP or AurA, as indicated. **B.** In vitro kinase assay. Comparable levels of GST-fusion proteins, or histone H1 or H3 (left panel) were incubated with AurA and gamma-32-P in vitro. Right panel, autoradiograph of in vitro phosphorylated AurA substrates. **C.** MCF7 cells were treated with either scrambled siRNA (Scr), or AurA-targeting siRNA (-AurA). Nocodazole

arrested or thymidine arrested cells, either treated or untreated with ALLN, were lysed, and blotted with antibodies as indicated at left.

Figure 6. Mapping the HEF1-Ajuba interaction. **A.** Cells were transfected with FLAG-tagged full length HEF1 (Flag-FL), N-terminus (Flag-N), or C-terminus (Flag-C), in combinations with GFP or Myc-tagged full length Ajuba (Aj) or the Ajuba Pre-LIM domain (PL). Top three panels, left: input Ajuba derivatives, visualized with Myc antibody. Right panel: input HEF1 derivatives, visualized with FLAG antibody. Bottom three panels, left: Ajuba co-immunoprecipitated by FLAG antibody, visualized with Myc antibody. **B.** Cells transfected with HA-tagged full length HEF1, and either Myc vector or Myc tagged full length Ajuba (Aj), Ajuba pre-LIM domain (PL), or LIM domain (L). Right panels, input. Left panels, top, coimmunoprecipitated HEF1, visualized with antibody to HA; bottom, immunoprecipitated Ajuba. **C.** Experimental setup as in B, except cells contain full length HEF1 (left) or N-terminal HEF1 (right). **D.** Experimental setup as in B., except HA-HEF1 co-transfected with Myc vector or full length Ajuba (Aj), LIMD1 (LM), LPP1 (LP), or zyxin (Zx).

Figure 7. Comparison of HEF1 and p130Cas action at the centrosome. **A.** FF2425, MCF7, or HeLa cells were depleted with siRNA targeting HEF1 (-HEF1), p130Cas (-130) or a scrambled control (Scr). The percent of split centrosomes was scored; blue, un-split; red, split centrosomes. For each data point, 50 cells were counted in each of 3 separate experiments (150 cells total). **B.** Western blot, analyzing levels of HEF1 and p130Cas in MCF7 cells treated with siRNA as for A. beta-actin represents a loading control. **C.** GFP-fused p130Cas (GFP-Cas) or GFP-fused HEF1 (GFP-HEF1) were expressed in either FF2425 or MCF7 cells. Inset, enlarged view of centrosomes. **D.** MCF7 cells with siRNA-depleted p130Cas, visualizing AurA, phospho-AurA (P-AurA), and phospho-histone H3 (P-H3).

Figure 8. Transient appearance of >4N populations in HEF1-depleted cells. FACS analysis of fraction 5 of elutriated MCF7 cells 48 hours after treatment with HEF1-directed (-HEF1) or scrambled control (Scr) siRNAs (Top); or after 24 additional hours of growth following elutriation prior to FACS analysis. See results for details. Comparable results were obtained in MCF12F cells (data not shown).

A.

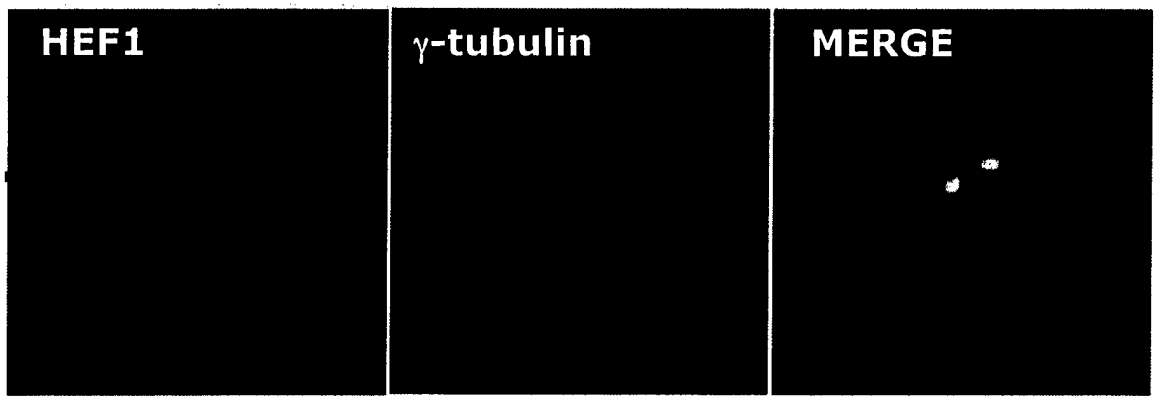

C.

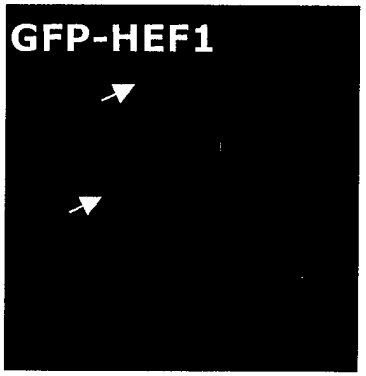

B.

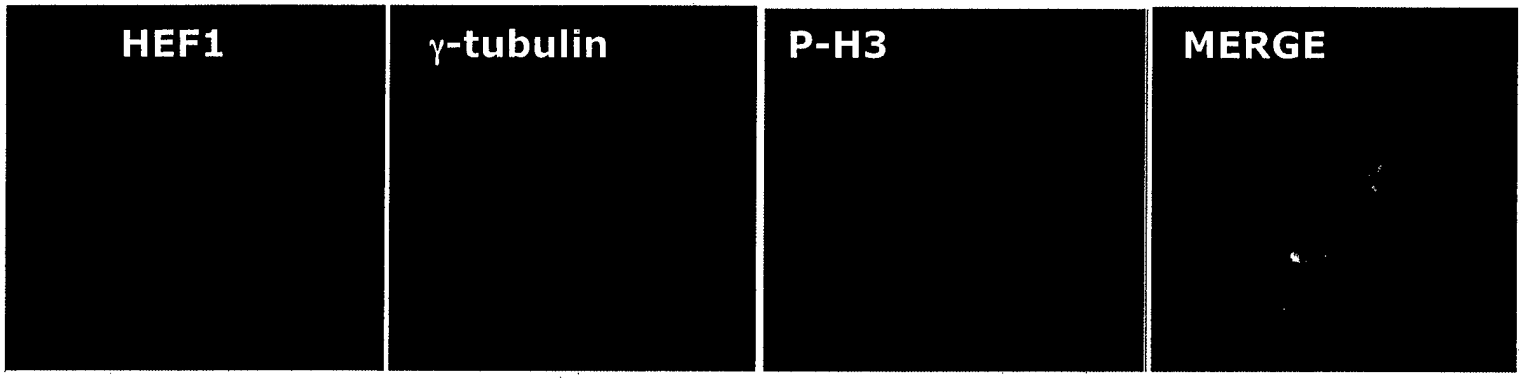

Figure 1

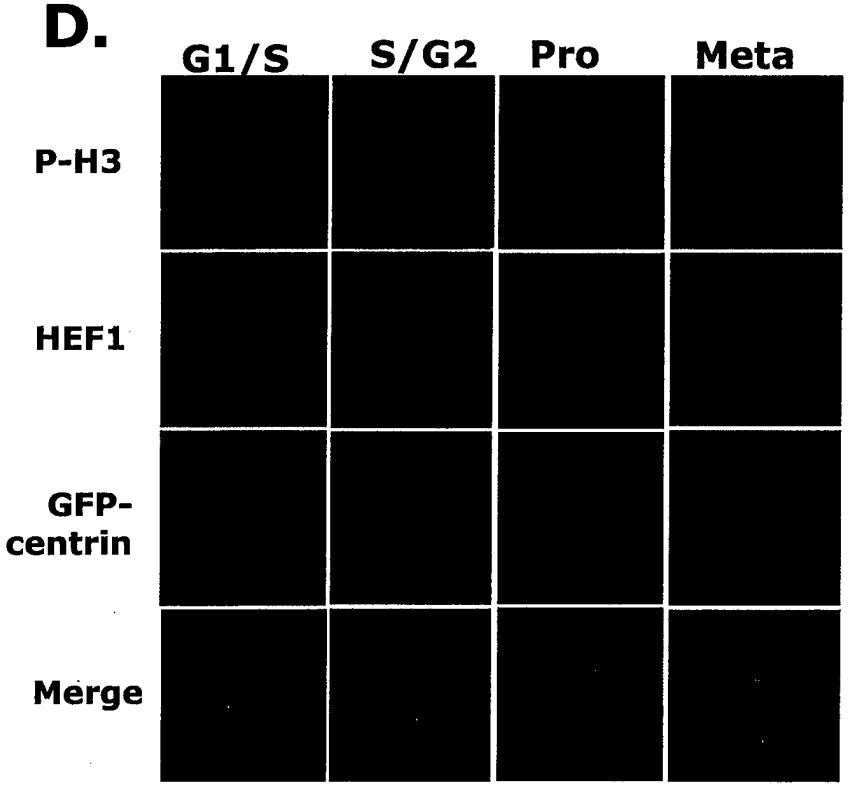
D.
G1/S
S/G2
Pro
Meta
P-H3
HEF1
GFP-centrin
Merge

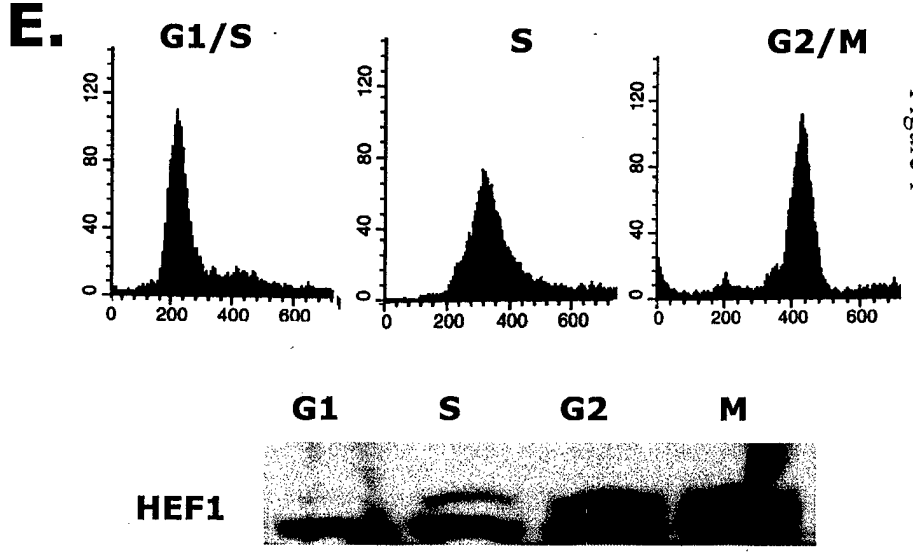
E.
G1/S
S
G2/M
0
40
80
120
0
200
400
600
G1
S
G2
M
HEF1

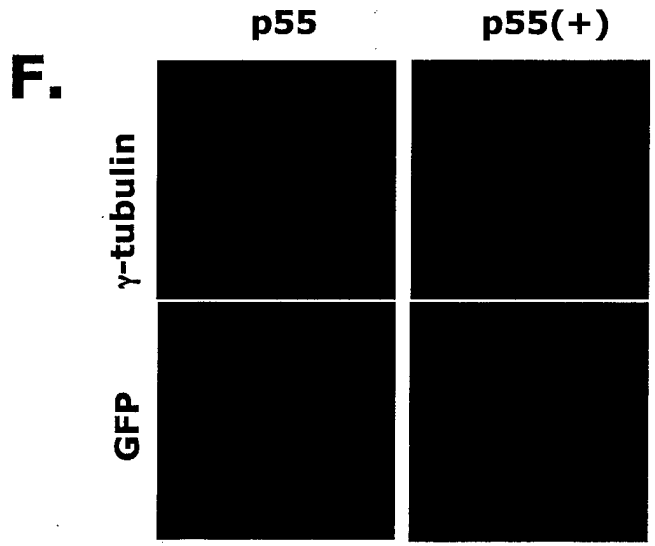
F.
p55
p55(+)
γ-tubulin
GFP

Figure 1

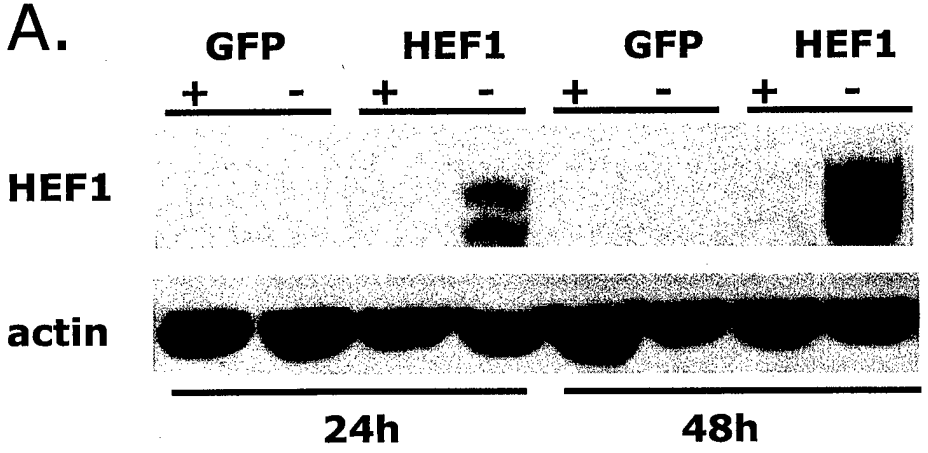
A.
GFP
HEF1
GFP
HEF1
+ - + - + - + -
HEF1
actin
24h
48h

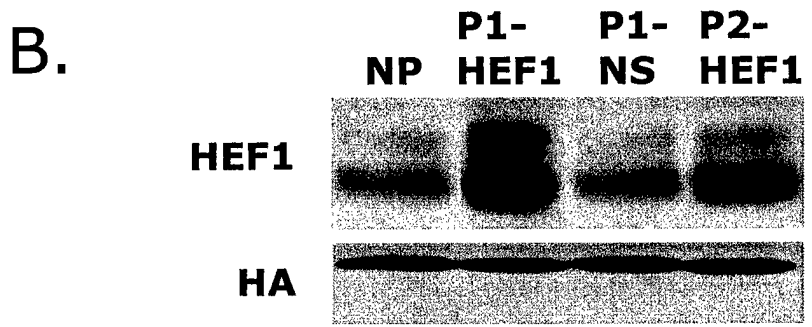
B.
NP
P1-HEF1
P1-NS
P2-HEF1
HEF1
HA

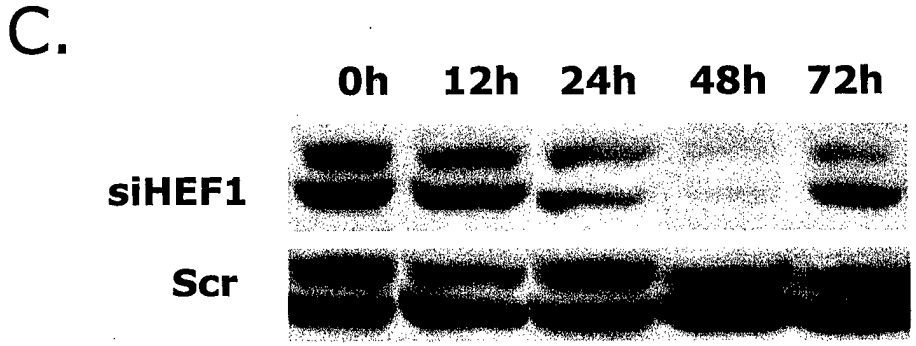
C.
0h
12h
24h
48h
72h
siHEF1
Scr

Figure 2

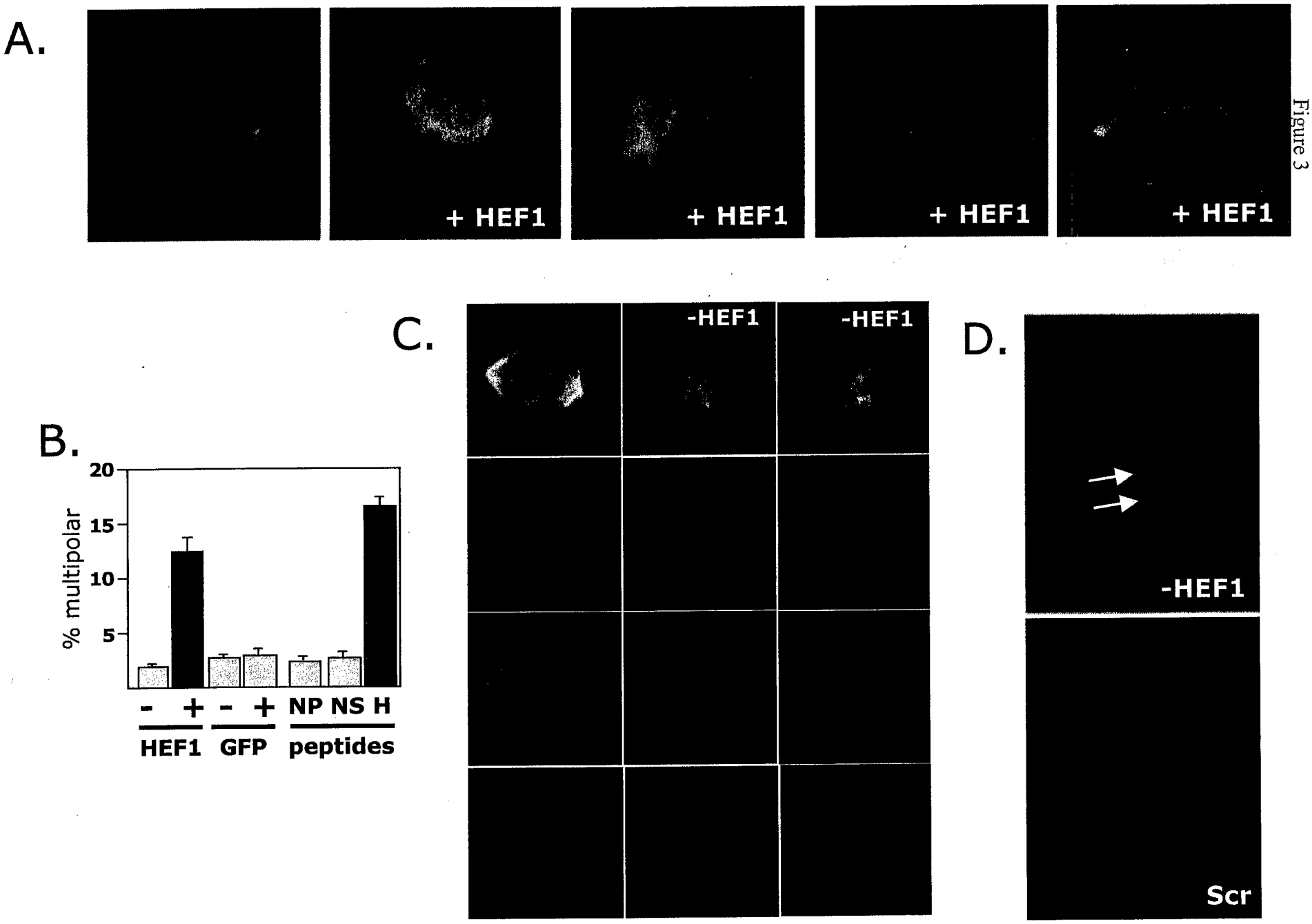
A.
+ HEF1
+ HEF1
+ HEF1
+ HEF1
B.
% multipolar
20
15
10
5
- + - + NP NS H
HEF1
GFP
peptides
C.
-HEF1
-HEF1
D.
-HEF1
Scr

Figure 3

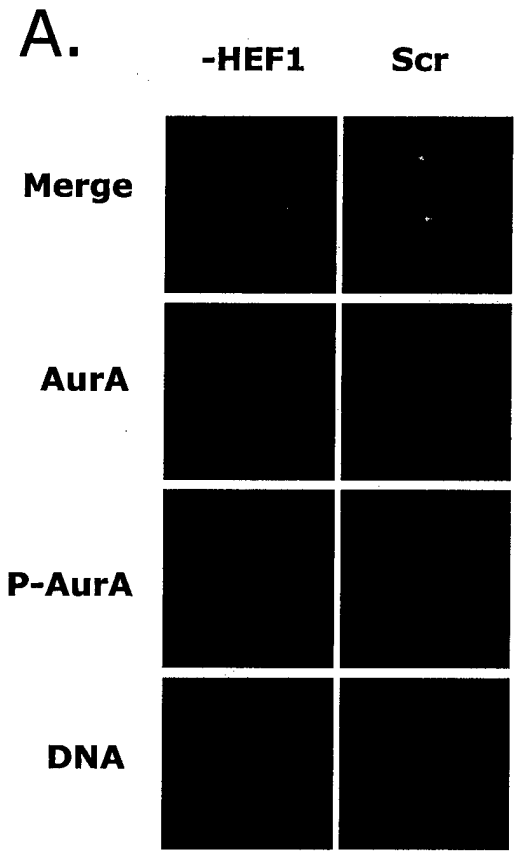
A.
-HEF1
Scr
Merge
AurA
P-AurA
DNA

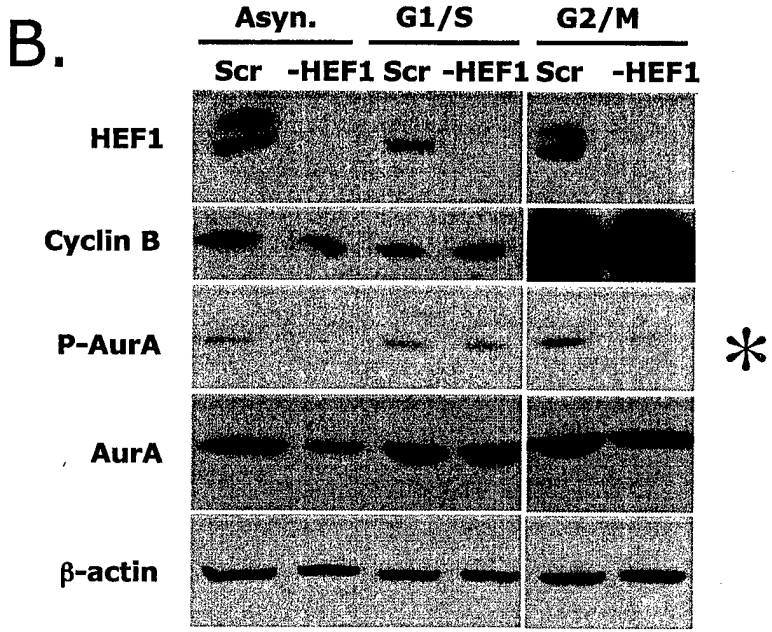
B.
Asyn.
G1/S
G2/M
Scr
-HEF1
Scr
-HEF1
Scr
-HEF1
HEF1
Cyclin B
P-AurA
AurA
β-actin
*

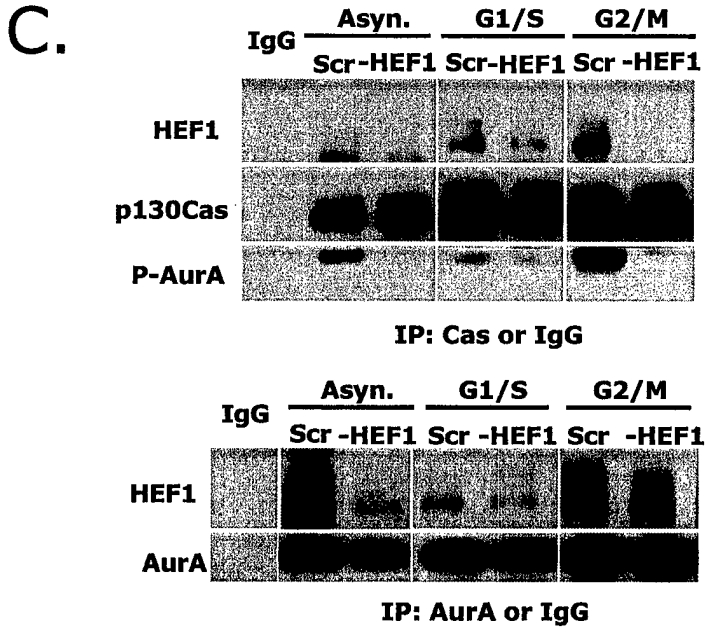
C.
IgG
Asyn.
G1/S
G2/M
Scr
-HEF1
Scr
-HEF1
Scr
-HEF1
HEF1
p130Cas
P-AurA
IP: Cas or IgG
IgG
Asyn.
G1/S
G2/M
Scr
-HEF1
Scr
-HEF1
Scr
-HEF1
HEF1
AurA
*
IP: AurA or IgG

Figure 4

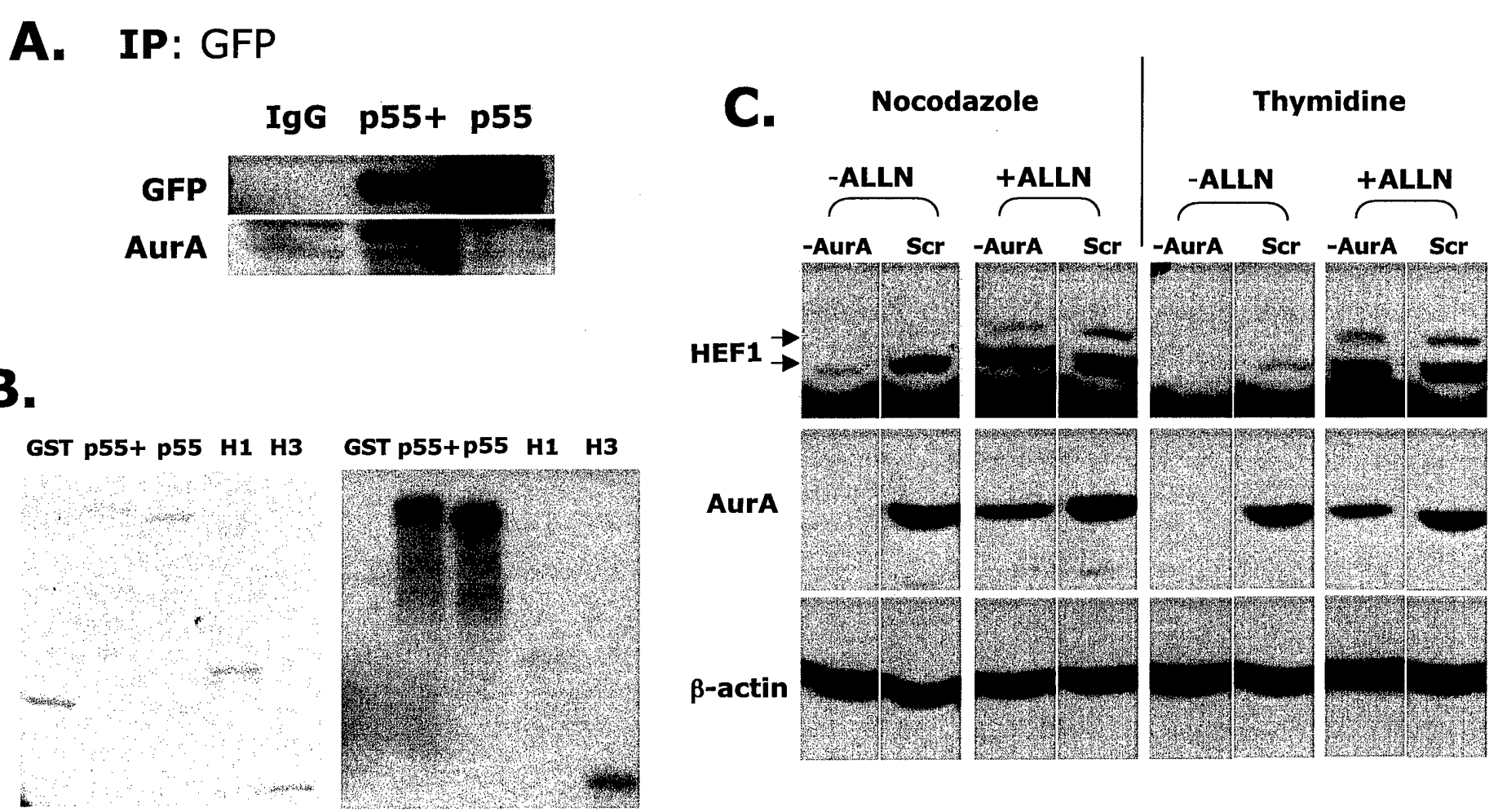
A.
IP: GFP
IgG
p55+
p55
GFP
AurA
B.
GST
p55+
p55
H1
H3
GST
p55+
p55
H1
H3
C.
Nocodazole
Thymidine
-ALLN
+ALLN
-ALLN
+ALLN
-AurA
Scr
-AurA
Scr
-AurA
Scr
-AurA
Scr
HEF1
AurA
β-actin

Figure 5

Figure 6

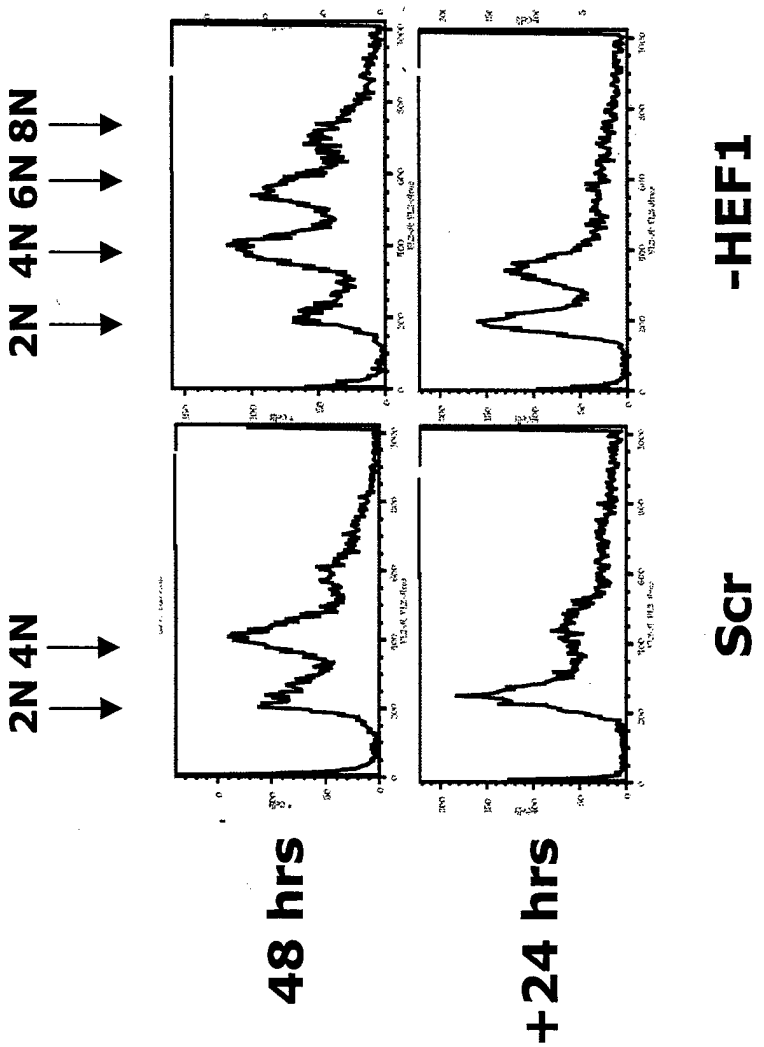

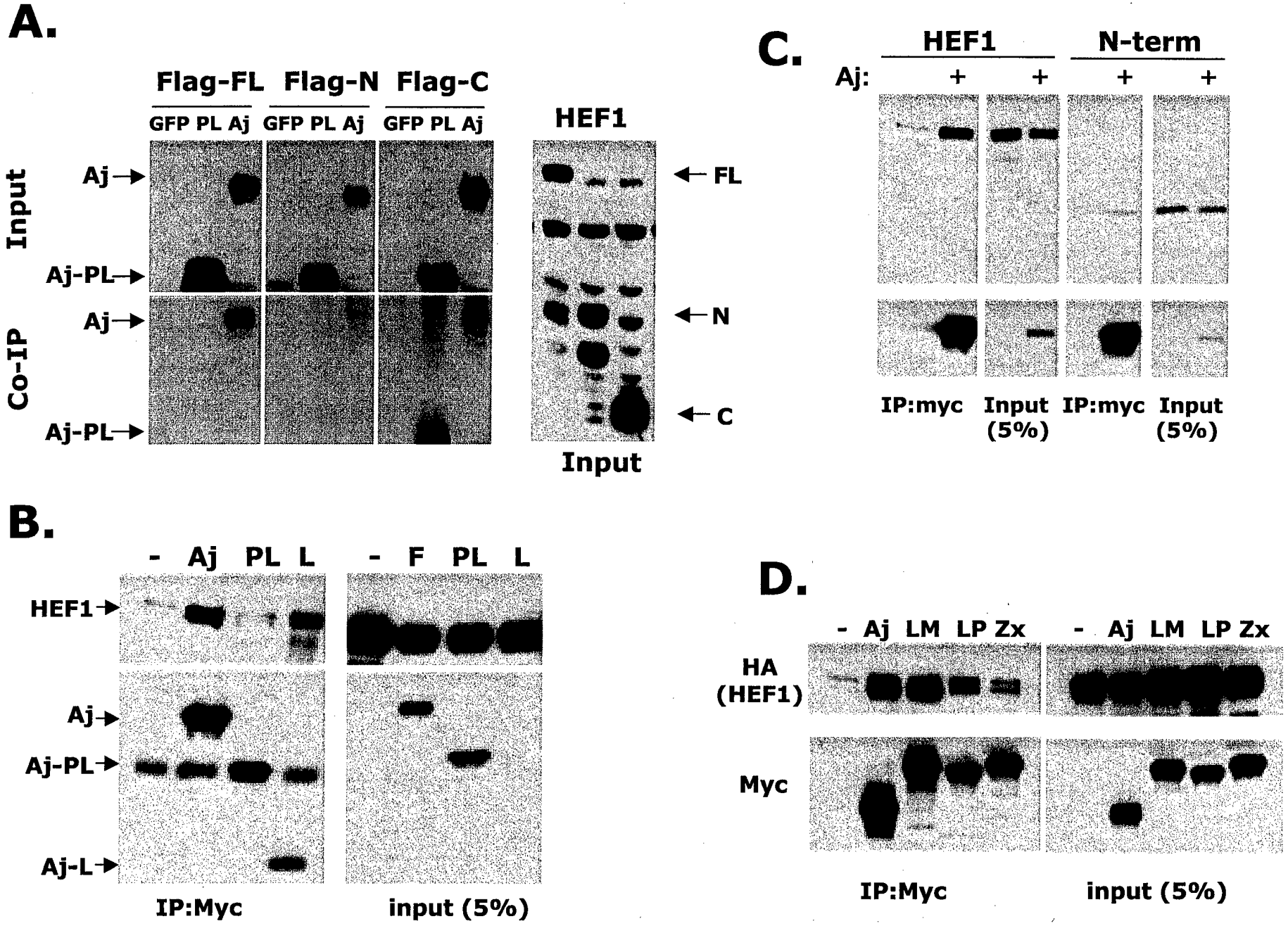
A.
Flag-FL
Flag-N
Flag-C
GFP PL Aj GFP PL Aj GFP PL Aj
Input
Co-IP
Aj
Aj-PL
Aj
Aj-PL
HEF1
FL
N
C
Input
B.
- Aj PL L
- F PL L
HEF1
Aj
Aj-PL
Aj-L
IP:Myc
input (5%)
C.
HEF1
N-term
Aj: + + + +
IP:myc
Input (5%)
IP:myc
Input (5%)
D.
- Aj LM LP Zx
- Aj LM LP Zx
HA (HEF1)
Myc
IP:Myc
input (5%)

Figure 7

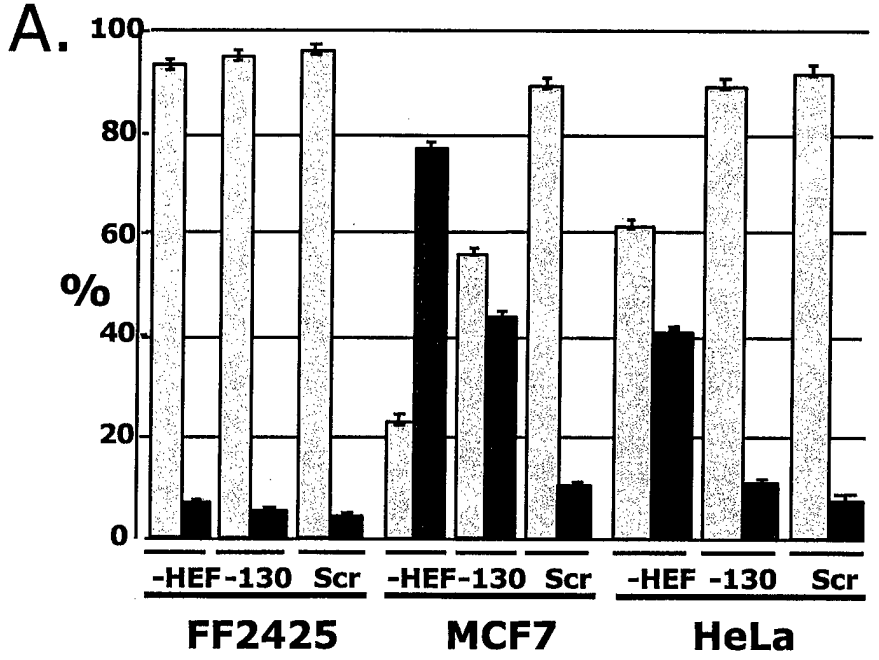
A.
100
80
60
%
40
20
0
-HEF -130 Scr
-HEF -130 Scr
-HEF -130 Scr
FF2425
MCF7
HeLa

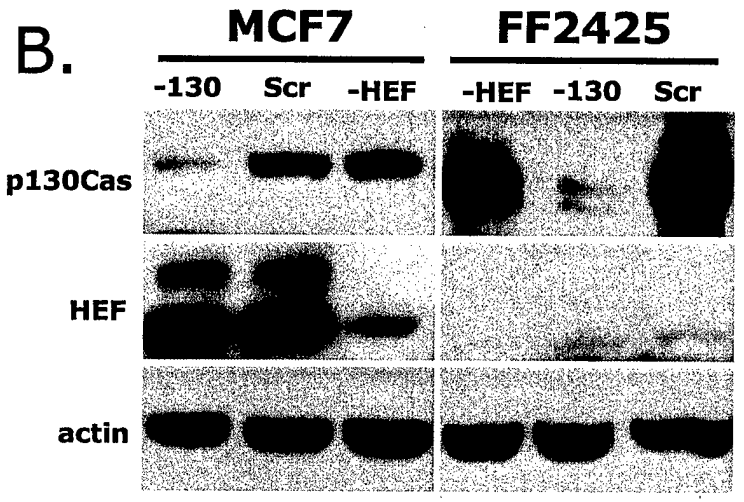
B.
MCF7
FF2425
-130 Scr -HEF
-HEF -130 Scr
p130Cas
HEF
actin

Figure 8

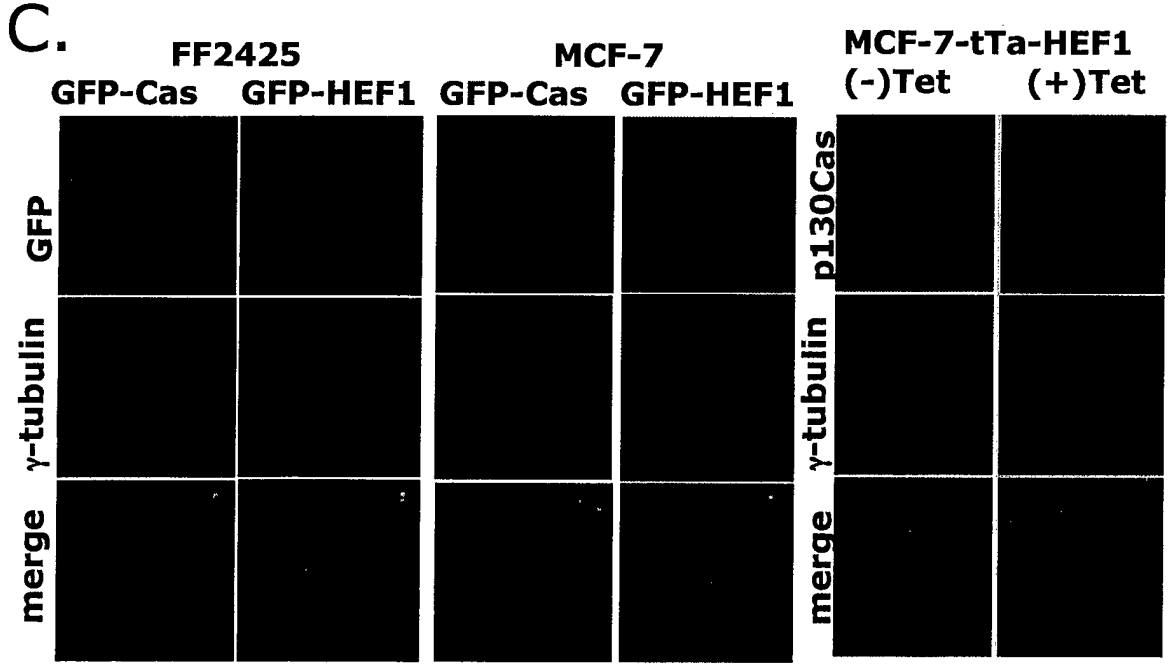
C.
FF2425
MCF-7
MCF-7-tTa-HEF1
GFP-Cas GFP-HEF1 GFP-Cas GFP-HEF1
(-)Tet (+)Tet
GFP
γ-tubulin
merge
p130Cas
γ-tubulin
merge

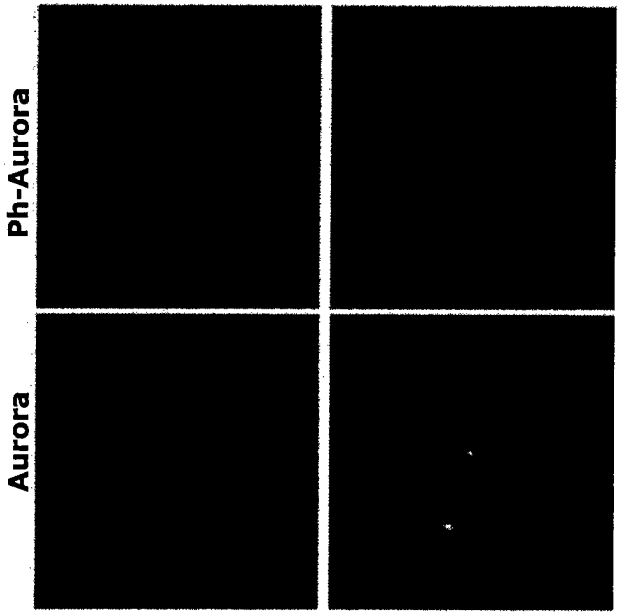
D.
Ph-Aurora
Aurora

FCCC-Poster for Postdoc Day, 2004

Involvement of Akt in vitamin E succinate-induced apoptosis

Huihong You and Joseph R. Testa

Human Genetics, Fox Chase Cancer Center, Philadelphia, PA 19111

Vitamin E succinate (VES; RRR-α-tocopheryl succinate) is a derivative of natural vitamin E. Previous studies have shown that VES is a potent antitumor agent. Treatment of human breast cancer cells with VES is known to induce apoptosis, at least in part, via the mitogen-activated protein kinase (MAPK) signaling pathway. Whether other cell signaling cascades are affected by VES has not been addressed to date. AKT is activated by various growth factors and mediates signals involved in diverse cellular processes, including cell growth and cell survival. AKT is frequently activated in human breast cancers and may contribute to chemoresistance. In this investigation, we sought to determine whether VES attenuates AKT signaling. We found that VES markedly inhibits the growth of breast cancer cell lines and induces apoptosis in a time- and dose-dependent manner. We also found that treatment with VES results in decreased AKT activity. Pharmacologic inhibition of PI3K/AKT signaling by LY294002 potentiated the growth inhibitory and pro-apoptotic effects of VES, in connection with dephosphorylation of various downstream effectors of AKT, such as GSK3β and mTOR. Other experiments showed that the protein phosphatase PP2A modulates AKT activity during VES-induced apoptosis. Collectively, these data suggest that the apoptotic effect of VES on human breast cancer cells is mediated not only via MAPK signaling but also by inhibiting AKT. These findings provide mechanistic evidence in support of the potential use of VES as a chemopreventive or chemotherapeutic agent, and suggest that VES may have enhanced effects on breast cancer cells dependent on AKT activity for survival.

*This work was performed by a DOD training grant DAMD17-00-1-0249 to J. Russo.

Control/Tracking Number : 04-AB-3854-AACR
Activity : Abstract Submission
Current Date/Time : 11/7/2003 10:58:47 AM

"Role of 17p13.2 in the neoplastic transformation of human breast epithelial cells."

Sandra V. Fernandez, Mohamed Lareef, Irma Russo, Binaifer R. Balsara, Joseph Testa, Jose Russo. Fox Chase Cancer Center, Philadelphia, PA

Role of 17p13.2 in the neoplastic transformation of human breast epithelial cells.
Mohamed Lareef, Sandra V. Fernandez, Irma H. Russo, Binaifer R. Balsara, Joseph Testa, and Jose Russo. *Breast Cancer Research Laboratory and Human Genetics Program, Fox Chase Cancer Center, Philadelphia, PA.*
Genomic alterations on chromosome 17 play an important role in breast cancer development. To further investigate the role of chromosome 17 in the initiation and progression of breast cancer, we have used an *in vitro* experimental system in which a human chromosome 17 was introduced into BP1E, a transformed cell line derived from benzo(a)pyrene (BP)-treated human breast epithelial cells MCF-10F (Carcinogenesis 14:483-492,1993). Microcell mediated chromosome transfer technique (MMCT) was used for chromosome transfer. MCF-10F cells do not form colonies in agar methocel and form ductules in collagen, whereas the transformed BP1E cells do form colonies and have lost their ductulogenic capacity. Transfer of chromosome 17 originated BP1E-17neo cells, which, like MCF-10F cells, did not form colonies in agar methocel, formed ductules in collagen, and their doubling time was reduced two-fold below the values observed in BP1E cells. Cytogenetic characterization of the cell lines MCF-10F, BP1E and BP1E-17neo was performed using a combination of the standard G-banding analysis and comparative genomic hybridization (CGH). BP1E-17neo cells exhibit the same chromosomal abnormalities observed in BP1E cells, having an additional chromosome 17. The extra copy of chromosome 17 appeared to be rearranged, containing most of the p arm and a portion of 17q. CGH analyses showed that it had only the most telomeric region of the q arm (q24.3 through q25.2). Microsatellite analysis performed using more than 30 markers for chromosome 17 revealed that the transformed cell line BP1E had an allelic imbalance on chromosome 17 p13.2 (D17S796), and that the transfer of chromosome 17 abrogated the transformed phenotype and corrected the allelic imbalance on this locus. Allelic imbalances in chromosome 17p13.2 (D17S796) have been identified by others investigators in atypical ductal hyperplasia and ductal carcinoma *in situ* of the breast (J. Pathol. 187:272-278, 1995). In summary, transfer of chromosome 17 suppressed the growth and transformation phenotypes of BP1E cells indicating that chromosome 17 p13.2 (D17S796) hosts one or more tumor suppressor genes that could be involved in early stages of breast cancer. (This work was supported by DAM17-01-0249 and DAM17-02-1-0384).
Author Disclosure Block: S.V. Fernandez, None; **M. Lareef**, None; **I. Russo**, None; **B.R. Balsara**, None; **J. Testa**, None; **J. Russo**, None.

Category and Subclass (Complete): CB3-02 Identification of new cancer genes

Keyword (Complete): Breast cancer ; Tumor suppressor genes ; Comparative genomic hybridization
Sponsor (Complete):
2004 Travel Awards (Complete):
Payment (Complete): Your credit card order has been processed on Thursday 6 November 2003 at 7:29 PM.
Status: Complete

If you have any questions or experience any problems, please contact Customer Support at aacr@dbpub.com or call (617) 621-1398 or (800) 375-2586.

Role of 17p13.2 in the neoplastic transformation of human breast epithelial cells.

Mohamed Lareef [1], Sandra V. Fernandez [1], Irma H. Russo [1], Binaifer R. Balsara [2], Joseph R. Testa [2] and Jose Russo [1,3].

[1] Breast Cancer Research Laboratory, Fox Chase Cancer Center, Philadelphia, Pennsylvania.
[2] Human Genetics Program, Division of Population Sciences, Fox Chase Cancer Center, Philadelphia, Pennsylvania.

[3]To whom correspondence should be addressed:

Jose Russo, MD, FCAP

Director

Breast Cancer Research Laboratory

Fox Chase Cancer Center

7701 Burholme Avenue

Philadelphia, PA 19111, USA

Phone: 215- 728-4782

FAX: 215-728-2180

E-mail: J_Russo@fccc.edu

Key words: Breast cancer, MCF10F, Cell transformation, 17p13.2, D17S796.

Short title: 17p13.2 in cell transformation

Abstract

Genomic alterations of chromosome 17 play an important role in breast cancer development. To further investigate the role of chromosome 17 in the initiation and progression of breast cancer, we have used an *in vitro* experimental system in which a human chromosome 17 was introduced into BP1E, a transformed cell line derived from benzo(a)pyrene (BP)-treated human breast epithelial cells MCF-10F. Microcell mediated chromosome transfer technique (MMCT) was used for chromosome transfer. MCF-10F cells do not form colonies in agar methocel and form ductules in collagen, whereas the transformed BP1E cells do form colonies and have lost their ductulogenic capacity. Transfer of chromosome 17 originated BP1E-17neo cells, which, like MCF-10F cells, did not form colonies in agar methocel, formed ductules in collagen, and their doubling time was increased 1.5-fold compared to that observed in BP1E cells. Cytogenetic analysis confirmed the presence of an additional chromosome 17 in BP1E-17neo cells. The extra copy of chromosome 17 was rearranged, containing most of the p arm and a portion of 17q. Comparative genomic hybridization analyses showed that it had only the telomeric region of the q arm (q22-ter). Microsatellite analysis performed using 33 markers for chromosome 17 revealed that the transformed cell line BP1E had an allelic imbalance at chromosome 17p13.2 (D17S796), and that the transfer of chromosome 17 abrogated the transformed phenotype and corrected the allelic imbalance at this locus. Allelic imbalances in chromosome 17p13.2 (D17S796) have been identified by others investigators in atypical ductal hyperplasia and ductal carcinoma *in situ* of the breast. In summary, transfer of chromosome 17 suppressed the growth and transformation phenotype of BP1E cells, suggesting that chromosome 17p13.2, in the vecinity of D17S796, harbors one or more tumor suppressor genes that could be involved in early stages of breast cancer.

Introduction.

Genomic alterations of chromosome 17 play an important role in the initiation and progression of human breast cancer (Bieche et al., 1995; Callahan et al., 1993; Chen et al., 1991; Radford et al, 1995). This chromosome contains the oncogene HER2/neu located at 17q21.1 (Gullick, 1990) and three known tumor suppressor genes (TSG) (Futreal et al., 1992; Seizinger, 1993; Harris and Hollstein, 1993); TP53 located at 17p13.1, NF1 at 17q11.2 and BRCA1 at 17q21.31. There are also several putative TSGs such as HIC1 and OVCA2 both located at 17p13.3, ELAC2 at 17p12, TOC at 17q25 and DMC1 at 17q25.2 (Kirchweger et al., 1994; Risk et al., 1994; Wales et al., 1995; Phillips et al., 1996; Schultz et al., 1996; Bruening et al., 1999; Harada et al., 2001; Tavtigian et al., 2001). Allelic losses from 17p have been observed in the absence of any detectable anomaly at the TP53 locus (Coles et al., 1990; Biegel et al., 1992; Osborne et al., 1991), and alterations on 17q have been found in addition to the amplification of the HER2/neu or the inactivation of NF1 (Cornellis et al., 1993). The PHB gene (prohibitin) at 17q21.33 may be important in breast cancer progression, whereas the RARA gene on 17q21.2 has been implicated in acute promyelocytic leukemia (Sato et al., 1992; Borrow et al., 1990).

To further investigate the role of chromosome 17 in the initiation and progression of human breast cancer, we have used an *in vitro* experimental system in which a normal human chromosome 17 was introduced into the transformed cell line BP1E using microcell mediated chromosome transfer (MMCT). Transfer of chromosome 17 into BP1E cells produced the cell line BP1E-17neo. We have used Comparative Genomic Hybridization (CGH) to evaluate chromosomal imbalances in the whole genome and microsatellite analysis to narrow down the

different areas of chromosome 17 that have been modified by the transformation process. We show that the transformed BP1E cell line has an allelic imbalance on chromosome 17p13.2 in the D17S796 region. Introduction of chromosome 17 corrected this imbalance with the concomitant reversion of the transformed phenotype.

Materials and Methods.

Cell lines.

The following human breast epithelial cells were used: MCF-10F (passage 126), BP1E (passage 37) and BP1E-17neo (passage 13). The MCF-10F cell line is a spontaneously immortalized human breast epithelial cell line (Soule et al, 1990; Tait and Russo, 1990). The BP1E cell line was derived from MCF-10F transformed by the carcinogen benzo(a)pyrene (BP) (Calaf et al., 1993). The BP1E cells express all the phenotypes indicative of neoplastic transformation such as colony formation in agar methocel and loss of ductulogenesis in collagen matrix (Calaf et al., 1993). BP1E was used for MMCT of human normal chromosome 17, which generated a cell line designated BP1E-17neo. This cell line (BP1E-17neo II-3) was maintained in high calcium media with 5% horse serum and geneticin (400 μg/ml).

Microcell mediated chromosome transfer (MMCT).

BP1E cells were fused with microcells prepared from mouse A9 cells containing a human chromosome 17 tagged with the selectable gene *neo*. Human chromosome donor cells A9-17 neo were treated with 0.1μg/ml colcemid for 48h. Microcells were collected in DMEM medium

containing 10μg/ml cytochalasin B by centrifugation at 8,000 rpm for 60 min. Microcells were purified through 8, 5 and 3 μm-pore polycarbonate filters and resuspended in serum free medium containing 100μg/ml phytohemaglutinin. Exponentially growing BP1E cells were incubated with the microcell suspension at 37°C for 15 min. They were treated with polyethylene glycol (MW=13-16K) for 1 min and washed with serum free medium. The cells were allowed to recover in regular medium overnight. Following trypsinization, 10^6 cells were plated in 100-mm^2 Petri dishes with medium containing geneticin (400 μg/ml) for selection. As a representative of the chromosome 17 transfer experiments, the BP1E-17neo clone II-3 was chosen for this work (Lareef et al, 2003).

Growth curve.

The cells were plated in a 96-well plate at a density of $2x10^3$ cells in each well chamber. The quantification of cell proliferation was measured using the colorimetric assay based on the cleavage of the tetrazolium salt WST-1 (Roche) to Formazan by mitochondrial dehydrogenases (Berridge et al., 1996). The cells were counted at 24, 48, 72, 96 and 120h post plating. The doubling time was calculated using a growth curve that was plotted using relative cell number as Y-axis and time as X-axis. Each experiment was made in triplicate.

Colony efficiency assay.

For this assay, 24-well chambers pre- coated with 500 μl 0.8% agar base were used. The cells were plated at 10^4 cells per well in 0.8% agar methyl cellulose 25% horse serum (Basolo et al., 1991; Freshney, 1987), and they were feed twice a week with high calcium medium containing 5% horse serum. The number of cells plated was determined by a count of cell number at 24h

post-plating. The number and size of the colonies were determined 21 days later. Colony efficiency (CE) was defined as the ratio between number of colonies (≥100 μm in diameter) and the total number of viable cells after 24h of plating.

Ductulogenesis assay in collage matrix.

Collagen gels were prepared for studying the three-dimensional growth of the cells. The collagen gel was prepared by making a final solution containing 8% (v/v) F-12, 2% (v/v) $NaHCO_3$ (58.8mg/ml), 89.3% (v/v) Vitrogen Collagen (Cohesion Technologies, CA), and 0.36% (v/v) NaOH (2.78N). The final collagen concentration was 2.5mg/ml. A base layer of 0.5 ml was added to each well and 0.5ml collagen containing 12,500 cells was added to the top after the base became hard. Twenty-four wells chamber were used and four wells were made for each cell line. The cells were incubated at 37°C, and after 24h high calcium media plus 5% horse serum was added to each well and changed twice a week. The three-dimensional structures were evaluated 21 days post-plating.

DNA isolation.

DNA was prepared from MCF-10F, BP1E and BP1E-17neo (II-3). The cells were treated with lysis buffer (100 mM NaCl, 20 mM Tris-Cl pH 8.0, 25 mM EDTA pH 8.0, 0.5% SDS) with 200μg/ml proteinase K and incubated at 65°C for 15 minutes with gentle agitation. The samples were cooled down on ice and treated with 100 μg/ml RNase at 37°C for 30 minutes. One phenol extraction was done followed by another with chloroform: isoamyl alcohol (24:1). The aqueous layer was adjusted to 0.75M with ammonium acetate and the DNA was precipitated with 100% ethanol. The samples were centrifuged, dried and dissolved in distilled water.

Chromosome banding and cytogenetic analysis.

Cell were arrested in metaphase using colcemid at a final concentration of 0.01μg/ml and removed from the culture flask by trypsinization prior to treatment with hypotonic solution (0.075M KCl) for 20 min at 37°C. The cells were fixed in three changes of a 3:1 mixture of methanol: glacial acetic acid at –20°C. Metaphase cells were prepared by the steam-drying technique (Miura et al., 1990). Chromosomes were analyzed after G-banding. At least 20 cells were counted and five cells were karyotyped. Chromosome identification and karyotypic designations were in accordance with the ISCN (1985), as updated in ISCN (1992).

CGH Analysis

Protocols for DNA labeling and hybridization were as previously described (Sonoda et al., 1997; du Manoir et al., 1995). Gray-level images of fluorescence were captured with a Zeiss (Thorndale, NY) microscope connected to a cooled, charge-coupled-device camera (Photometrics, Tucson, AZ). Digital image analysis was performed using the Quipps software (Vysis, Downers Grove, IL). The threshold was set at 0.8 and 1.2 for losses and gains, respectively. The mean values of individual ratio profiles were calculated from at least 7 metaphase spreads. Averaged values were plotted as profiles alongside individual chromosome ideograms. Overrepresentation exceeding a threshold value of 1.50 was designated a high level gain (HLG). A HLG defined by a sharp peak was considered indicative of DNA sequence amplification.

Microsatellite analysis.

PCR reactions were performed in 20μl final volume containing 1X PCR buffer (Invitrogen), 1.5 mM $MgCl_2$, 0.6 μM of each primer, 200μM dNTPs, [^{33}P-α] dCTP (3,000Ci/mmol), 1U TaqPlatinum (Invitrogen), and 120ng DNA. The PCR cycler conditions were: 94°C, 5 minutes, 35 cycles: 94°C, 45 sec; annealing temperature, 45 sec; 72°C, 45 sec and an extension step: 72°C, 10 min. The following markers for chromosome 17 were used: D17S849, D17S926, D17S1583, D17S513, D17S796, TP53, D17S786, D17S945, D17S1852, D17S520, D17S793, D17S1358, D17S798, D17S518, D17S800, D17S1320, D17S1323, D17S1327, D17S930, D17S791, D17S806, D17S787, D17S808, D17S807, D17S789, D17S968, D17S785, D17S722, D17S937, D17S801, D17S802, D17S836, D17S784. The sequences and characteristics of microsatellite oligonucleotide primers were obtained from the GDB database (http://www.gdb.org). The PCR products were run on a 6% polyacrylamide gel for 3-4 h. The gel was dried and autoradiographed. For the marker D17S796, the PCR reaction was also analyzed by capillary electrophoresis. The D17S796 forward primer was fluorescent-labeled (Proligo, CA), and the PCR was carried out in a final volume of 10 μl containing 1X PCR buffer (Invitrogen), 1.5 mM $MgCl_2$, 0.5 μM pmol of each primer, 100μM dNTPs and 0.25U TaqPlatinum (Invitrogen) and 20ng DNA. The PCR conditions consisted of a denaturation step followed by 16 cycles at 94°C for 20 sec, 60°C for 45 sec (decreasing 0.5°C per cycle) and 72°C for 30 sec; 34 cycles at 94°C, 20 sec, 50°C for 45 sec and 72°C for 30 sec. The fluorescent PCR was mixed with an internal standard size marker and fractionated using CEQ8000 (Beckman Coulter). Microsatellite instability was defined as a shift of the allelic band or a change (increase or decrease) in the broadness of the allelic band. LOH was defined as a total loss (complete

deletion) or a 30% or more reduction in the signal of one of the heterozygous alleles compared with the control MCF-10F DNA (Dietmaier et al., 1999).

Results.

Transformation phenotypes.

In order to test whether chromosome 17 plays a functional role in the transformation of BP1E cells, we transferred a normal chromosome 17 to this cell line using MMCT. Nine clones were obtained from MMCT, and these clones were called BP1E-17neo (Lareef et al., 2003). One of these clones, BP1E-17neo clone II-3, was chosen for these studies. MCF-10F, BP1E and BP1E-17neo cells were used to evaluate growth rate, colony formation in agar methocel, and ductulogenesis in collagen matrix, all markers of cell transformation (Kakunuoka, 1978; DiPaolo, 1983; Shin et al., 1975; McCormick et al., 1989; Basolo et al., 1991; Calaf et al., 1993). BP1E-17neo grew at slower rate compared with the transformed cell line BP1E (Figure 1). The doubling time for BP1E-17neo was 24h, 1.5-fold longer than the BP1E cell that has a doubling time of 16h and similar to MCF-10F that was 24.6h. The cell line BP1E formed colonies over 100μm in diameter in agar methocel, whereas BP1E-17neo behaved like the cell line MCF-10F by not forming colonies in agar methocel (Figure 2).

In collagen matrix, BP1E-17neo like the control cells MCF-10F formed ductule-like structures (Figure 3 and Table 1) lined by a monolayer of cubical epithelial cells. BP-1E cells on the other hand, grew forming solid spherical masses (Figure 3 and Table 1).

Karyotype and CGH analysis.

The cytogenetic characterization of the human breast cell lines MCF-10F, BP1E and BP1E-17neo were made using a combination of standard G-banding and CGH analysis (Figure 4). All the cell lines had extra genetic material on chromosome 1 at band p34 as well as balanced translocation between chromosome 3 and chromosome 9 t(3;9)(p13;p21). The CGH analysis helped to identify the extra genetic material on chromosome arm 1p34 to be from 8q24. The modal number of chromosomes of the control cell line MCF-10F was 46, XX and for BP1E transformed cell line was 47, XX. BP1E had an additional isochromosome 10q (Figure 4). DNA losses were not observed in BP1E cell line using CGH. The modal chromosome number for BP1E-17neo was 48. BP1E-17neo has the same chromosomal abnormalities observed in BP1E and in addition has an extra copy of chromosomes 17 (Figure 4). It shows the same gain of chromosome 10q as seen in BP1E. The extra copy of chromosome 17, probably the one that was microinjected, was rearranged being composed of most of the p arm and a portion of 17q22-ter (Figure 4).

Microsatellite analysis.

Microsatellite analysis was performed using 33 markers for chromosome 17 (Figure 5). Retention was observed with most of the markers for 17p indicating that the extra chromosome 17 had most of this arm as CGH results indicated. For 17q, two markers out of twenty one showed retention and the others were not informative. The markers that showed retention were located at 17q22 and 17q25.3 respectively. We found differences between the three cells lines using the marker D17S796 located at 17p13.2 (Figure 5). The PCR products obtained using the marker D17S796 were analyzed using 6% polyacrylamide gels and by capillary electrophoresis (Figure 6). BP1E showed allelic imbalance in 17p13.2 using the marker D17S796. However,

BP1E-17neo showed a pattern similar to MCF-10F. This indicated that the introduction of chromosome 17 in BP1E had reverted this mutation.

Discussion.

The human breast epithelial cell line MCF-10F transformed with the chemical carcinogen benzo(a)pyrene gave rise to BP1E cells which form colonies in agar methocel and lose their ductulogenic capacity in collagen gel. In the present work, we have shown that the transfer of chromosome 17 reverted the transformed phenotype and reduced the growth rate of these cells to values similar to that of MCF-10F cells. Bp1E-17neo cells did not form colonies in agar methocel and formed ductule-like structures in collagen, as is the case with MCF-10F cells. The transfer of human chromosome 17 was associated with this reversion. BP1E cells acquired an isochromosome 10 not found in the parental MCF-10F cells, and this isochromosome was also present in BP1E-17neo cells. In addition, BP1E-17neo cells acquired an extra, rearranged chromosome 17. Taken together, these findings suggest that although BP1E cells have gained and isochromosome 10 in the process of chemical transformation by benzo(a)pyrene, this carcinogen also has produced a mutation(s) in chromosome 17 that was likely responsible for the observed changes in growth rate, colony efficiency and ductulogenic capacity.

The extra chromosome 17 found in BP1E-17 neo cells appears to contain most of the p arm and part of the q arm, q22-ter. Our observations that transfer of chromosome 17 into BP1E suppressed the growth of this cell line suggests that this chromosome harbors a tumor suppressor gene(s), confirming studies reported in the literature (Theile *et al*, 1995; Plummer *et al.*, 1997;

Negrini *et al.*, 1994; Levine *et al.*, 1991; Albertsen *et al.*, 1994; Coles *et al.*, 1990; Sato *et al.*, 1990; Andersen *et al*, 1992; Isomura *et al.*, 1994). Transfer of human chromosome 17 into CAL51 breast cancer cells resulted in loss of tumorigenicity and anchorage independent growth, changes in morphology, and reduction of cell growth rates. As in our study, these hybrid clones also contained a rearranged chromosome composed of 17p and the distal portion of 17q (Theile et al., 1995).

CGH is a useful molecular cytogenetic method for screening the entire tumor genome for chromosomal imbalances, but it has some methodological limitations, including the inability to detect balanced chromosomal rearrangements and limited resolution for detection of gains or losses of at least 5-15Mb (du Manoir *et al.*, 1995). Therefore, to map the 17p and 17q gains with higher resolution, we performed microsatellite analyses with a panel of different polymorphic markers distributed along 17p and 17q. We have found retention of most of the markers for 17p and two markers located near the telomeric region of 17q, consistent with the CGH results. The microsatellite analysis revealed that BP1E had an allelic imbalance in chromosome 17p13.2 as assessed by the marker D17S796, and this region was restored in BP1E-17neo cells. Allelic imbalances in chromosome 17p have been reported in 40-60% of sporadic breast carcinomas (Sato el al., 1990; Stack et al., 1995; Phelan et al., 1998). Deletion mapping analyses have shown that the region between the markers D17S938 and TP53 is one of the most frequently deleted regions in sporadic breast carcinoma (Seitz et al., 2001). The marker D17S796 resides between the marker D17S938 and TP53, and D17S796 is located approximately 2kb from D17S938. Allelic imbalances in the 17p13.2 region have been identified by others investigators in atypical ductal hyperplasia and *in situ* ductal carcinoma of the breast (Lakhani *et al*, 1995).

Furthermore, a high frequency of LOH was detecting in hepatocellular tumors with the marker D17S796 (Suzuki et al., 2000).

The marker D17S796 is approximately 1.5cM upstream of the tumor suppressor gene TP53, and the DEFCAP gene (death effector filament-forming Ced-4-like apoptosis protein) is 1.1cM downstream from D17S796. The DEFCAP protein contains a caspase recruitment domain, and it has been shown that its overexpression in MCF7 cells induces apoptosis (Hlaing et al., 2001). Others genes near the marker D17S796 are the LOC342530 and AIPL1 (aryl hydrocarbon receptor interacting protein-like 1).

Note (Dr Testa) : Reviewers will certainly expected you to state whether you saw any mutations of TP53 and/or altered protein expression in BP1E cells.

Collectively, these data indicate that 17p13.2 near the marker D17S796 contains one or more tumor suppressor genes that when inactivated is/are associated with cell transformation. In vitro, the transformed phenotype is characterized by increased cell proliferation, colony formation in semisolid media, and loss of the ability to from ductules in collagen matrix which and *in vivo* has been associated with ductal hyperplasia and carcinoma in situ of the breast (Lakhani *et al*, 1995), consistent with early stages of breast cancer.

References.

Andersen TI, Gaustad A, Ottestad L, Farrants GW, Nesland JM, Tveit KM, and Borresen AL. 1992. Genetic alterations of the tumor suppressor gene regions 3p, 11p, 13q, 17p, and 17q in human breast carcinomas. Genes Chromosomes Cancer 4: 113-121.

Albertsen H, Plaetke R, Ballard L, Fujimoto E, Connolly J, Lawrence E, Rodriguez P, Robertson M, Bradley P, Milner B, Fuhrman, D., Marks, A., Sargent, R., Cartwright, P., Matsunami, N., White, R. 1994. Genetic mapping of the BRCA1 region on chromosome 17q21. Am J Hum Genet 54: 516- 525.

Basolo F., Elliott J., Tait L., Chen X.Q., Maloney T, Russo IH., Pauly R., Momiki S., Caamano J., Klein-Szanto AJP., Koszalka M., and Russo J. 1991. Transformation of human breast epithelial cells by c-Ha-ras oncogenes. Mol. Carcinogenesis 4, 25-35.

Berridge M. V., Tan A. S., McCoy K. A. & Wang R. 1996. The biochemical and cellular basis of cell proliferation assays that use tetrazolium salts. Biochemica **4**, 15–19.

Bieche I, Lidereau R., 1995. Genetic alterations in breast cancer. Genes Chromosomes Cancer14: 227- 251

Biegel JA, Burk CD, Barr FG, Emanuel B. S. 1992. Evidence for a 17p tumor related locus distinct from p53 in pediatric primitive neuroectodermal tumors. Cancer Res., 52, 3391-3395.

Borrow J, Goddard A.D, Sheer D, Solomon E. 1990. Molecular analysis of acute promyelocytic leukemia breakpoint cluster region on chromosome 17. Science 28, 249 (4976): 1577-80.

Bruening W, Prowse AH, Schultz DC, Holgado-Madruga M, Wong A, Godwin AK. 1999. Expression of OVCA1, a candidate tumor suppressor, is reduced in tumors and inhibits growth of ovarian cancer cells. Cancer Res. 59 (19): 4973-83.

Calaf G. and Russo J. 1993. Transformation of human breast epithelial cells by chemical carcinogens. Carcinogenesis: 483- 492.

Callahan R, Cropp C, Sheng ZM, Merlo G, Steeg P, Liscia D, and Lidereau R. 1993. Definition of regions of the human genome affected by loss of heterozygosity in primary human breast tumors. J Cell Biochem Suppl 17G: 167-172.

Chen LC, Neubauer A, Kurisu W. , Waldman F M., Ljung B M., Goodson III W., Goldman ES., Moore II D., Balazs M., Liu E., Mayall BH., and Smithe H S. 1991. Loss of heretozygosity on the short arm of chromosome 17 is associated with high proliferative capacity and DNA aneuploidy in primary human breast cancer. Proc Natl Acad Sci USA 88: 3847-3851.

Coles C, Thompson AM, Elder PA, Cohen BB, Mackenzie IM, Cranston G, Chetty U, Mackay J, Macdonald M, Nakamura Y, Hoyheim, B.; Steel, C. M. 1990. Evidence implicating at least two genes on chromosome 17p in breast carcinogenesis. Lancet 336, 761- 763.

Cornelis RS, Devilee P, van Vliet M, Kuipers-Dijkshoorn N, Kersenmaeker A, Bardoel A, Khan PM, Cornelisse CJ. 1993. Allele loss patterns on chromosome 17q in 109 breast carcinomas indicate at least two distinct target regions. Oncogene 8, 781-785.

Dietmaier W, Riedlinger W, Köhler A, Wegele P, Beyser K, Sagner G, Wartbichler R, and Rüschoff J, 1999. Detection of microsatellite instability (MSI) and loss of heterozygosity (LOH) in colorectal tumor by fluorescent-based multiplex PCR. Biochemica 2.

DiPaolo, J. A. 1983. Relative difficulties in transforming human and animal cells *in vitro*. J. Natl. Cancer Inst., 70, 30-35.

du Manoir S., Schröck E., Bentz M., Speicher M.R., Joos S., Ried T., Lichter P., Cremer T. 1995. Quantitave analysis of comparative genomic hybridization. Cytometry 19: 27- 41:

Freshney R.I. 1987. Culture of Animal Cells, 2nd edn. Alan R. Liss, New York, pp.137- 153.

Futreal PA, Soderkvist P, Marks JR, Iglehart JD, Cochran C, Barrett JC, Wiseman RW. 1992. Detection of frequent allelic loss on proximal chromosome 17q in sporadic breast carcinoma using microsatellite length polymorphisms. Cancer Res 52, 2624- 2627.

Gullick, WJ. 1990. The role of the epidermal growth factor receptor and the c-erbB-2 protein in breast cancer. Int J Cancer Suppl. 5: 55-61.

Harada H, Nagai H, Tsuneizumi M, Mikami I, Sugano S, Emi M. 2001. Identification of DMC1, a novel gene in the TOC region on 17q25.1 that shows loss of expression in multiple human cancers. J Hum Genet. 46 (2): 90-5.

Harris CC and Hollstein M. 1993. Clinical implications of the p53 tumor-suppressor gene. N Engl J Med. 329 (18): 1318- 27.

Hlaing T., Guo RF, Dilley KA, Loussia JM, Morrish TA, Shi MM, Vincenz C. and Ward PA, 2001. Molecular cloning and characterization of DEFCAP-L and –S, two isoforms of a novel member of the mammalian Ced-4 family of apoptosis protein. J Biol Chem 276: 9230- 9238.

Isomura M, Tanigami A, Saito H, Harada Y, Katagiri T, Inazawa J, Ledbetter DH, Nakamura Y. 1994. Detailed analysis of loss of heterozygosity on chromosome band 17p13 in breast carcinoma on the basis of a high-resolution physical map with 29 markers. Genes Chrom. Cancer 9, 173- 179.

Kakunuoka 1978. Neoplastic transformation of human diploid fibroblast cells by chemical carcinogen. Proc. Natl. Acad. Sci. USA, 75: 1334- 1388.

Kirchweger R., Zeillinger R, Schneeberger C, Speiser P, Louason G and Theillet C. 1994. Patterns of allele losses suggest the existence of five distinct regions of LOH on chromosome 17 in breast cancer. Int J Cancer 56: 193- 1999.

Lakhani SR. 1995. The transition from hyperplasia to invasive carcinoma of the breast. J. Pathol. 187: 272- 278.

Lareef MH, Quivo T, Song J, Russo IH, Mihaila D, Slater CM, Balsara B, Testa JR, Broccoli D, Grobelny JV, Mor G, Cuthbert A and Russo J., 2003. Chromosome 17p13.2 reverts transformation phenotypes and Fas mediated apoptosis in breast epithelial cells. Mol. Carcinog. (In Press)

Levine AJ., Momand J, Finlay CA., 1991. The p53 tumour suppressor gene. Nature 351: 453-6.

McCormick J.J., and Maher VM. 1989. Malignant transformation of mammalian cells in culture, including human cells. Environ. Mol. Mutagenesis, 14: 105- 113.

Miura I., Siegfried JM., Resau J., Keller SM., Zhou J-Y, Testa JR. 1990. Chromosome alterations in 21 non-small cell lung carcinomas. Genes Chrom Cancer 2: 328- 338.

Negrini M, Sabbioni S, Haldar S, Possati L, Castagnoli A, Corallini A, Barbanti-Brodano G, Croce CM., 1994. Tumor and growth suppression of breast cancer cells by chromosome 17-associated functions. Cancer Res. 54: 1818-24.

Osborne RJ, Merlo GR, Mitsudomi T, Venesio T, Liscia DS, Cappa AP, Chiba I, Takahashi T, Nau MM, Callahan R, et al. 1991. Mutations in the p53 gene in primary human breast cancers. Cancer Res., 51, 6194-6198.

Phelan CM, Borg A Cuny M, Crichton DN, Baldursson T, Andersen TI, Caligo MA, Lidereau R, Lindblom A, Seitz S, Kelsell D, Hamann U, Rio P, Thorlacius S, Papp J, Olah E, Ponder B, Bignon YJ, Scherneck S, Barkardottir R, Börresen-Dale AL, Eyfjord JE, Theillet C, Thompson AM, Larsson C, et al. 1998. Consortium study on 1280 breast carcinomas: allelic loss on chromosome 17 targets subregions associated with family history and clinical parameters. Cancer Res. 58:1004-12.

Phillips NJ, Ziegler MR, Radford DM, Fair KL, Steinbrueck T., Xynos FP., Donis-Keller H. 1996. Allelic deletion on chromosome 17p13.3 in early ovarian cancer. Cancer Res. 56(3): 606-611.

Plummer SJ, Adams L, Simmons JA, Casey G., 1997. Localization of a growth suppressor activity in MCF7 breast cancer cells to chromosome 17q24-q25. Oncogene 14: 2339-45.

Radford DM, Fair KL, Phillips NJ, Ritter JH, Steinbrueck T, Holt MS and Donis-Keller H. 1995. Allelotyping of ductal carcinoma *in situ* of the breast: deletion of loci on 8p, 13q, 17p and 17q. Cancer Res 55: 3399-3405.

J.M. Risk, J. Whittaker, A. Fryer, A. Ellis, J.M. Shaw, E.A. Field, P.S. Friedmann, D.T. Bishop, J. Bodmer, I.M. Leigh & J.K. Field. 1994. Tylosis oesophageal cancer mapped. Nature Genetics 8:319-321.

Sato T, Tanigami A, Yamakawa K, Akiyama F, Kasumi F, Sakamoto G, Nakamura Y. 1990. Allelotype of breast cancer: cumulative allele losses promote tumor progression in primary breast cancer. Cancer Res., 50, 7184-7189.

Sato T, Saito H, Swensen J, Olifant A, Wood C, Danner D, Sakamoto T, Takita K, Kasumi F, and Miki Y. 1992. The human prohibitin gene located on chromosome 17q21 is mutated in sporadic breast cancer. Cancer Res 52, 1643-1646.

Schultz DC, Vanderveer L, Berman DB, Hamilton TC, Wong AJ, Godwin AK. 1996. Identification of two candidate tumor suppressor genes on chromosome 17p13.3. Cancer Res. 56 (9): 1997-2002.

Seitz S, Poppe K, Fischer J, Nothnagel A, Estevez-Schwarz L, Haensch W, Schlag PM, Scherneck S. 2001. Detailed deletion mapping in sporadic breast cancer at chromosomal region 17p13 distal to the TP53 gene: association with clinicopathological parameters. J Pathol. 194: 318- 26.

Seizinger BR. 1993. NF1: a prevalent cause of tumorigenesis in human cancers? Nat Genet. 3 (2): 97-9.

Shin S I, Freedman, VH, Rismer R, and Pollack, R. 1975. Tumorigenicity of virus-transformed cells in nude mice is correlated with anchorage independent growth in vitro. Proc. Natl. Acad. Sci. USA, 72: 4435- 4439.

Sonoda G, Palazzo J, du Manoir S, Godwin AK, Feder M, Yakushiji M, Testa JR. 1997. Comparative genomic hybridization detects frequent overrepresentation of chromosomal material from 3q26, 8q24, and 20q13 in human ovarian carcinomas. Genes Chromosomes Cancer 20 (4): 320-8.

Soule HD, Maloney TM, Wolman SR, Peterson WD Jr, Brenz R, McGrath CM, Russo J, Pauley RJ, Jones RF, Brooks SC. 1990. Isolation and characterization of a spontaneously immortalized human breast epithelial cell line, MCF-10. Cancer Res. 50: 6075-86.

Stack M, Jones D, White G, Liscia DS, Venesio T, Casey G, Crichton D, Varley J, Mitchell E, Heighway J. et al. 1995. Detailed mapping and loss of heterozygosity analysis suggests a suppressor locus involved in sporadic breast cancer within a distal region of chromosome band 17p13.3. Hum Mol Genet. 4: 2047-55

Suzuki K., Hirooka Y., Tsujitani S., Yamane Y., Ikeguchi M., and Kaibara N, 2000. Relationship between loss of heterozygosity and microsatellite loci and computerized nuclear morphometry in hepatocellular carcinoma. Anticancer Research 20: 1257- 1262.

Tavtigian SV, Simard J, Teng DH, Abtin V, Baumgard M, Beck A, Camp NJ, Carillo AR, Chen Y, Dayananth P, Desrochers M, Dumont M, Farnham JM, Frank D, Frye C, Ghaffari S, Gupte JS, Hu R, Iliev D, Janecki T, Kort EN, Laity KE, Leavitt A, Leblanc G, McArthur-Morrison J, Pederson A, Penn B, Peterson KT, Reid JE, Richards S, Schroeder M, Smith R, Snyder SC, Swedlund B, Swensen J, Thomas A, Tranchant M, Woodland AM, Labrie F, Skolnick MH, Neuhausen S, Rommens J, Cannon-Albright LA. 2001. A candidate prostate cancer susceptibility gene at chromosome 17p. Nat Genet. 27 (2): 172-80.

Tait L., Soule HD and RussoJ. 1990. Ultrastructural and immunocytochemical characterization of an immortalized human breast epithelial cell line, MCF-10. Cancer Res. 15, 50(18):6087-94.

Theile M, Hartmann S, Scherthan H, Arnold W, Deppert W, Frege R, Glaab F, Haensch W and Scherneck S. 1995. Suppression of tumorigenicity of breast cancer cells by transfer of human chromosome 17 does not require transferred BRCA1 and p53 genes. Oncogene 10: 439- 447.

Wales MM, Biel MA, el Deiry W, Nelkin BD, Issa JP, Cavenee WK, Kuèrbitz SJ, Baylin SB. 1995. p53 activates expression of HIC-1, a new candidate tumour suppressor gene on 17p13.3. Nat Med. 1(6): 570-577.

Legends of Figures

Figure 1. Comparative growth rates *in vitro* among MCF-10F, BP1E and BP1E-17neo cells. The doubling time, estimated from the growth curves, was significantly higher for BP1E-17neo (24) than for BP1E (16h). The doubling time for BP1E-17neo was similar to MCF10F (24.6h).

Figure 2. Colony formation in agar methocel. A) MCF-10F, B) BP1E and C) BP1E-17neo cells. The number and size of the colonies were determined 21 days post-plating. MCF-10F and BP1E-17 neo cells did not form colonies although BP1E cells formed colonies over 100 μm in diameter. Magnification: 10X

Figure 3. Ductulogenesis assay in collagen matrix. A) MCF-10F, B) BP1E and C) BP1E-17neo cells. MCF-10F and BP1E-17 neo cells formed ductule-like structures in collagen, whereas BP1E cells did not. Magnification: 10X

Figure 4. Karyotypic and CGH analysis of MCF-10F, BP1E and BP1E-17neo cells. Differences among the cell lines are shown. In the three cell lines, the arrow on chromosome 1 shows the extra material at 1p34 present in the three cell lines. The arrows on chromosome 3 and chromosome 9 indicated the translocated regions between these chromosomes. The isochromosome 10 present in BP1E and BP1E-17neo are also indicated. The extra chromosome 17 present only in BP1E-17neo is also indicated. Vertical green lines on the right of each chromosome in the CGH analysis represent gains, whereas red vertical lines on the left indicate loss of genetic material.

The codon 47 polymorphic variant of p53 is associated with altered phosphorylation pattern and decreased apoptosis

Xiaoxian Li[#], Patrick R.G.G. Dumont[#], Anthony Della Pietra, Cory Shetler and Maureen E. Murphy*
Department of Pharmacology, Fox Chase Cancer Center, Philadelphia PA 19111

Running title: Serine 47 polymorphism impairs p53 function
Keywords: p53, apoptosis, transcription, polymorphism, phosphorylation.

[#]These authors contributed equally to this work
*To whom correspondence may be addressed:
Department of Pharmacology
Fox Chase Cancer Center
333 Cottman Avenue
Philadelphia PA 19111
(215) 728-5684
Maureen.Murphy@FCCC.edu

In addition to a common functionally significant polymorphism at codon 72, the p53 tumor suppressor gene also contains a rarer coding region polymorphism at amino acid 47. Wild type p53 encodes proline at this residue (P47), but in approximately 1% of African Americans this amino acid is serine (S47). Phosphorylation of a neighboring residue, serine 46, is critical for p53's ability to induce programmed cell death; one responsible kinase is the proline-directed kinase p38 Map kinase (refs). We reasoned that the codon 47 polymorphism, which replaces the proline residue critical for recognition by p38, might have decreased phosphorylation of serine 46. We show that the S47 protein is a poorer substrate for phosphorylation on serine 46 by p38, and has decreased ability to induce apoptosis *in vivo* compared to wild type p53. Mechanistically, this is the result of decreased ability to transactivate two p53-target genes, p53AIP1 and PUMA. The combined data indicate that, like the codon 72 polymorphism, the codon 47 polymorphism of p53 is functionally significant, and may play a role in cancer risk and efficacy of therapy.

The serine 47 (S47) polymorphism in the p53 tumor suppressor gene was first described eleven years ago (ref). In that study, no functional differences were found between the S47 and wild type p53 proteins. However, the ability to induce apoptosis was not assessed, and this study was performed before it was known that phosphorylation of serine 46 was critical for that function. In a small sample number, the S47 polymorphism was found in less than 5% of African Americans, and not at all in Caucasians (ref). Before embarking on a functional study of this polymorphic variant, we reasoned that its low allele frequency, combined with its proximity to another polymorphic residue at codon 72, indicated that S47 might exist in linkage disequilibrium with a particular codon 72 variant (P72 or R72). To address this issue we analyzed both p53 polymorphisms in genomic DNA isolated from 200 healthy African Americans. We found four individuals who were heterozygous for the S47 variant, for an allele frequency of 1%. Notably, in all four cases these individuals were homozygous for proline at 72. This indicated that the S47/P72 allele was a relevant allele to study in a functional analysis. Therefore, we focused this study

on the function of the S47/P72 protein, which we designate S47, and compare it to the P72 protein, which we designate wild type (wt).

In order to assess the impact of the S47 polymorphism on serine 46 phosphorylation by the proline-directed kinase p38, we created GST fusion proteins encoding p53 amino acids 1-92 encoding wild type p53 (P72) or the S47 variant. Additionally, we constructed a synthetic mutant that could not be phosphorylated on serine 46 (A46). These fusion proteins were used in *in vitro* kinase assays using purified, active p38 kinase. Because serine 33 of p53 can also be phosphorylated by p38 (ref), we generated these proteins with serine 33 mutated to alanine (S33A), in order to reduce background; however, identical results were obtained in the serine 33 background as well (see below). Equal microgram amounts of each GST fusion protein, compared to GST alone and a positive control (myelin basic protein, MBP) were incubated with equal units of purified active p38 kinase and γ^{32}P-ATP. As depicted in Figure 1, the S47 recombinant protein was phosphorylated approximately 2-fold less well than wild type p53 protein, while the A46 variant was undetectably phosphorylated (Fig 1A). Coomassie staining of the input proteins confirmed equal loading and purity of the substrate (Fig. 1B). Comparable results were obtained without mutation of serine 33 to alanine, except the basal level of phosphorylation of all three proteins was higher (see Supplementary Fig. 1).

To determine if the S47 polymorphism alters p53 function *in vivo*, we generated stably-transfected cell lines containing wild type p53 (wt), the S47 variant, and the A46 mutant. These p53 variants were generated in the background of the temperature sensitive version of p53 encoding valine at amino acid 138. This mutant of p53 is widely used and well characterized; the p53 protein is denatured and inactive when cells are cultured at 39 degrees, but temperature shift of cells to 32 degrees results in wild type p53 conformation and apoptosis induction (ref). Stably transfected cell lines were generated in the human lung adenocarcinoma line H1299. This p53-null cell lines was chosen because it contains high levels of constitutively active p38 kinase, as determined by western blotting using antisera specific for the active enzyme (X. Li and M.

Murphy, unpublished observations). Twenty independent clones were generated for each variant (wt, S47 and A46), and two clones of each were selected based upon western analysis that revealed comparable levels of p53 protein (Fig. 1C). These six clones were analyzed for apoptosis induction following temperature shift using the Guava personal Cell Analysis machine (Guava PCA), which is a flow cytometer that performs multiple quantitative assays for apoptosis. As depicted in Figure 1C, TUNEL analysis in these cell lines after temperature shift indicated that the S47 variant routinely had a 2 to 5-fold decreased ability to induce apoptosis, relative to wt p53. As predicted by previous studies, the A46 mutant was also significantly compromised for apoptosis induction (Fig. 1C). This difference was consistent and statistically significant ($p<0.01$), and this difference was recapitulated using independent assays (for example, caspase activation, see Supplemental Fig. 2). To confirm these findings in another cell background, we generated stably-transfected wt and S47 cell lines in the p53-null osteosarcoma cell line Saos2. Again, clones were selected that contained equivalent levels of p53. For this comparison we also included a Saos2 cell line containing temperature-sensitive R72; in this way, all three polymorphic variants of p53 could be compared for apoptosis induction (S47, P72 and R72). As shown in Figure 1D, in the cellular background of Saos2, the S47 variant has over 2-fold decreased ability to induce apoptosis compared to P72 ($p= 0.01$), and over 7-fold decreased ability when compared to R72 ($p<0.001$).

To measure the timing of apoptosis, we performed a time course in three selected lines (clones wt-4, S47-8 and A46-8 from Fig. 1C) following p53 induction in the presence of genotoxic stress. For this analysis, cells were treated with gamma radiation to enhance apoptosis, and apoptosis was measured by the appearance of the 85 kDa caspase cleavage product of Poly(ADP) ribose polymerase (PARP). Differences between wt p53, S47 and A46 in apoptosis induction could be seen at all time points, though at later time points the difference in apoptosis was more marked (up to 10-fold decrease for S47 at 24 hours). Comparable results were obtained in the presence of ultra-violet light as a source of DNA damage (not shown). Interestingly, these differences did not appear to reflect significant differences in the transcriptional activities of these

p53 variants, as the induction of the p53 target gene MDM2 appeared indistinguishable in all three clones at all time points (Fig. 2A).

In efforts to compare the phosphorylation pattern of the S47 variant to wt p53, we used antisera specific for p53 phosphorylated at serines 15, 20, 46 and 392. Western analysis of our stably transfected H1299 clones revealed no difference in the phosphorylation pattern on serines 15 or 392 between the wt, S47 and A46 proteins. As expected, there were marked differences in S46 phosphorylation between these variants, though we cannot rule out the possibility that the S47 change alters the epitope for this antibody. Interestingly, there were also consistent differences in serine 20 phosphorylation between these variants; specifically, the S47 variant had a 2-3 fold decrease in serine 20 phosphorylation, and A46 had a 10-fold decrease (Fig. 2B). Though serine 20 phosphorylation has in some studies been linked to the transactivation potential of p53, we saw no evidence of this, and the ability of S47 and A46 variants to transactivate MDM2 and p21/waf1 was indistinguishable from wt (Fig. 2C).

The combined data support the hypothesis that the S47 variant has decreased ability to be phosphorylated on serine 46 by p38, and potentially also serine 20, leading to decreased ability to induce apoptosis. To test this hypothesis further, we treated our inducible H1299 clones with the well-characterized inhibitor of p38, SB-203580. Following treatment we measured p53 phosphorylation by immunoblot, as well as apoptosis induction. As expected, SB-203580 effectively inhibited serine 46 phosphorylation of wild type p53 (Figure 3A, compare lanes 4 and 7 for S-46), despite the fact that some p53 was already phosphorylated on serine 46 prior to temperature shift (lane 1). TUNEL analysis of treated cells indicated that the p38 inhibitor SB-203580 also dramatically inhibited apoptosis induced by wt p53, bringing it to levels comparable to the untreated S47 variant (Fig. 3B). The residual levels of serine 46 phosphorylation and apoptosis in cells with wild type p53 cells likely reflects phosphorylation of this residue by another kinase, such as Hipk2, which is also known to target serine 46 (ref). Interestingly, analysis of serine 20 phosphorylation of wt p53 also revealed consistent decreases in serine 20

phosphorylation (Fig. 3A, S-20). In contrast, phosphorylation of serine 20 was unaffected by SB-203580 in the S47 and A46 lines, suggesting that serine 20 phosphorylation may rely on previous phosphorylation of S46. This is consistent with work from two other groups, who have previously shown that phosphorylation of serine 46 facilitates phosphorylation of other N-terminal residues of p53, including serine 20 (refs). Similar results were obtained in MCF-7 cells (endogenous wt p53) treated with ultra-violet light to stimulate p38-mediated phosphorylation of serine 46. In these cells, the p38 inhibitor SB-203580 inhibited serine 46 phosphorylation 2-fold, leading to a comparable 2-fold decrease in serine 20 phosphorylation (S-20) and decreased apoptosis (p85-PARP, Fig. 3C).

It has been reported that serine 46 phosphorylation is not required for the full ability of p53 to transactivate the majority of target genes; however, at least one, the pro-apoptotic target gene p53AIP1, requires this phosphorylation event for transactivation (ref). As shown in Figure 4A, analysis of poly-adenylated RNA isolated from our inducible cell lines indicated that there was a modest induction of p53AIP1 in cells containing wt p53, but no evidence for induction in lines containing the S47 or A46 variants. Analysis of other p53 target genes in these cells revealed no difference in the ability of these variants to transactivate the p53 response genes Killer/DR5, Gadd45, p21/waf1, Mdm2 or bax, or to repress the genes encoding survivin or cyclin B1 (Fig. 4B). Interestingly, however, there was a consistent 2-fold decrease in the ability of the S47 and A46 variants to transactivate the p53 response gene PUMA (Fig. 4B). To analyze this further, we performed western analysis for PUMA in cells shifted in a time course experiment. This analysis confirmed that the S47 variant had a decreased level of PUMA induction (2-fold less at 8 hours, 5-fold less at 24 hours). These levels correlated with decreased apoptosis, as measured by the appearance of p85-PARP (Fig. 4C). Along these lines, incubation with the p38 inhibitor SB-203580 effectively impaired the ability of wt p53 to transactivate PUMA in MCF-7 cells (see Supplementary Fig. 3). Consistent with these results, we found that the S47 and A46 variants of p53 possessed 5 to 10 fold decreased ability to

transactivate a reporter gene driven by the PUMA promoter (Fig. 4D) but not the MDM2 promoter (not shown).

Our data are consistent with the hypothesis that decreased phosphorylation of serine 46, and possibly also serine 20, at the amino terminus of the S47 variant impairs its ability to induce apoptosis, and to transactivate the known pro-apoptotic p53 target genes p53AIP1 and PUMA. In contrast, we have seen no differences in the ability of S47 to bind to DNA, repress gene expression, induce G1 arrest, or traffic to mitochondria (X. Li and M. Murphy, unpublished observations). Notably, transcription of the PUMA gene has been reported to be uniquely sensitive to phosphorylation at the N-terminus of p53 (ref). Additionally, while the changes in PUMA transactivation by S47 appear to be only 2-4 fold, PUMA transactivation is known to be particularly critical for apoptosis induction by p53 (ref). In fact, the heterozygous PUMA knock-out mouse, with approximately 2-fold less PUMA, has a marked defect in apoptosis compared to wild type (ref). The combined data indicate that there are two polymorphisms in p53 that are functionally significant, at codons 47 and 72. Interestingly, both variants with decreased apoptotic potential (P72 and S47) are more prevalent in African American populations, suggesting that the selection for these variants may occur as a response to high exposure to ultraviolet light, which has been suggested (ref). It remains to be determined if the S47 polymorphism has an impact on cancer risk or the efficacy of chemo-and radiation therapy, or if the ethnic bias of this polymorphism in part explains some of the differences in cancer risk between Caucasian and African American populations.

Methods

Plasmid Construction

The human p53 cDNA construct encoding temperature sensitive p53 (valine 138, ref) was modified by site-directed mutagenesis using Stratagene's Quick-Change Kit. The A46 p53 mutant was made by introducing alanine at codon 46 using primers: 5′-GATTTGATGCTGGCCCCGGACGATATTG-3′ and 5′-CAATATCGTCCGGGGCCAGCATCAAATC-3′. The S47 p53 polymorphic variant was made by introducing serine at codon 47 using primers: 5′-GATTTGATGCTGTCCTCGGACGATATTGAAC-3′ and 5′-GTTCAATATCGTCCGAGGACGACATCAAATC-3′. These mutations were confirmed by DNA sequencing. All p53 constructs have proline at codon 72. The GST-p53 construct contains amino acids 1-92 in the pGEX-4T-3 vector was also modified as described above. In addition, the GST-p53(1-92) was mutated by introducing alanine at codon 33 using primer: 5′-AAGAACGTTCTGGCCCCCTTGCCGTCC-3′ and 5′-GGACGGCAAGGGGGCCAGAACGTTCTT-3′

Cell culture, p53 induction

The H1299 and Saos2 cell lines containing temperature-sensitive p53 were generated by stable transfection with CMV promoter-driven human p53 cDNA containing the temperature-sensitive Val138 mutation. The ts H1299 and Saos2 cells were maintained at 39°C in Dulbecco's Modified Eagle medium (DMEM) supplemented with 10% fetal bovine serum (FBS), 100 U/mL penicillin and streptomycin, and 400μg/mL (SaoS2) or 800μg/mL (H1299) G418 in a 5% CO_2 humidified atmosphere. For temperature shift and p53 induction, cells were plated at $2x10^6$ cells per 100-mm plate and either shifted to 32°C (active p53) or maintained at 39°C (mutant conformation p53). The p53-null lung cancer cell line H1299 and the breast cancer cell line MCF7 were maintained at 37°C in DMEM supplemented with 10% FBS and 100 U/mL penicillin and streptomycin in a 5% CO_2 humidified atmosphere. For experiments with the p38 kinase inhibitor, cells were incubated with SB-203580 (Upstate Biotechnology) to a final

concentration of 40 uM, or vehicle alone (DMSO) for 30 minutes prior to temperature shift or irradiation. Cells were irradiated with 7.5 J/m2 of UV-C with a Spectroline X series UV lamp, and output was measured with a traceable UV light meter (Fisher Scientific).

Western and Northern analysis

Cells were lysed in Nonidet P40 buffer (50mM Tris, pH 8.0, 5mM EDTA, 150mM NaCl, 0.5% Nonidet-P40, 1mM phenylmethylsulfonyl fluoride, 10μg/mL pepstatin A, 10μg/mL aprotinin and 5μg/mL leupeptin). The protein concentration was determined using the Bio-Rad Dc assay kit (BioRad). Equal amounts of protein were loaded on a Nupage Novex 10% Bis-Tris gel (Invitrogen). Gels were transferred overnight onto Immuno-blot PVDF membrane (BioRad) at 4°C. The membrane was blocked with phosphate-buffered saline (PBS) supplemented with 0.2% Tween-20 and 5% nonfat dry milk for 10 min. Primary antibody was incubated for 1h at room temperature or overnight at 4°C. Antisera for p53 (Ab-6, Calbiochem), phospho-p53 (Cell Signalling), PUMA (Oncogene Sciences) were used at 1:1000 dilution, and for cleaved PARP (p85PARP, Promega) was used at 1:400 dilution. The membrane was then washed 3 times for 15 min using PBS containing 0.2% Tween-20 (PBST), followed by a 1h incubation with peroxidase-conjugated secondary antibody (Jackson Immunoresearch Laboratories), and then washed 3 times for 20 min using PBST. The proteins were detected by chemiluminescence using the ECL Western Blotting Detection Reagents (Amersham Biosciences).

For analysis of RNA, cells were harvested 24 hrs after temperature shift. Total RNA was prepared using Trizol (Gibco-BRL) or via cesium chloride, gradients, as described (ref). Polyadenylated RNA was purified from cesium gradient total RNA using Poly A Quick columns, as per the manufacturer (Stratagene). Eight micrograms of total RNA, or two micrograms polyA RNA were resolved by denaturing agarose gel electrophoresis and transferred onto a nylon membrane, as described (ref). The membrane was hybridized with probes and exposed to an X-ray film as described (ref).

Preparation of GST fusion proteins and in-vitro p38 kinase assay

After a 6h induction with 0.1mM IPTG, the BL21 cells were centrifuged and the pellet was resuspended in STE buffer supplemented with protease inhibitors (10mM Tris, pH 8.0, 150mM NaCl, 1mM EDTA, 1mM phenylmethylsulfonyl fluoride, and 10 μg/mL aprotinin) and incubated on ice for 15 minutes. The lysate was brought to 5mM DTT and 1.5% Sarkosyl, sonicated three times for 30sec and centrifuged at 10,000g for 15 min. The supernatant was adjusted to 2% Triton X-100 and incubated at 4°C for 15 min. Glutathione-Sepharose 4B beads were added as per the manufacturer (Amersham Biosciences) and incubated for 30 minutes at 4°C. The GST-p53/glutathione-sepharose complex was washed 3 times with 20 volumes of PBS and eluted from the beads with 10mM reduced glutathione in 50mM Tris-HCl, pH 8.0. The GST-p53 proteins were concentrated using Microcon columns as per the manufacturer (Millipore).

For the *in vitro* kinase reactions, twenty micrograms of purified GST-p53 (wt, S47 or A46) or myelin basic protein (MBP) was mixed with 10μL ADBI buffer (20mM Tris, pH 7.4, 20mM β-glycerol phosphate, 5mM EGTA, 1mM Na_3VO_4, 1mM DTT and 20mM $MgCl_2$), 0.6 mM cold ATP, 20 μCi [γ-^{32}P]ATP (NEN), and 100 ng active p38β2 (Upstate Biotechnology). After a 15 min incubation at 30°C, the reaction was stopped by adding Lithium Dodecyl Sulfate and boiling for 10 min. Then the samples were loaded on a Nupage Novex 10% Bis-Tris gel (Invitrogen), and the gel was dried and exposed to an X-ray film.

Apoptosis assays

Temperature-sensitive H1299 clones were seeded onto 6-well plates at a density of 500,000 cells per well. Saos2 cells were plated at 250,000 cells/100-mm plate. Cells were shifted to 32°C and harvested at the times indicated after temperature shift. Control cells were maintained at 39°C. TUNEL or multi-caspase assays were conducted using the Guava Personal Cytometer (Guava Technologies) following the manufacturers protocol. Briefly, for the TUNEL

assay, cells were trypsinized and resuspended in 1% paraformaldehyde. After a 1h incubation on ice, cells were spun down at 300g for 5 min, washed twice with PBS and fixed overnight with 70% ethanol. The next day, the cells were labeled with BrdU and analyzed. For the multi-caspase assay, cells were trypsinized, washed with PBS and incubated with SR-VAD-FMK and 7-AAD before analysis on the Guava flow cytometer.

Luciferase Assays

The Puma promoter was cloned from human genomic DNA (Promega) using SuperScript RT-PCR (Invitrogen) and cloned into pCDNA 3.1D/V5-HIS Topo Expression Vector (Invitrogen). The following primers were used: 5'-CACC*GAATTC*GCGACTGTG-3' and 5'-*GCTAG*CGCCCCCGCGTGACGC-3' (nucleotides in *italics* represent engineered restriction sites Eco R1 and Nhe 1, respectively). The promoter was then subcloned into the luciferase reporter vector pGL3-E1bTATA, provided by James Manfredi (Mount Sinai School of Medicine). H1299 cells were plated in triplicate into six well plates (60,000 cells/well) and allowed to grow overnight. Each p53 construct or empty vector (CMV-neo-Bam) was added in increasing concentration to 250ng Puma pGL3-E1bTATA and 5ng of pCMV Renilla were transfected into cells using FUGENE (Roche). 24h after transfection cells were harvested, lysed and analyzed according to the manufacturer's protocol (Promega). Samples were analyzed on a Monolight 2010 luminometer (Analytical Luminescence Laboratory). Luciferase activity was normalized to Renilla luciferase activity. Fold induction was obtained by dividing the normalized values with the average value of normalized p53 -/- sample.

References

Acknowledgments

This work was supported by a generous grant from the McGrorty Foundation, and by Health Research Formula Funds from the Commonwealth of Pennsylvania Tobacco Settlement Act. We thank Cindy Spittle and acknowledge the Biomarker and Genotyping Facility for this work. We thank Ettore Appella, Steve McMahon, and Donna George for critical reading of this manuscript.

Figure Legends

Figure 1. The S47 polymorphic variant of p53 is phosphorylated less well by p38 Map kinase, and has decreased ability to induce apoptosis *in vivo*.

A, B. GST fusion proteins containing amino acids 1-92 of human p53 were generated that contain wild type p53 (wt, proline at amino acid 72), serine at amino acid 47 (S47) or alanine at 46 (A46, cannot be phosphorylated by p38), all in the background of alanine 33. *In vitro* kinase reactions were performed using purified, active p38β2 kinase and run on SDS-PAGE. In B, the loading and purity of GST fusion proteins is indicated by Coomassie staining; BSA is included as a standard. MBP= myelin basic protein.

C, D. TUNEL assay results from individual clones of cells stably transfected with inducible versions of p53, as indicated. Western analysis for total p53 in each clone is indicated in the inset. Values of TUNEL positive cells are given at 39 degrees (mutant p53) and 32 degrees (wild type p53 conformation) following twenty-four hours of temperature shift. Values given are the mean +/- SD from three independent experiments. p values reflect comparison to clone wt-4. In D, clones of Saos2 cells stably transfected with each p53 polymorphic variant (R72, P72 and S47) are analyzed by western analysis for p53 level (see inset) and for TUNEL positive cells after twenty-four hours of temperature shift. Values are expressed as the mean +/- SD. p values are given for each cell line (R72 and S47) compared to P72.

Figure 2. The S47 variant has reduced apoptotic ability after genotoxic stress, and decreased phosphorylation on Serines 46 and 20.

A. Western analysis of p53 level, MDM2 induction, and apoptosis (appearance of the caspase-cleaved form of poly (ADP) ribose polymerase, p85-PARP) in cells harvested at the indicated timepoints after temperature shift. Prior to temperature shift, cells were exposed to 6Gy of radiation. The clones depicted are, from Fig. 1C, wt-4, S47-8, and A46-8. 39 degrees is mutant (inactive) p53, and 32 degrees is wild type conformation and activity. Levels of β-actin are included as a loading control.

B. Western analysis for p53 level, apoptosis (p85-PARP) and phosphorylated serines 46, 20, 15 and 392, using phospho-specific antisera (Cell Signaling). Cells were temperature shifted for 24 hours.

C. Western analysis of the same lysates used in (B) for transactivation of the p53 target genes p21 and MDM2. Levels of β-actin are included as a loading control.

Figure 3. The p38 inhibitor SB-203580 inhibits phosphorylation of p53 serine 46 and serine 20, and abrogates p53-dependent apoptosis.

A. Western analysis of H1299 clones containing the indicated inducible proteins (wt, S47 and A46) treated with the p38 inhibitor SB-203580 or vehicle alone (dimethyl sulfoxide, DMSO) and temperature-shifted to 32 degrees to induce wild type p53 conformation. Cells were pre-treated for 30 minutes with kinase inhibitor prior to temperature shift. The data depicted are representative of three independent experiments.

B. Quantitation of apoptosis using the Guava Personal Cell Analysis machine (Guava PCA). TUNEL assay was performed on the inducible H1299 clones indicated 24 hours after temperature shift; cells were pre-treated for 30 minutes prior to temperature shift with p38 kinase inhibitor (SB-203580) or vehicle alone (DMSO).

C. Western analysis of asynchronously growing MCF-7 breast carcinoma cells treated with ultra-violet light (7.5 J/m2) and harvested after the times indicated; cells were pre-treated for 30 minutes with SB-203580 to a final concentration of 40 uM before harvesting and western analysis with the antisera indicated.

Figure 4. The S47 variant has impaired ability to transactivate the p53-response genes p53AIP1 and PUMA.

A. Northern analysis of 2 ug polyadenylated RNA isolated from the inducible H1299 clones indicated, and probed with cDNA specific for p53AIP1 and gapdh (glyceraldehyde 3 phosphate dehydrogenase); temperature shift is for 24 hours.

B. Northern analysis of total RNA isolated from the H1299 clones indicated, following 24 hours of temperature shift. Results are representative of 3 independent experiments. Densitometry indicates a consistent 2-fold decrease in PUMA level in S47 and A46. Gapdh is included as a control for loading and integrity.

C. Western analysis of a time course of p53 induction in the H1299 clones indicated for p53 level, apoptosis (p85-PARP) and PUMA level. Levels of β-actin are included as a loading control.

D. Analysis of the fold induction of luciferase activity in cells transfected with a PUMA-driven luciferase reporter (PUMA-luciferase) along with a co-transfected Renilla luciferase control. Numbers depicted represent the fold increase over cells transfected with PUMA-luciferase alone, in the absence of p53. Data depicted represent three independent experiments, with standard deviation.

Supplemental Figures

Figure 1. The S47 variant is a poorer substrate for phosphorylation of active p38 kinase.
A, B. The indicated GST fusion proteins (amino acids 1092 of p53) were used as substrates for phosphorylation by active, purified p38 kinase. Myelin basic protein (MBP) is used as a positive control, and GST is used as a negative control. Coomassie staining of input substrates is included in B.

Figure 2. Induction of caspase activity in cell lines containing inducible versions of wild type p53 (wt), S47 and A46. Levels of caspase activity in uninduced samples (39 degrees, mutant conformation p53) were set to 1, and the fold increase is depicted. Numbers represent the results from three independent experiments, plus standard deviation. Cells were temperature shifted for 24 hours.

Figure 3. Western analysis of PUMA levels in MCF-7 cells treated with 7.5 J.m2 of UV-C and harvested at the indicated timepoints. 30 minutes prior to irradiation, cells were treated with the p38 inhibitor SB-203580 or vehicle alone (DMSO).

Li *et al.*, Fig. 1

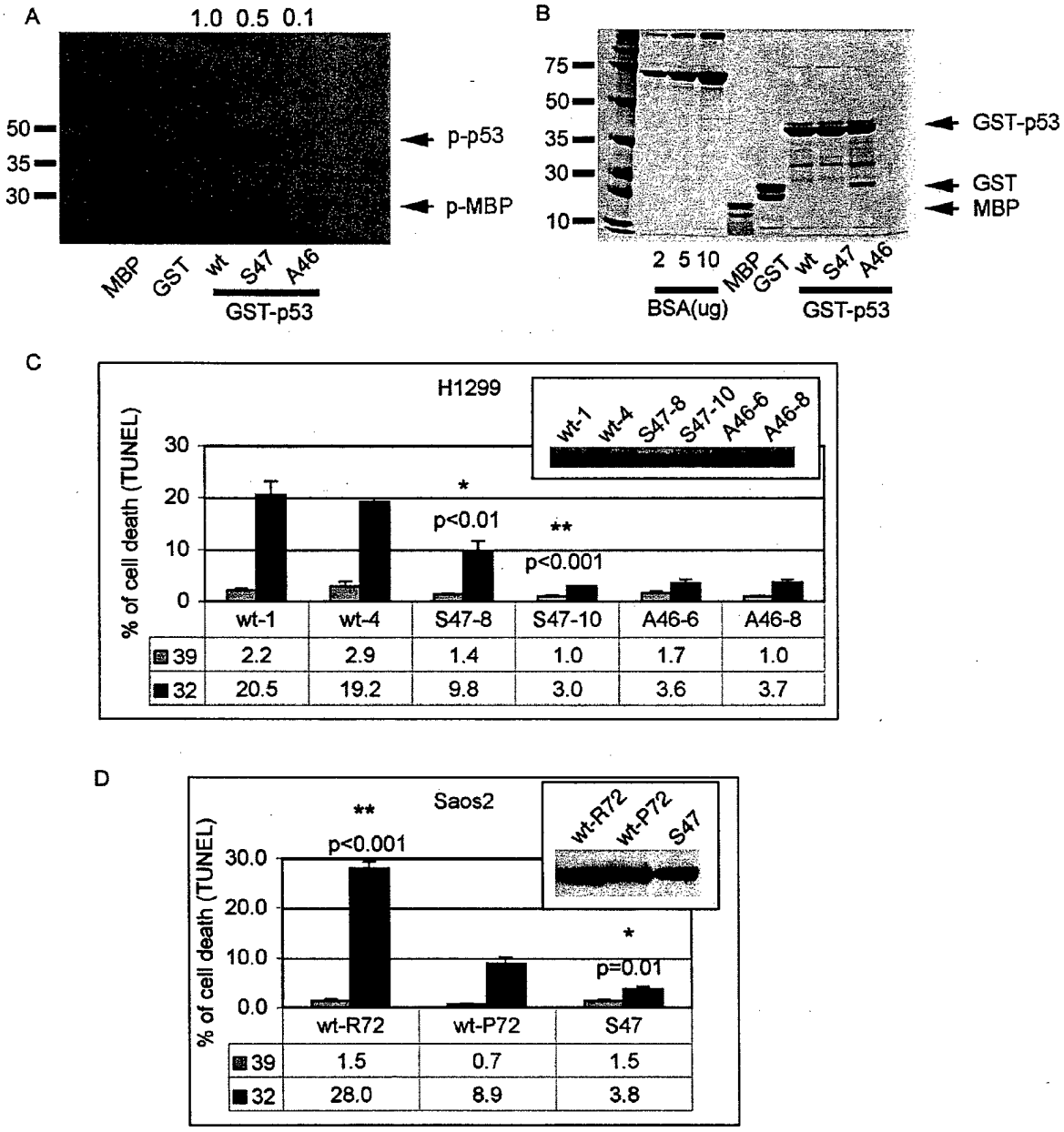
A
1.0 0.5 0.1
50
35
30
p-p53
p-MBP
MBP
GST
wt
S47
A46
GST-p53
B
75
50
35
30
10
GST-p53
GST
MBP
2 5 10
MBP
GST
wt
S47
A46
BSA(ug)
GST-p53
C
H1299
wt-1
wt-4
S47-8
S47-10
A46-6
A46-8
% of cell death (TUNEL)
30
20
10
0
*
p<0.01
**
p<0.001
wt-1 wt-4 S47-8 S47-10 A46-6 A46-8
39 2.2 2.9 1.4 1.0 1.7 1.0
32 20.5 19.2 9.8 3.0 3.6 3.7
D
Saos2
wt-R72
wt-P72
S47
% of cell death (TUNEL)
**
p<0.001
30.0
20.0
10.0
0.0
*
p=0.01
wt-R72 wt-P72 S47
39 1.5 0.7 1.5
32 28.0 8.9 3.8

Li *et al.*, Fig. 2

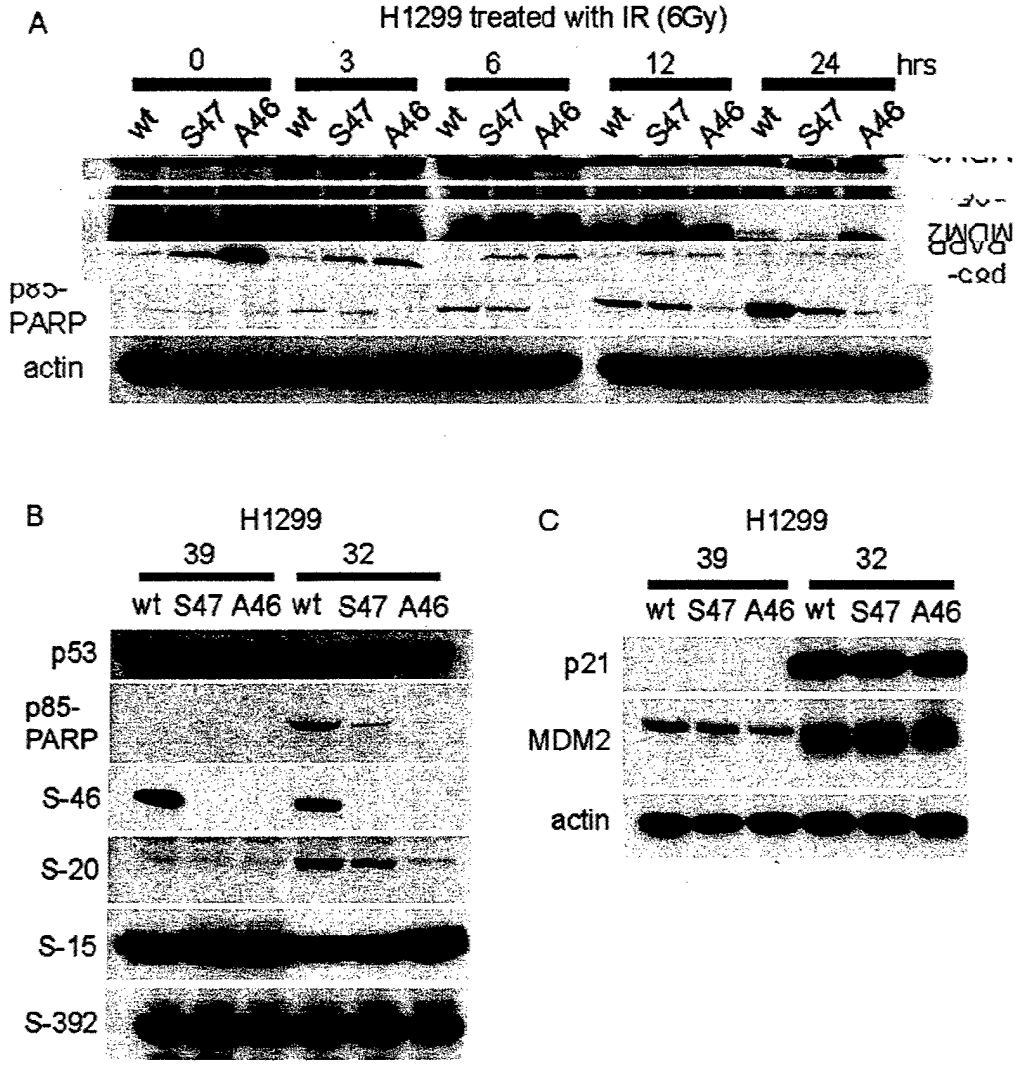
A
H1299 treated with IR (6Gy)
0
3
6
12
24
hrs
wt S47 A46 wt S47 A46 wt S47 A46 wt S47 A46 wt S47 A46
p85-PARP
actin
B
H1299
39
32
wt S47 A46 wt S47 A46
p53
p85-PARP
S-46
S-20
S-15
S-392
C
H1299
39
32
wt S47 A46 wt S47 A46
p21
MDM2
actin

Li *et al.*, Fig. 3

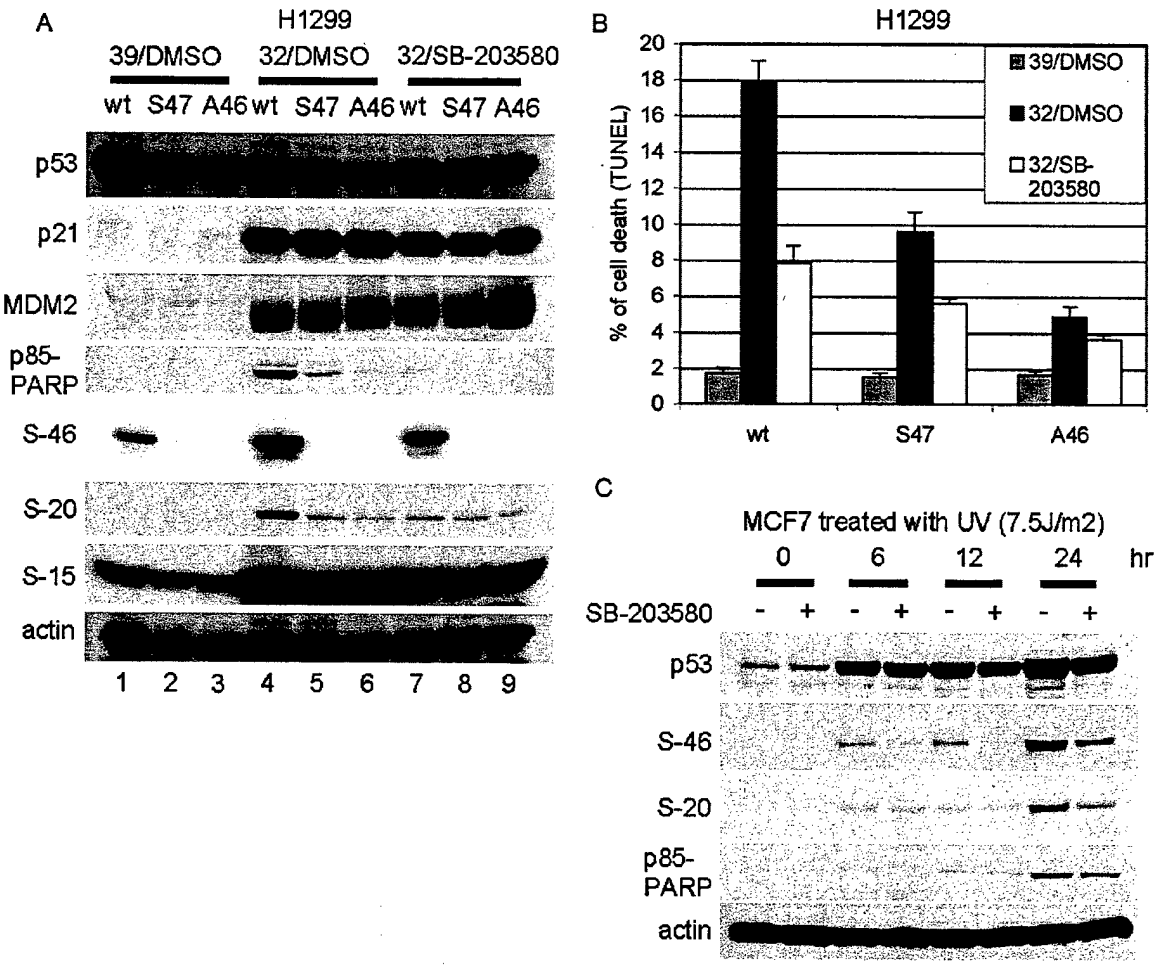
A
H1299
39/DMSO
32/DMSO
32/SB-203580
wt S47 A46 wt S47 A46 wt S47 A46
p53
p21
MDM2
p85-PARP
S-46
S-20
S-15
actin
1 2 3 4 5 6 7 8 9
B
H1299
% of cell death (TUNEL)
39/DMSO
32/DMSO
32/SB-203580
wt
S47
A46
C
MCF7 treated with UV (7.5J/m2)
0 6 12 24 hr
SB-203580 - + - + - + - +
p53
S-46
S-20
p85-PARP
actin

Li *et al.*, Fig. 4

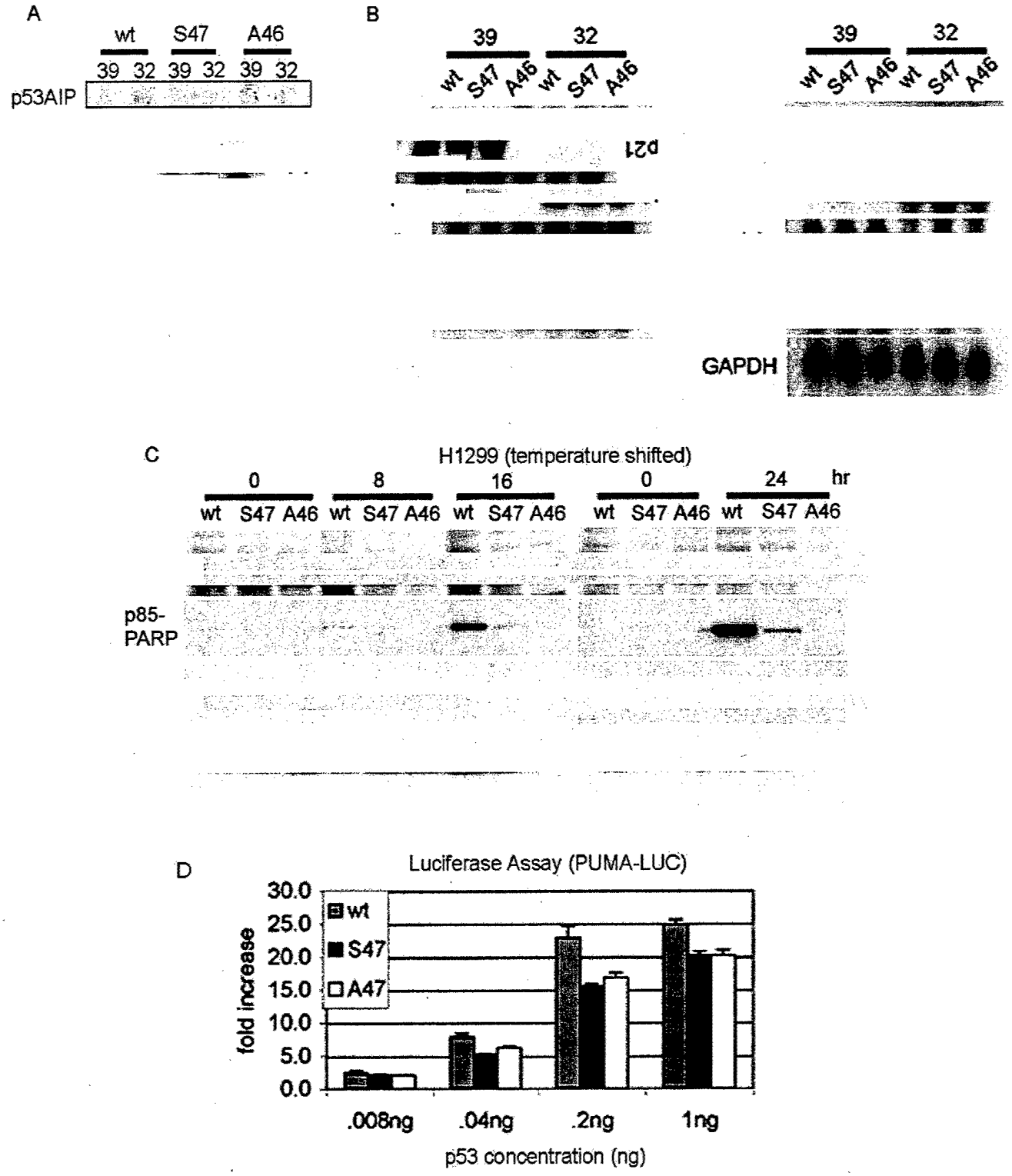
A
wt
S47
A46
39 32 39 32 39 32
p53AIP
B
39
32
wt S47 A46 wt S47 A46
p21
GAPDH
C
H1299 (temperature shifted)
0
8
16
0
24
hr
wt S47 A46 wt S47 A46 wt S47 A46 wt S47 A46 wt S47 A46
p85-
PARP
D
Luciferase Assay (PUMA-LUC)
fold increase
30.0
25.0
20.0
15.0
10.0
5.0
0.0
wt
S47
A47
.008ng
.04ng
.2ng
1ng
p53 concentration (ng)

Supplemental Figures, Li et al.

Supp. Figure 1.

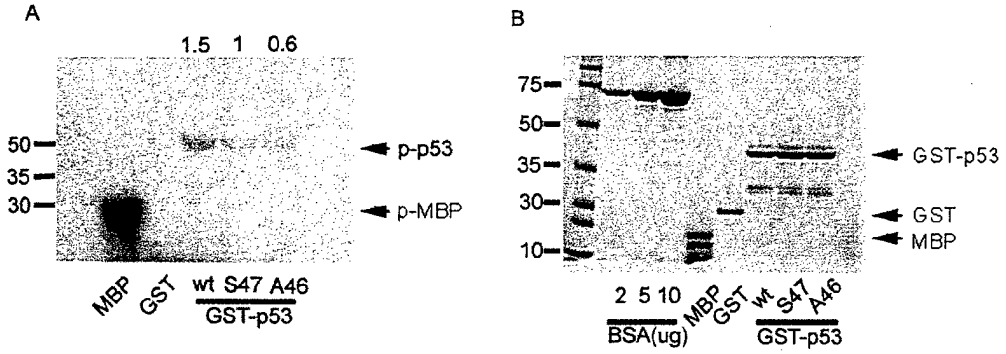

Supp. Figure 2.

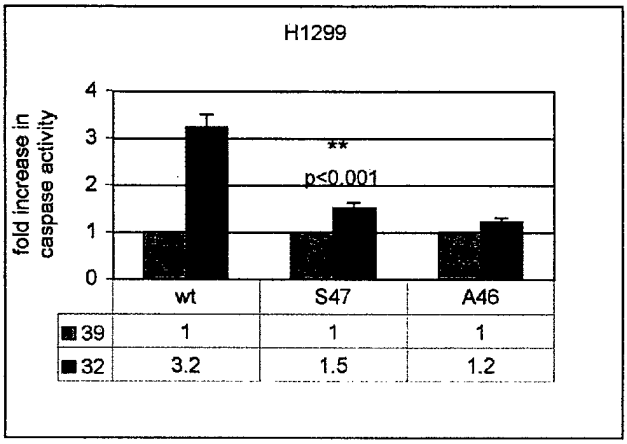

Supp. Figure 3.